University of Southern Queensland
FACULTY OF HEALTH, ENGINEERING AND SCIENCES
SCHOOL OF CIVIL ENGINEERING AND SURVEYING

Quantification of the measurement error associated with *in situ* measurements of water absorption and attenuation using the AC-9 instrument.

A dissertation submitted by

Alex Darton

in fulfilment of the requirements of

ENG4111/4112 Engineering Research Project

towards the degree of

Bachelor of Spatial Science: Surveying

Submitted: 30th October 2014

Abstract

Remote sensing has become a major resource for the monitoring of the concentrations of suspended and dissolved particulates in a water body. Measurement of the characteristics of the water body being analysed is a requirement to correctly calculate the concentrations of the particulates.

The Inherent Optical Properties of a water body are those characteristics that affect the path of a photon. They are caused by interaction of photons with dissolved and particulate matter. The properties that are of importance for measurements are absorption and attenuation with measurements carried out on water samples to quantify the effects these properties have on light within the sample. The measurement process, due to the effects of scattering contains errors when determining the coefficient of each property.

The aim of this project is to quantify the errors and determine the error drivers in the measurement of the IOPs with the WETLabs AC-9 resulting in a correction procedure. This will be carried out by evaluating a simulated dataset generated by an AC-9 instrument in SimulO.

The results of the simulation analysis found that for measurements of the attenuation coefficient the backscatter ratio and absorption formed the primary drivers of the error, with the backscatter ratio determined as the primary error driver. The absorption tube was determined to be a complex function of scattering, absorption and the backscatter ratio.

The correction method generated utilises a small amount of external data to determine the error factor for measured attenuation and absorption. The error factor is used to correct the measured coefficients to 'true' values.

University of Southern Queensland

Faculty of Health, Engineering and Sciences

ENG4111/ENG4112 Research Project

Limitations of Use

The Council of the University of Southern Queensland, its Faculty of Health, Engineering & Sciences, and the staff of the University of Southern Queensland, do not accept any responsibility for the truth, accuracy or completeness of material contained within or associated with this dissertation.

Persons using all or any part of this material do so at their own risk, and not at the risk of the Council of the University of Southern Queensland, its Faculty of Health, Engineering & Sciences or the staff of the University of Southern Queensland.

This dissertation reports an educational exercise and has no purpose or validity beyond this exercise. The sole purpose of the course pair entitled "Research Project" is to contribute to the overall education within the student's chosen degree program. This document, the associated hardware, software, drawings, and other material set out in the associated appendices should not be used for any other purpose: if they are so used, it is entirely at the risk of the user.

University of Southern Queensland

Faculty of Health, Engineering and Sciences

ENG4111/ENG4112 Research Project

Certification of Dissertation

I certify that the ideas, designs and experimental work, results, analyses and conclusions set out in this dissertation are entirely my own effort, except where otherwise indicated and acknowledged.

I further certify that the work is original and has not been previously submitted for assessment in any other course or institution, except where specifically stated.

Alex Darton

Student Number: 0061019481

_____

Signature

_____

Date

Acknowledgements

This project was carried out under the supervision of Dr Glenn Campbell of the University of Southern Queensland. Without his supervision and guidance this project would not have been possible.

I would also like to thank my Family and the residents of McGregor College for providing support, encouragement and lollies throughout the process.

Table of Contents

List of Figures

List of Tables

List of Graphs

List of Abbreviations and Symbols

Abbreviations

IDL	Interactive Data Language
IOP	Inherent Optical Property
VSF	Volume Scattering Function
CDOM	Coloured Dissolved Organic Matter
OAS	Optically Active Substance
FF	Fournier-Forand
FOV	Field Of View
NIR	Near-Infrared
PSICAM	Point Source Integrating Cavity Absorption Meter

Symbols

a	spectral absorption coefficient
a_{715}	spectral absorption at 715nm
a_{CDOM}	spectral absorption of CDOM
a_m	measured absorption coefficient
a_{m715}	measured spectral absorption at 715nm
a_p	spectral absorption of particulates
a_t	true absorption coefficient
a_{TR}	spectral absorption of Tripton
a_w	spectral absorption of water
a_ϕ	spectral absorption of phytoplankton
b	spectral scattering coefficient
b_b	spectral backscattering coefficient
$\frac{b_b}{b}$	backscatter ratio
b_f	spectral forward scattering coefficient
b_m	measured scattering coefficient
b_{nf}	spectral near-forward scattering coefficient
b_t	true scattering coefficient
c	spectral attenuation

$C(\mu_0)$	zenith angle function for reflectance
c_{CDOM}	spectral attenuation of CDOM
c_m	measured attenuation coefficient
c_t	true attenuation coefficient
c_{TR}	spectral attenuation of Tripton
c_w	spectral attenuation of water
c_ϕ	spectral attenuation of phytoplankton
E_{fa}	Error factor for absorption
E_{fc}	Error factor for attenuation
$f(\lambda)$	complex function of IOPs for remote sensing
f_a	Fraction of scattered light not collected by sensor
f_c	Fraction of scattered light collected by sensor
k_a	spectral absorption correction
k_c	spectral attenuation correction
L	instrument length
n_w	real refractive index
$P^x_{a_t,b_t}(\lambda)$	Probability of detection for the sample
$P^x_{0,0}(\lambda)$	Probability of detection for pure water
$Q(\lambda)$	ratio of upwelling irradiance to upwelling radiance
R	photon path length
$R(0^-)$	remotely sensed reflectance beneath the surface
$R_{rs}(\lambda)$	remotely sensed reflectance
$t_{(a,w)}$	coefficient of transmittance from air to water
$t_{(w,a)}$	coefficient of transmittance from water to air
$T(\lambda)$	spectral transmittance
x_m	measured coefficient
$\beta(\theta, \phi)$	volume scattering function for a sphere
$\beta(\theta)$	volume scattering function
$\tilde{\beta}_{ms}(\theta)$	volume scattering function for multiple scattering
θ_0	Acceptance angle of the sensor
ω	single scattering albedo
ω_{ms}	multiple scattering albedo

Chapter 1

Introduction

1.1   Project Outline

It has been noted in recent studies by McKee et al. (2013) and (Röttgers, McKee & Woźniak 2013) that the established correction methods used for the correction of in-situ measurements of the Inherent Optical Properties (IOP) of water rely on a major assumption for use. They note that due to this assumption systematic errors are propagated through the adjustment and a better method is required. McKee et al. (2013) proposed a method however noted that the requirement of extra data to perform the correction renders it less useable while Röttgers, McKee and Woźniak (2013) provide a correction for absorption errors in the near-infrared at the wavelength 715nm. The purpose and scope of the project are covered in Section 1.4 Research Objectives.

1.2   Introduction

Remote sensing has become a major resource for the monitoring of the concentrations of particulates and Coloured Dissolved Organic matter (CDOM) in a water body. This has become the preferred method to obtain data on the variability of a water body in relation to optical type, seasonal changes and human impacts (Herlevi 2002; Paavel, Arst & Herlevi 2007). These

concentrations of water quality parameters influence the reflectance values of water that are detected by the remote sensing system. The IOPs of a water body are those properties that affect the interaction of light with water (McKee et al. 2013). As the inherent optical properties are determined partly by the particulate and dissolved material, if the IOPs are known for a water body then the concentrations of material can be determined from remote sensing data.

The IOPs are the properties that define the changes that light particles undergo when impacting on the particles that are suspended in the water body. These changes can be in the direction or the intensity of the particle and are defined as scattering and absorption. This scattering and absorption affect the light as it propagates through the water body and thus affect the spectral signature of the light through a process called beam attenuation. In order to use IOPs, measurements must be made to obtain values for each IOP. The reflecting type absorption meter was developed for the measurement of water in 1939 (Kirk 1992) where it was used in the pioneering studies on water absorption. Kirk (1992) notes that this instrument has increased in popularity with recent advances in technology. These advances however, have shown that there are a number of errors associated with the measurements taken using these instruments.

The common instrument for *in-situ* measurement of the IOPs is the WETLabs ac-9. The standard correction method that was proposed by Zaneveld, Kitchen and Moore (1994) which uses a proportionality function to correct the scattering error when using the ac-9. A recent study by Röttgers, McKee and Woźniak (2013) questioned a number of the assumptions that are used by

Zaneveld in the creation of the 'proportional' method and creates doubt over the validity of the 'proportional' correction method. McKee et al. (2013) have created a correction scheme that does not rely on this assumption but relied on other external data. They also state that a correction method that does not require the extra data used in the study would be beneficial due to time savings.

While all of these methods are correction methods for the optical properties they focus on the correction of the measurements from the absorption tube of the ac-9. Zanevelds 'proportional' correction method study only contains explicit corrections for the values in the absorption tube (Leymarie, Doxaran & Babin 2010) and does not account for any possible errors in the attenuation tube which may affect the measured values. It is due to this lack of definition that a correction method must be proposed that accounts for the change in the assumption of non-zero absorption (Röttgers, McKee & Woźniak 2013) and the lack of quantification of errors in the attenuation tube of the ac-9 to ensure that the scattering coefficient error is reduced.

1.3   The Problem

Despite there being a number of proposed correction methods for AC-9 measured data (McKee et al. 2013; Röttgers, McKee & Woźniak 2013; Zaneveld, Kitchen & Moore 1994) there is no definitive correction method that produces results with a minimum of residual error. The methods that are the currently established corrections rely on an assumption that has been proven

to be incorrect to a certain degree. Current research has accounted for some of this error; however further work is required to create an effective correction method requiring minimal data. The nature of the errors and the correction methods are investigated in Chapter 2.

1.4   Research and Testing Objectives

This research analysed the problems and current solutions regarding the determination of the Inherent Optical Properties of a water body. As such the following objectives were set to fulfil the aim of the project.

1. Perform a literature review to identify and understand the following:

    i.   The Inherent Optical Properties of waters and how they interact with photons

    ii.   The relationship that exists between IOPs and the remote sensing process

    iii.   The WETLabs AC-9 instrument, both its operation and the theory behind its use

    iv.   The pre-existing correction methods in use with AC-9 data

    v.   The current research into correction methods to account for assumptions in pre-existing corrections

2. Based off the literature design a suite of simulations for an AC-9 instrument modelled in SimulO to generate experimental measurements.

3. Using the Experimental data, identify the primary drivers behind the error that is generated through operation of the AC-9 to measure IOP coefficients.

4. Having identified the primary error drivers, develop a correction scheme that can be implemented to account for the modelled errors.

1.5   Conclusion

This dissertation aims to address in some manner the issues involved with the determination of the errors associated with *in-situ* measurement of IOPs with the AC-9. The literature review is expected to identify the range within which the data is to be generated to establish bounds for Australian natural waters. It is also expected to identify the theory behind the IOPs and remote sensing, the operation of the WETLabs AC-9 and the errors inherent within measurements. It also aims to identify the existing and in-progress correction methods and the procedures and constraints involved in the creation of the methods. A simulated dataset for usage in analysis of the error and the primary drivers of the error will be generated.

The outcomes of this study are to be used to further the research and development of a robust correction method that can be applied to a wide range of water bodies with a high level of accuracy from the corrected IOP values.

Chapter 2

Literature Review

2.1   Introduction

This literature review provides an overview of the background information relevant to the project along with a number of established and current research areas that are important. First to be looked at is the basis of this project, that of the Inherent Optical Properties (IOPs) of water (Section 2.2). This is broken down into its component parts of Absorption (Section 2.2.1), Scattering (Section 2.2.2), the Volume Scattering Function (VSF) (Section 2.2.3) and Attenuation (Section 2.2.4) and details how each of these elements are relevant to the nature of the project.

The relationship between the particulate matter in a water body and the IOPs is then discussed (Section 2.2.5) with a focus on how changes in particulates affect the IOPs with respect to water body types. This then moves onto an explanation of how the IOPs are linked to the surveying practice of remote sensing and why they are relevant (Section 2.3).

Following this the instrument that is used to determine IOP values, the WETLabs AC-9 is noted and discussed (Section 2.4). In particular the individual operation of each tube is detailed along with the construction and natural causes that introduce error into the measurements.

Having established the operation of the AC-9 and the errors that occur in measurements with the instrument, the established correction schemes that

are in place to account for these errors are discussed (Section 2.5). In particular the methods detailed are the "Flat" correction, Zanevelds "Proportional Correction" and Kirks "Fixed Contribution" method.

The research into corrections for the errors experienced when using the AC-9 is an ongoing field of work and so this chapter finishes by examining the current corrections that are being developed (Section 2.6). In particular the correction methods of McKee and Röttgers are detailed and discussed while noting that elements of the methods require further work and investigation.

2.2   The Inherent Optical Properties of Water

The inherent optical properties (IOPs) are defined by a number of authors to be any property that is independent of the ambient light field and determines the magnitude and spectral signature of the light propagating through the water body (Barnard, Pegau & Zaneveld 1998; McKee et al. 2013; Pegau, Gray & Zaneveld 1997). These IOPs must be clearly defined and values accurately known in order to carry out accurate analysis on the concentrations of particulate matter in the water body. The particulate matter is generally comprised of optically active substances such as phytoplankton, CDOM and non-algal suspended sediment (Tripton) (Paavel, Arst & Herlevi 2007) based on the effect they have on the attenuation of light in the medium. The IOPs for water bodies are the absorption, scattering and the VSF.

2.2.1 Absorption

Absorption is defined as a reduction in radiance that occurs when a photon encounters a particle as it passes through a water body (Arst & Arst 2003). It is one of the IOPs that influence the reflectance of a water body and is required to perform measurement of the scattering coefficient *in-situ* (Leymarie, Doxaran & Babin 2010).

In order to accurately determine the contribution that particulate matter has on the levels of absorption in a water body the absorption coefficient is broken down into its component parts as per equation 2.1 to ensure that measured coefficients have the pure water component removed, leaving only the particulate.

$$a = a_w + a_\varphi + a_{CDOM} + a_{TR} \tag{2.1}$$

The removal of the pure water component is required as the absorption that is detected *in-situ* includes not only the absorption for phytoplankton (ϕ), coloured dissolved organic matter (CDOM) and tripton which are classified as optically active substances (OAS).

The traditional technique that has been used to estimate the coefficient for absorption for particulate matter was performed *in-vitro* in a laboratory. This method used a filter pad to separate the particulate and dissolved material from the water in the sample (Barnard, Pegau & Zaneveld 1998) which allows for the determination the absorption coefficient for the particulate matter as shown by equation 2.2 where a_p is the coefficient of the particulate and dissolved material.

$$a = a_w + a_p \qquad\qquad\qquad\qquad (2.2)$$

Use of laboratory pigment extraction techniques is then used to separate the tripton and phytoplankton absorption portions of the absorption (Barnard, Pegau & Zaneveld 1998). While this method calculates the absorption values for discrete portions of the water column (Barnard, Pegau & Zaneveld 1998) the data is of a high spectral resolution. That the data is only for discrete portions of the water body is a drawback to this method. As such improvements in optical instrument have allowed for the use of non-invasive determination of the absorption coefficient of the sample at a greater vertical scale than the traditional method through beam attenuation measurements (Barnard, Pegau & Zaneveld 1998). This is achieved through the use of an instrument such as the WETLabs ac-9 (WETLabs Inc. 2005) which is used for the determination of the measureable IOPs of a water body.

2.2.2 Scattering

Scattering of photons in a water body is considered as an IOP, however due to the nature of scattering it is not readily measured (Piskozub et al. 2004). It is characterised by the scattering coefficient, which defines the amount of scattering that occurs due to the particulate matter in the water body, and the VSF, which defines the probability of a photon being scattered in a particular direction. Section 2.2.3 provides further insight on the VSF. Scattering causes photons to take non-regular paths through the water body if they are not absorbed before they exit the water body. This scattering can occur in all directions away from the point of impact and causes significant levels of error

in the determination of the measureable IOPs. The coefficient of scattering for all directions from the point of scattering can be determined using equation 2.3

$$b = \int_0^{2\pi} \int_0^{\pi} \beta(\theta, \phi) \sin(\theta) \, d\theta \, d\phi \quad \text{(Pegau, Zaneveld \& Voss 1995)} \quad (2.3)$$

Where $\beta(\theta, \phi)$ is the volume scattering function for the sample, θ is the plane scattering angle and ϕ is the scattering angle above and below the plane of forward momentum. This double integral is simplified down to a single integral of $\int_0^{2\pi} \beta(\theta)$ as the scattering above and below the plane is symmetrical (Bukata et al. 1995).

Equation 2.3 provides the scattering coefficient *b* for all directions in a sphere provided that the VSF for the water body is known. The simplified integral provides the scattering coefficient in a plane away from the point the scattering event. This scattering is categorised into two categories that are used as separate indicators of the scattering nature of the sample. These are the forward scattering and the backscattering components of the water body. Each of these is important for determination of a number of errors in *in-situ* measurements and reflectance analysis as the particulate scattering needs to be determined as it differs from the scattering of pure water. The particulate scattering can be broken down further into the contribution due to phytoplankton and tripton particles. CDOM is not included in the scattering equation due to the complex equations that govern scattering by CDOM particles (Paavel, Arst & Herlevi 2007). The amount of scattering contributed to the total scattering by CDOM has been found to be approximately 1% of the

total scattering coefficient and as such is classed as negligible (Paavel, Arst & Herlevi 2007)

It has been generally assumed that scattering levels within a water body are independent of the wavelength of light that is being measured (Zaneveld, Kitchen & Moore 1994) however it has been recently noted that there is evidence that shows that this may not be entirely valid (McKee et al. 2013). Scattering is complex in nature and cannot be measured by conventional techniques or equipment. Therefore obtaining a measured value for scattering requires the measurement of the absorption and attenuation before determining the scattering value. This introduces errors as scattering effects the determination of these values and deviates them from the true coefficient.

2.2.2.1   Forward Scattering

The forward scattering is a property of water constituents that is important to analysis and determination of error due to the effects it has on *in-situ* measurements (Voss & Austin 1993).

$$b = 2\pi \int_0^{\frac{\pi}{2}} \beta(\theta) sin\theta \, d\theta \qquad\qquad (2.4)$$

The definition of forward scattering is that it is those scattering events which occur and deviate the path of the photon at angles less than 90° from the original path. The coefficient of forward scattering can be calculated using equation 2.4 and it is this error that causes errors in determination of the coefficient of attenuation due to the collection of photons that have been scattered at small angles and not discounted due to the angle of scattering

(Voss & Austin 1993). Where the scattering angle is <10° the scattering is referred to as near-forward scattering. This error is discussed in greater detail in section 2.4.

The scattering has been found to be more highly peaked in the forward direction in water bodies where the majority of particulate matter has a large particle size (Voss & Austin 1993). This results in lower values of forward scattering in water bodies where the particle size is reduced, however this will result in larger amounts of forward and backscattering for the sample. In samples of seawater the particulate scattering is very highly peaked in the near-forward direction with small deviations of angle (Voss & Austin 1993). This shows that seawater predominately is composed of larger particle sizes that form the largest contribution to near-forward scattering (Voss & Austin 1993). As such, transmissometers, which measure transmitted light intensity, can receive a large amount of light which has been scattered by a seawater sample and measure it as part of the unscattered light (Voss & Austin 1993).

In order to determine the angle which is termed as near-forward scattering Voss & Austin (1993) note that the near forward scattering that contributes to a majority of the error is scattered at an angle equal to that of the acceptance angle of the sensor. By using this information forward scattering can be separated into both a near-forward scattering coefficient and a value for the remainder of the forward scattering.

$$b_{nf} = 2\pi \int_0^{\theta_0} \beta(\theta)\sin\theta \, d\theta \qquad\qquad (2.5)$$

$$b_f = 2\pi \int_{\theta_0}^{\pi} \beta(\theta)\sin\theta \, d\theta \qquad\qquad (2.6)$$

Equations 2.5 and 2.6 show the integrals that can be used to calculate coefficients for the near forward and forward scattering given the acceptance angle of the sensor θ_0 and the VSF. These can be used to estimate the percentage of scattering that will be in a near forward direction when given the total scattering coefficient as calculated from equation 2.3.

2.2.2.2 Backscattering

Where the scattered photons are scattered away from the direction of travel at angles between 90° and 180° the scattering is deemed to be backscatter.

$$b_b = 2\pi \int_{\frac{\pi}{2}}^{\pi} \beta(\theta)sin\theta\ d\theta \qquad\qquad (2.7)$$

Equation 2.7 shows that the calculation for the backscattering coefficient is the same calculation used for forward scattering with a change in the angle values used in the integral to account for backscatter being any scatter event greater than 90°.

As backscatter is a scatter event of such magnitude, the remotely sensed diffuse reflectance is highly influenced by the amount of backscatter that occurs when the photons interact with the water body (Ulloa, Sathyendranath & Platt 1994). This is due to the photons that are backscattered upon interaction with the surface of the water forming the part of the photons that are collected by the satellite. The general method used to define the effect that the backscatter has is by using the backscatter ratio $\frac{b_b}{b}$ (Aas, Høkedal &

Sørensen 2005) which is the ratio of the backscattering to the scattering coefficient.

Equation 2.7 is the generally accepted and adopted method of calculating the backscattering coefficient of the particulates and pure water. Another method, which uses bio-optical models for particulates, can also be used to determine the backscattering coefficient (Ulloa, Sathyendranath & Platt 1994). This method requires knowledge of the scattering coefficient and the backscatter ratio of the sample. From this data pigment concentrations are used to calculate the backscatter for each of the particulates (Ulloa, Sathyendranath & Platt 1994). This method is restricted to the algal particles within a sample as the non-algal particles cannot be modelled with a bio-optic model and contribute significantly more to the backscatter (Herlevi 2002). This restricts the effectiveness to waters where the algal particles form the greater contribution of backscatter than the non-algal particles (Herlevi 2002) which does not occur in inland waters due to high tripton levels.

2.2.2.3 Multiple Scattering

In high scattering environments multiple scattering events can occur within a water body or an *in-situ* testing sample (Piskozub & McKee 2011). Therefore the more times a photon is scattered the longer its path length, that is the distance the photon has travelled. While this in itself can lead to small errors in radiance calculations (Leymarie, Doxaran & Babin 2010) there is a greater error which can occur due to multiple scattering. By having a photon scatter multiple times there is a possibility that the photon will intersect at an angle

that can be detected in an attenuation measurement test with an ac-9 (Piskozub et al. 2004). It is assumed that there is always some photons which contribute to measurement error by being scattered away from the beam length in the first instance and then back to the beam path due to subsequent scattering events (Piskozub et al. 2004). As there is a scattering phase function that can be used to describe single scattering events there can similarly be a phase function that can be used to describe multiple scattering events (Equation 2.8) (Piskozub & McKee 2011).

$$\tilde{\beta}_{ms}(\theta) = \frac{\tilde{\beta}_1(\theta) + \omega\tilde{\beta}_2(\theta) + \omega^2\tilde{\beta}_3(\theta) + \cdots + \omega^{n-1}\tilde{\beta}_n(\theta)}{1 + \omega + \omega^2 + \cdots + \omega^{n-1}} \tag{2.8}$$

Where $\tilde{\beta}_{ms}(\theta)$ is the multiple scattering function, $\tilde{\beta}_n(\theta)$ is a scattering phase function and ω is the scattering albedo calculated as the ratio of scattering to attenuation. When analysing samples of water for IOP values it is important to note that there is likely to be multiple scattering events. The concentration of particles is the greatest indicator of this (Piskozub et al. 2004) with the particle size of inorganic particles also playing a large part in the probability of multiple scattering occurring (Voss & Austin 1993) as an increase in concentration of small sized particles is likely to lead to an increase in multiple scattering events.

2.2.3 Volume Scattering Functions

Mie scatterers are the models that are used to define the scattering of a light particle off a surface (Fournier & Forand 1994). They describe the angular distribution that defines the likelihood of a particle being scattered in a

particular direction and are generally expressed in terms of a volume scattering function. This volume scattering function is used in the equation 2.3 to determine the scattering coefficient and is represented by $\beta(\theta)$ (Fournier & Forand 1994; Pegau, Zaneveld & Voss 1995). Mie theory can be broken down into a small angle component called diffraction theory (Voss & Austin 1993). This component of scattering theory is generally adopted for VSF calculations as it allows for simplification of small angle descriptions in the VSF (Voss & Austin 1993)

As has been noted, scattering is affected by the particle size of the particulates in the water body (Voss & Austin 1993). As such the determination of any phase function that describes the scattering events requires the input of a particle size distribution function to describe the size of the particles (Fournier & Forand 1994). It has been found that for oceanic waters the size distribution is associated with an inverse power law (Junge distribution) (Fournier & Forand 1994) for spherical particles. This inverse power relationship however has been shown to not be valid when dealing with non-spherical particles (Ulloa, Sathyendranath & Platt 1994) and is especially important when applying Mie theory. Due to the difficulty of performing scattering function measurements assumptions are generally made about the particulate matter and the choice of VSF that will be suitable (Freda & Piskozub 2007).

Fournier and Forand (1994) created a VSF (FF) which has been used as an established VSF, however it should be noted that the function relies on the determination of a relative refractive index which impacts on the usage of the FF VSF (Freda & Piskozub 2007). However various studies have obtained a

modified FF method which removes this requirement and increases the usability of the function (Freda & Piskozub 2007).

As there are a number of differing parameterizations for VSFs it is then valid that for differing 'chemical' makeups of water bodies there should be a different VSF used for the determination of scattering (Herlevi 2002). Therefore a water body with high refractive index particles require the usage of a different VSF to that of a water body with low refractive index particles (Herlevi 2002).

2.2.4 Attenuation

Beam attenuation is a function of the combined effects of particulate scattering and absorption (Piskozub et al. 2004) and is defined by equation 2.9.

$$c = a + b \qquad\qquad\qquad (2.9)$$

The attenuation is the second measureable IOP and forms the basis of the operation of the WETLabs ac-9 meter (WETLabs Inc. 2005) which comprises direct measurement of the attenuation coefficient of a water sample. It is an important optical property as it is the main tool of *in-situ* measurements to obtain scattering coefficients. This method of data collection has been used for an extensive period of time (Piskozub et al. 2004) with reflecting type absorption meters being the instrument of choice. The measuring process uses transmittance in a wavelength (λ) over a pathlength R (Voss & Austin 1993) as shown in equation 2.10 which leads to the attenuation coefficient value for a wavelength.

$$c(\lambda) = -\ln[T(\lambda)]/R \qquad\qquad\qquad (2.10)$$

Where $c(\lambda)$ is the attenuation coefficient for a particular wavelength, $T(\lambda)$ is the transmittance factor of the water for the wavelength and R is the pathlength. As the attenuation is the sum of the absorption and scattering it is subject to the cumulative effects of the particulate and dissolved material in a water body which leads to knowledge of the water body being required to obtain an accurate measurement (Paavel, Arst & Herlevi 2007). As with the scattering and absorption coefficients the attenuation of a water sample is dependant on the contributions by the optically active substances to the total attenuation (Paavel, Arst & Herlevi 2007).

$$c = c_w + c_\varphi + c_{CDOM} + c_{TR} \qquad\qquad\qquad (2.11)$$

This is generally broken down into the same categories of phytoplankton, CDOM and the nonchlorophyllous or tripton material. The tripton can be classified further for attenuation by breaking it down into contributions based on particle size which can be used to evaluate the variability between water bodies and their IOPs (Paavel, Arst & Herlevi 2007).

2.2.5 Influence of water constituents on the Inherent Optical Properties

As has been discussed a number of times so far, the water particulates greatly effect the IOPs. The effects are generally seen in the determination of the attenuation, absorption and the scattering coefficients, which vary with changes in the constituents. These changes have been linked to the classification of water bodies into two distinct classes for the purposes of

remote sensing known as class 1 and class 2 waters (Paavel, Arst & Herlevi 2007) and are classified based on the influence that OAS have on them. Class 2 waters are multicomponental water systems with inorganic particles having a higher concentration than organic particles. Resuspended sediments and particles form the major contribution to the optical properties (Paavel, Arst & Herlevi 2007). The class 1 waters are defined as the rest of the water bodies where phytoplankton dominates the water sample (Paavel, Arst & Herlevi 2007). This classification system has been noted to be vague (Paavel, Arst & Herlevi 2007) however for the purposes of determining a monitoring system for the concentration of particulates it is suitable.

The changes which particulate material and the concentrations affect range across a number of scopes and include scattering and absorption changes in the water nature (Herlevi 2002; Paavel, Arst & Herlevi 2007). The scattering of light due to particles is a function of the VSF and therefore the particle size (Fournier & Forand 1994; Pegau, Zaneveld & Voss 1995) which causes changes in scattering directions and amounts. It is noted that larger particle sizes cause higher amounts of near forward scattering (Voss & Austin 1993) especially in waters dominated by inorganic particles. This causes a change in the coefficient in scattering and a change in the VSF, as it must change to acknowledge the increase in forward scattering and therefore the subsequent reduction in scattering at all other angles (Voss & Austin 1993). The increase of inorganic material also creates an increase in the absorption of the water body and creates problems due to the difficulty in determining the specific absorption value of the tripton while the phytoplankton and CDOM is solved

easily (Paavel, Arst & Herlevi 2007). While an increase is shown to occur in the forward scattering it has also been noted that tripton particles contribute significantly more backscatter than organic particles, especially for the smaller particle sizes where forward scattering is less prevalent (Herlevi 2002). All of this is caused by changes in the concentrations and particle sizes of the optically active substances and greatly affect the IOP values for each individual water body.

2.3 Inherent Optical Properties and Remote Sensing

The remote sensing of a water body for the determination of concentration requires the use of a number of the IOPs in order to obtain an accurate value. This is because the reflectance of the photons by the water body is affected by the IOPs effects on the nature of the water in terms of the backscattering $b_b(\lambda)$ and the absorption $a(\lambda)$ for the particular wavelength being analysed (Tzortziou et al. 2007). This reflectance is detected by the sensor that is attached to the satellite and then captured and turned into a manipulable image which requires the IOP values to correctly calibrate for the concentrations (Tzortziou et al. 2007).

There are a number of different methods that can be used to calculate the reflectance values based on IOP inputs along with other input data. Equation 2.12 shows an equation that is used for reflectance sensed beneath the surface of the water body. $C(\mu_0)$ is a function of the angle of refracted photons, $b_b(\lambda)$ is the particulate backscattering and $a(\lambda)$ is the particulate absorption.

Equation 2.13 shows another derivation of the calculation of reflectance, this time for reflectance above the surface where $t_{(w,a)}$ and $t_{(a,w)}$ are the transmittance from air to water and vice versa. n_w is the real part of the refractive index, $f(\lambda)$ is a complex function of water IOPs and $Q(\lambda)$ is a ratio of upwelling irradiance to upwelling radiance.

$$R(0^-) = C(\mu_0) \times \frac{b_b(\lambda)}{a(\lambda)+b_b(\lambda)} \qquad \text{(Herlevi 2002)} \qquad (2.12)$$

$$R_{rs}(\lambda) = \frac{f(\lambda)}{Q(\lambda)} \times \frac{t_{(w,a)}t_{(a,w)}}{n_w^2} \times \frac{b_b(\lambda)}{a(\lambda)+b_b(\lambda)} \qquad \text{(Tzortziou et al. 2007)} \qquad (2.13)$$

These two equations (2.12 & 2.13) both show that the IOPs are a part of the analysis that is performed on remotely sensed imagery. The multiple scattering albedo $\frac{b_b(\lambda)}{a(\lambda)+b_b(\lambda)}$ is comprised of particulate information as is $f(\lambda)$ from equation 2.13.

This is only a small amount of reflectance models, a large number of other methods have been created and all of these models can be applied to remote sensing monitoring, with different requirements and data used for each. Some of these, like the method described by Lee et al. (1999) are designed for a specific purpose and as such should only be used as appropriate to ensure that measurements are accurate. These different methods also make use of differing equipment and remote sensing systems and should only be used with the appropriate equipment to ensure optimal results.

As the most common usage of the measured reflectance values is to obtain concentration information on the particulate matter the backscattering is highly important due to it's dependence on the nature of the particulate matter

(Tzortziou et al. 2007). In particular it is the concentration, composition, size, shape and refractive index of all particles which provides the information about the constituents that effect a variety of processes including biological and carbon cycle information (Tzortziou et al. 2007) which are two of the main drivers for monitoring of water systems.

2.4   The ac-9 instrument

The WETLabs ac-9 is a reflecting type absorption meter that is used to analyse and determine the attenuation and absorption coefficients of a water body (Barnard, Pegau & Zaneveld 1998). Scattering values for the water sample are then obtained by using Equation 2.14:

$$b = c - a \qquad \text{(Leymarie, Doxaran \& Babin 2010)} \qquad (2.14)$$

The instrument is made up of a collimated laser diode, two sample tubes, a photon detector and other miscellaneous components. These tubes are used to calculate the coefficient values for attenuation and absorption respectively. Each tube is designed to be used for the determination of a specific coefficient with the amount of scattering being determined by Equation 2.14. Figure 2.1 provides a schematic overview of the internal systems of the ac-9.
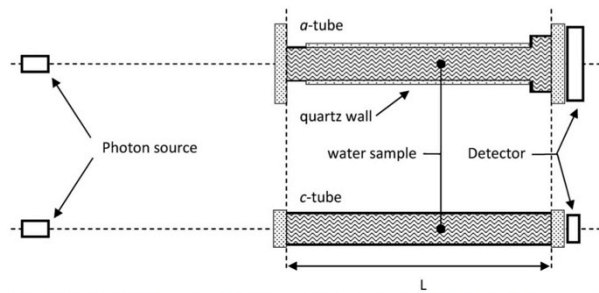
Fig. 1. Schematic modeling of the absorption and attenuation tubes including the light sources and detectors.

Figure 2.1 - Schematic diagram of the WETLabs ac-9 measurement tubes (Leymarie, Doxaran & Babin 2010)

The absorption tube (*a*-tube) is constructed with a reflective exterior covering of quartz at the edge of the water sample tube. This quartz wall is designed to prevent the escape of scattered photons from the water medium while facilitating the travel of forward scattered photons to reach the detector (Leymarie, Doxaran & Babin 2010). The photon detector at the end of the tube is set with a wide Field of View (FOV) that allows it to accept the large angles with which the scattered photons can impact against the sensor. This results in photon losses due to absorption. It is from this sensor data that the coefficient for absorption is obtained for the water sample.

The attenuation tube (*c*-tube) is constructed with a fully absorbent interior in contrast to the fully reflective exterior of the absorption tube (Leymarie, Doxaran & Babin 2010). This design means that any photons that are scattered away from the initial beam direction are absorbed by the walls and stopped. As some photons are only scattered by a small degree, due to near-forward scattering, the detector is set with a small FOV that is set to be slightly larger than the diffusion angle of the photon emitter (Voss & Austin 1993). This construction ensures that the scattered photons are discounted from the collected photons, with only un-scattered and non-absorbed photons being

23

detected. This sensor data allows for the calculation of the attenuation coefficient of the sample of water.

Due to the nature of the construction of the ac-9 tubes however there are errors that can occur during the measurement of the coefficients for attenuation and absorption (Leymarie, Doxaran & Babin 2010). Due to the nature of the attenuation tube the following is known about the error:

- The error is proportional to the backscatter ratio

- The error is proportional to the scattering coefficient

This is due to the scattering nature of the VSF, which determines the likelihood of a photon being scattered in a particular direction (Piskozub & McKee 2011). As the attenuation is measured using the photons which are not scattered or absorbed (Piskozub et al. 2004) the nature of the VSF is of high importance in the definition of the amount of near-forward, forward scattering and multiple scattering which can introduce errors into the sample where the scattered photons are then detected by the sensor (Piskozub & McKee 2011; Voss & Austin 1993).
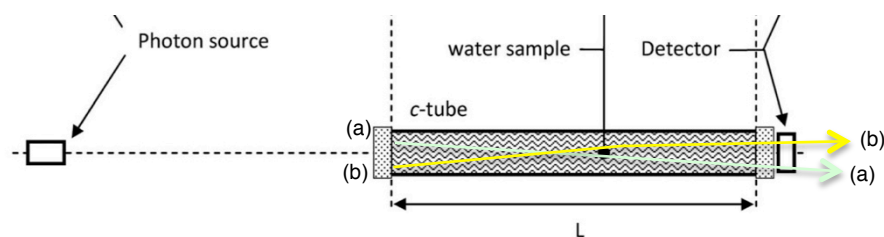
Figure 2.2 – Diagram showing the effect of near-forward (a) and multiple scattering (b) (Leymarie, Doxaran & Babin 2010)

These effects are shown in an exaggerated state in figure 2.2 with the overlay where (a) represents the near-forward scattering event that causes detection at an angle that is accepted as non-scattered (Voss & Austin 1993), while (b) provides an example of the multiple scattering which can result in detection of the photon as non-scattered (Piskozub & McKee 2011). As this results in an increase in measured photons a correction such as that shown in equation 2.15 must be applied to the measurements to ensure that the correct value is obtained.

$$c = c_m + k_c b_t \hspace{4cm} (2.15)$$

For the measurement of the absorption there are also design flaws within the instrument that lead to errors. A number of studies have been performed on the errors caused by the scattering within this tube and have identified a number of relationships between IOP data and the error (Kirk 1992; Leymarie, Doxaran & Babin 2010; Zaneveld, Kitchen & Moore 1994). This can be summarised as follows:

- The error is proportional to the backscatter ratio
- The error is proportional to the scattering coefficient
- The error is proportional to the absorption of the medium

These relationships affect the behaviour of the photons when they interact with the sample during a test with the ac-9 unit and causes scattering error to be included in the measured absorption value (Leymarie, Doxaran & Babin 2010). The backscattering of photons can result in a portion of the photons being 'lost' as they travel out the input point of the ac-9 and do not get detected and is an

error that is compounded by the errors that occur from the reflective surface of the tube (Leymarie, Doxaran & Babin 2010). The reflective material on the tube is generally a quartz interface and this surface will reflect a large amount of photons into the water sample upon contact (Leymarie, Doxaran & Babin 2010). It has been found that as the quartz ages it is more likely to transmit the photons through the interface and emit them out of the tube where they are again 'lost' (McKee et al. 2013). It has also been noted that the quartz interface has a critical angle of 41.7° where the photons will be trapped in the interface and result in total internal reflection (Leymarie, Doxaran & Babin 2010; McKee et al. 2013).
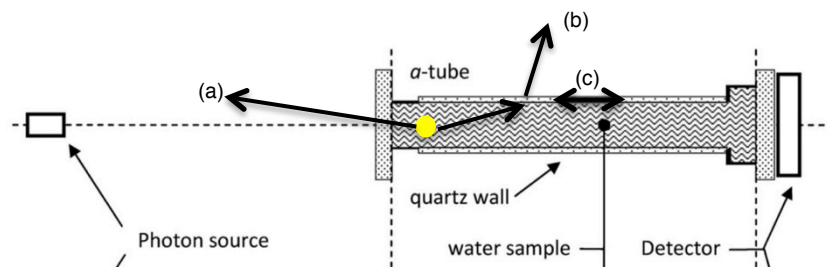
Figure 2.3 – Diagram showing backscatter (a) escaped photons (b) and total internal reflection (c) (Leymarie, Doxaran & Babin 2010)

As shown by the overlay in figure 2.3 all of these scattered photons thus fail to reach the detector in the ac-9 and are therefore recorded by the instrument as having been absorbed by the medium (Leymarie, Doxaran & Babin 2010). This results in a higher calculation of the coefficient of absorption for the water sample and requires a correction be applied for the correct value of the absorption. An example of this correction is shown in equation 2.16 and is part

of the proportional mathod of correction as discussed in Leymarie, Doxaran and Babin (2010).

$$a = a_m + k_a b_t \qquad\qquad (2.16)$$

Due to the errors that arise from the construction and nature of the ac-9 it is important that there are correction methods in place to account for these errors. The ac-9 protocol and user manuals (WET Labs Inc. 2006; WETLabs Inc. 2005) account and note these requirements and provide established correction methods for the errors. It also notes that measurements are generally not taken at a standard temperature and salinity level and provides data on the correction for these methods as well. These methods are well noted by a number of studies and the corrections account for the molecular changes which occur within the water sample and how they are different from the standard pure water calibration set (Pegau, Gray & Zaneveld 1997).

2.5 Established Correction Methods

There are a number of established and accepted correction methods that are adopted when correcting *in-situ* measurements collected using a reflecting type absorption meter such as the WETLabs ac-9. These have been extensively investigated to ascertain the error values that are associated with the correction methods and to improve the methods if possible. The methods are summarised and analysed below.

2.5.1 The 'Flat' correction method

The simplest of the established correction methods is the 'flat' method. This method corrects for scattering errors by subtracting the scattering value for a reference wavelength where the absorption is assumed to be zero (McKee et al. 2013; WETLabs Inc. 2005). The ac-9 protocol document (WETLabs Inc. 2005) notes that this correction also makes an assumption regarding the volume scattering function and its wavelength independence.

It is noted by numerous authors that the reference wavelength that is used is always in the near-Infrared (NIR), and is generally at wavelengths >700nm (Röttgers, McKee & Woźniak 2013; Stramski & Piskozub 2003) as this portion of the spectrum has lower absorption levels of absorption due to water constituents and that the detected levels of absorption are due to scattering error (Stramski & Piskozub 2003).

The 'flat' method uses this data about the scattering errors in the NIR as the basis for its correction method. It takes the absorption data obtained from the absorption tube of a reflecting type absorption meter (WETLabs ac-9) and assumes that the error in the reference wavelength is the same error across all the measured wavelengths. From this point a simple subtraction of the error from the measured value provides a corrected absorption coefficient for the sample (WETLabs Inc. 2005). While this method provides a sample correction it should be noted that it does not allow for any scattering variances due to changing particle sizes in the sample which can lead to errors in the corrected values (WETLabs Inc. 2005).

Given that the 'flat' correction method is a simple correction that aims to 'shift' the results so that the absorption is zero for the NIR wavelength and fails to account for other variables the method is less accurate and has more errors in the final results than more complex measurement correction methods like those of Zaneveld or Kirk (Kirk 1992; Zaneveld, Kitchen & Moore 1994)

Recent work has noted however that there is absorption that occurs in the NIR spectrum (McKee et al. 2013; Röttgers, McKee & Woźniak 2013). This is especially noted by McKee et al. (2013) where the correction that is used results in the measurement of absorption signals at 715nm after correction of the data for scattering errors. The use of a point source integrating cavity absorption meter (PSICAM) instrument to test absorption values in water samples with the results showing non-negligible values for absorption, which creates errors for the fundamental assumption of the 'flat' correction method.

A PSICAM is used in the determination of IOPs due to the nature of its construction. The sample of water is placed in a cavity within the instrument. The cavity walls are highly reflective and when the sample is illuminated the reflective interior ensures that even illumination of the sample. This makes the measurements insensitive to scattering error (Leathers, Downes & Davis 2000). The absorption losses are measured as the difference in the power input and the measured losses on the cavity walls. This makes it a better determinant of absorption losses within a sample.

2.5.2 Zanevelds Proportional correction method

To combat the errors which are inherent in the use of the fixed method Zaneveld, Kitchen and Moore (1994) performed a study on reflecting type absorption meters like the ac-9. This method looks at the proportion of the scattering error as a function of the scattering. It again uses the assumption that there is no absorption at a reference wavelength in the NIR (Leymarie, Doxaran & Babin 2010) which can be used along with the proportion of scattering to correct the absorption values for the entire measured spectrum (Zaneveld, Kitchen & Moore 1994). It is noted that the fraction of scattered light not received is assumed to be independent of the wavelength being measured (Zaneveld, Kitchen & Moore 1994). This is an assumption that is carried through all methods.

Given that the proportional correction method uses the assumption of the 'flat' correction method of zero absorption in the NIR (WETLabs Inc. 2005; Zaneveld, Kitchen & Moore 1994) combined with the assumption of a proportional error of scattering means that the correction scheme is robust unless the assumptions become incorrect (Leymarie, Doxaran & Babin 2010) where the errors become dramatic. Given that the assumption of zero absorption is the easier of the assumptions to test, the effect of a failure can only be measured in terms of this assumption.

By assuming a fixed proportion of the scattering is an error, the proportion method allows for the creation of a slope that can be extrapolated from the reference wavelength to correct for all wavelengths required in terms of percentage error (Zaneveld, Kitchen & Moore 1994). This slope is highly

variable and depends on the proportion of the scattering that is considered as the error. Equation 2.17 shows this correction method where a_t is the true absorption, a_m is the measured absorption and b_m is the measured scattering coefficient.

$$a_t(\lambda) = a_m(\lambda) - a_m(\lambda_r)\frac{b_m(\lambda)}{b_m(\lambda_r)} \qquad (2.17)$$

While the proportional correction method is more robust than the 'flat' correction it again is subject to the performance of the absorption at a reference wavelength (McKee et al. 2013; Röttgers, McKee & Woźniak 2013) that affects the accuracy of the corrected values. As the wavelength independence is also a fundamental aspect of the correction this has been tested by McKee et al. (2013) and has been found to be in doubt for differing water conditions with significant dependence found in studies of coastal waters (McKee et al. 2013). By noting that there is an error in the base assumption of zero absorption in the NIR Röttgers, McKee and Woźniak (2013) found that this method tends to underestimate absorption at shorter wavelengths with the error becoming significant when evaluated at longer wavelengths.

2.5.3 Kirks Fixed Contribution method

In order to facilitate the definition of the errors in the scattering, the fixed contribution method assumes that the contribution of the scattering error can be corrected from a known value calculated using an established formula that corrects measured absorption (Kirk 1992). The method uses three main assumptions, that the absorption in the reference wavelength in the NIR is

fixed, that the scattering error is proportional to the scattering and that the scattering error can be calculated using a function of the measured absorption (Kirk 1992).

The methods correction function is subject to changes in the VSF and the acceptance angle of the detector in the instrument (Kirk 1992). As such these parameters must be accurately known in order to perform a high accuracy correction on the data with the calculated correction factors. As the increase in scattering errors through the wavelengths is a linear increase (Kirk 1992) the effect of incorrect parameters can be significant if the error in the parameters is significant but can be small if the error is small.

By assuming that a linear function can be used to approximate the errors this method falls into the same pitfall as the proportional method of Zaneveld. It fails to account for variations that may cause the scattering error to change from a linear increase which is also a shortfall of the 'flat' method (WETLabs Inc. 2005). As such, this introduces errors into the corrected data if the water sample constituents create such variations. This can be combined with the evaluation of the absorption and other assumptions in recent studies (McKee et al. 2013; Röttgers, McKee & Woźniak 2013) which creates doubt as to the accuracy of the correction systems due to the assumptions. As accurate knowledge of the absorption in the NIR is required as per the 'flat' and proportional correction methods (WETLabs Inc. 2005; Zaneveld, Kitchen & Moore 1994), the errors in these systems are again possible error sources in this method.

2.6   Current Work

As the correction methods for water attenuation measurements are still an emerging field, there are a number of newer correction methods that are being investigated and improved with the aim to reduce the errors that are a part of the current standard correction methods. The major methods which are 'in progress' are the Monte Carlo correction method (McKee, Piskozub & Brown 2008; McKee et al. 2013) and the 'Absorption' correction formula (Röttgers, McKee & Woźniak 2013).

2.6.1   McKee's Monte Carlo correction

The Monte Carlo correction method is one correction method which is currently in development and testing and uses the Monte Carlo method for simulations to examine and correct for scattering values in an ac-9 (McKee, Piskozub & Brown 2008). The foundation of the method is to reduce the errors that arise through the use of established correction methods like the 'flat' or 'proportional' correction method and the assumptions inherent is those methods (McKee, Piskozub & Brown 2008).

The study that led to the creation of the method made use of *in-situ* measurements for absorption and attenuation using an ac-9 unit and backscattering data using a BB-9 (McKee, Piskozub & Brown 2008). The BB-9 data was used with the ac-9 measurements to obtain a set of parameters that could be used as a basis for the simulation. The method uses a number of processes to create a scattering correction method.
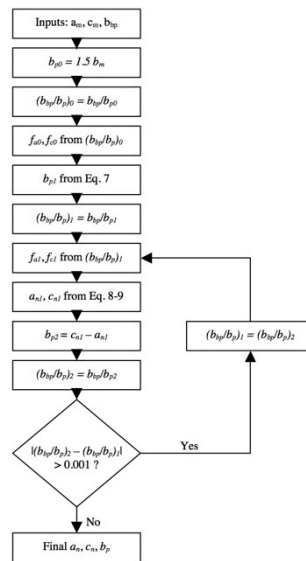
Figure 2.4 - McKee's Monte Carlo Correction Method (McKee, Piskozub & Brown 2008)

The first of these is a weighting function which is used to correct for uncollected photons based on the scattering angle (McKee, Piskozub & Brown 2008). This function allows for the photons that are 'lost' to be modelled for the simulation value and account for this error. This is only a viable correction method when it is combined with the phase function of the water body and provides fractions of scattered light not collected by the sensor (McKee, Piskozub & Brown 2008). It is noted by McKee, Piskozub and Brown (2008) however that the method requires the value of the scattering ratio (b_{bp}/b_p) to be either known or estimated. This creates a circular logic problem due to the requirement for the determination of the particle scattering which is an unknown value (McKee, Piskozub & Brown 2008). The first iteration of this method accounts for this error by forming an iterative correction method which is shown in figure 2.4 which uses an estimate of the scattering ratio to obtain

an initial value for absorption and attenuation and from there a new estimate of the scattering ratio (McKee, Piskozub & Brown 2008). This is then substituted back into the process until the change between the previous and new estimate is below the tolerance.

While this method does not suffer from a large number of assumptions it does suffer from the requirement for an estimation of the scattering ratio and the time that is taken to correct if the estimation is not close to the 'true' value.

While this is true, McKee et al. (2013) noted that this was not an optimal situation and moved to remedy the issue. In order to do so they performed tests using a PSICAM unit that was used to provide estimates of the absorption values instead of the ac-9 unit. This allows for more accurate estimation of the absorption values with the study finding that the original method provided values that overestimated the PSICAM results at the same wavelength (McKee et al. 2013). Other errors which occurred prompted an investigation into the effects of aging equipment and it was found that over time the reflectivity of the absorption tube decreases and needs to be accounted for as the tube allows for greater escape of photons as it loses its reflectivity (McKee et al. 2013). This introduces another variable that must be accounted for in the iterative scheme. By incorporating the age of the instrument into the method along with the correction data provided by PSICAM results McKee et al. (2013) managed to create a correction scheme that provided absorption values that closely matched the data obtained from the PSICAM unit. It also has the benefit of providing more accurate data in the NIR spectrum where the PSICAM data shows that there is non-negligible

absorption that is not accounted for in the established methods (McKee et al. 2013; Röttgers, McKee & Woźniak 2013).

The major shortcoming of this method is in the amount of data required to successfully utilise it. It requires *in-situ* measurements from not only an ac-9 unit but also a PSICAM and BB-9 or other scattering sensor (McKee et al. 2013) which takes extra time, money and means that the method cannot be used to correct historical data where PSICAM and BB-9 information is not available. This is explicitly stated by McKee et al. (2013) as an area which requires further work in order to allow for re-assessment of historic datasets in light of the knowledge of the doubt over negligible absorption in the NIR.

2.6.2 Röttgers Absorption correction

The most recent study of correction methods is that of Röttgers, McKee and Woźniak (2013) which looks at the assumptions taken by the established methods and tests the validity of these assumptions. The study makes use of measurements taken with both ac-9 and PSICAM units. In order to test the methods that have been established as accepted practice the use of a PSICAM was a requirement as it can provide absorption values that are closer to the 'true' value of the water sample than the ac-9 as the scattering error is negligible for particulate absorption (Röttgers, McKee & Woźniak 2013).

As the reference wavelength is assumed to have no particulate absorption and any ac-9 absorption measurements show that there is a measured absorption value it has been assumed that this is due to scattering error (Röttgers, McKee

& Woźniak 2013; WETLabs Inc. 2005; Zaneveld, Kitchen & Moore 1994). In particular for the ac-9 this has been the 715nm wavelength as it above 700nm (Röttgers, McKee & Woźniak 2013) where the absorption is assumed to be zero. This lead the study to concentrate only on this wavelength to evaluate the validity of the assumption that provides a major foundation for the established methods. The *in-situ* tests performed concurrently between the ac-9 and PSICAM units showed that there was a major source of difference between the assumption of zero absorption and the values that were detected from the PSICAM unit. Given that the reference wavelength has an error this error then propagates across the other wavelengths when the correction is applied.

By taking this absorption data for 715nm a number of tests where then performed on the ac-9 data using the established correction methods, in particular the 'flat' and proportional were investigated (Röttgers, McKee & Woźniak 2013) as they are more readily adopted. The tests showed that by adopting the 'true' value for the reference wavelength and then adopting the correction methods resulted in overestimation of true absorption levels for both correction methods.

In order to allow for the differences between the measured and 'true' absorption when using an ac-9 Röttgers, McKee and Woźniak (2013) analysed the values that were output for a set of samples from the ac-9 for the measured absorption in relation to the 'true' value. Using this analysis for the 715nm spectrum they established that the relationship was as per equation 2.18 for the correction of the measured absorption.

$$a_{715} = 0.212 \times a_{m715}^{1.135} \qquad \text{(Röttgers, McKee \& Woźniak 2013)} \qquad (2.18)$$

This formula has a high correlation with the data that was obtained using the PSICAM unit however the universal validity of the system is yet to be determined. As the formula was created using only a single set of collected field data there is no determination or validation of the formula for waters outside of the River Elbe, Baltic/German Bight, North Sea areas where field data was obtained (Röttgers, McKee & Woźniak 2013). As such this method is still in an exploratory phase and requires validation across a number of samples before it is fit for universal use.

2.7   Summary

This section has covered a large amount of information regarding the Inherent Optical Properties of water and how they relate to remote sensing and water. It has described the nature of Absorption, Scattering and all of its associated elements, the Volume Scattering Function and Attenuation.

The purpose of the AC-9 instrument was explained, with the construction of the instrument being detailed. Both the attenuation and absorption tubes functions were detailed with respect to the path travelled and interaction of photons within the sample being tested. The errors that occur as part of this process were also investigated and detailed.

It has also described how the properties of a water body play a role in determining the IOPs through the different particulate concentrations. The usage of IOPs in remote sensing was established and showed the complex

relationship that exists between IOPs and reflectance values that are sensed remotely.

Finally this section has covered the numerous correction methods that currently exist. It first looked at the three correction methods that are well established and currently used with AC-9 measurements alone. It also noted the assumptions that are used in the creation of the correction methods and how these assumptions impact on measurements corrected with these methods.

The methods that are currently being researched and are in development were also covered. McKee's iterative correction scheme showed that errors were systematically a part of the current correction methods and provided a method to account for this error by using converging estimates of the backscattering ratio to correct for the scattering coefficient. Further research into this method showed that extra data was required to increase a number of shortcomings and a revised method was proposed. The other current method that was covered was Röttgers absorption correction that exclusively looked at the error in the wavelength of 715nm and created a scheme to correct for that error.

Chapter 3

Methodology

3.1   Introduction

This section details the methods that were used to collect the data for the analysis. An outline of the resources used is provided and is followed by a larger and more detailed coverage of the processes used to generate and process the experimental data.

3.2   Resource Analysis

The number of resources used in the creation and processing of the data was limited due to the nature of the data that is to be generated.

The simulation environment that generates the experimental data is set inside the simulation program SimulO. A more detailed description of SimulO can be found in section 3.3.1.1.

The output data from SimulO requires processing to a usable form. To perform this analysis Exelis's IDL software was used as it allowed flexibility in the capture and usage of SimulO output files. Microsoft Excel was also utilised for data analysis. These programs were chosen due to the ability of IDL to allow for comprehensive data gathering while Excel was chosen for its data analysis and user-friendly interface.

3.3 Testing Method

3.3.1 Data Generation

3.3.1.1   SimulO

The SimulO simulation environment is based off the Monte Carlo random number method (Leymarie, Doxaran & Babin 2010). It uses this method to decide on the fate of the photons throughout the simulations that are run by the user in three dimensions, as the path taken by the photons is not a simple 2-dimensional problem. The program allows for the modelling of any known optical instrument through the creation and spawning of any number of virtual objects that can be connected to create an instrument (Leymarie, Doxaran & Babin 2010). It contains three main shapes for the objects at this current stage, cylinders, cubes and spheres. These can be manipulated to different sizes and have a number of properties that can be manipulated by the user to create the testing environment. These properties are the refractive index, the absorption, scattering, and phase function of the 'bulk' (interior volume) and absorption values can be set for the exterior and interior surfaces (Leymarie 2005; Leymarie, Doxaran & Babin 2010). In the process of joining these objects elements can to be set to not be 'seen' by the photons to allow for unimpeded access where the properties of the interior or exterior are not required to affect the photons path or state.

3.3.1.2 Monte Carlo Random Number Analysis

Monte Carlo analysis works off the assumption that if enough results are randomly generated then the overall average values obtained from the simulation will approximate the 'real' value (Niederreiter 1978). This guiding principle is the foundation of the Monte Carlo method and allows for its use in SimulO. Due to the numerical nature of computers, truly random numbers are not possible and instead quasi-random numbers are instead used (Niederreiter 1978). The term quasi-random is used as the 'random' numbers are generated based off a starting value or 'seed'. Due to this the numbers are generated by a system which an generate an endless string of random numbers (Niederreiter 1978).

3.3.1.3 AC-9 Modelling in SimulO

The WETLabs AC-9 was modelled as per the setup provided with the SimulO program. This setup merged a number of cylinders with varying properties in two separate environments to create the absorption and attenuation tubes. Each tube has a main cylinder that represents the water sample and its bulk is the element which allows for the particulate scattering, absorption, VSF and wavelength parameters to be defined for the water sample. Both tubes also feature cylinders at either end, which take the properties of the emission point and the detector. The emitter is placed a distance away from the tube to allow for some travel by the photon before interaction with the tube body. Both tubes also feature quartz windows at the start and end of the water samples that are modelled with cylinders of differing sizes dependant on the tube. From this
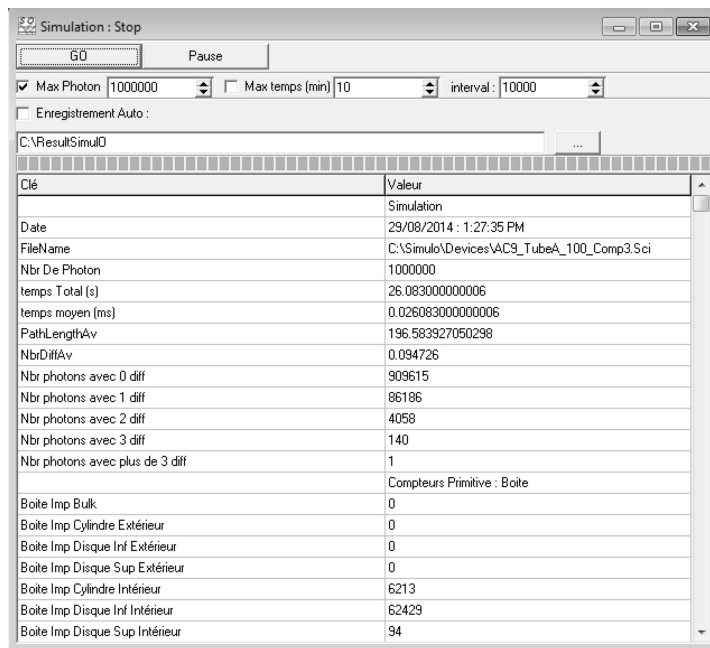
point on the design of the two tubes differs both in the simulation environment and in the real world as shown in figures 2.2 and 2.3.

The absorption tube has the larger of the quartz windows. These are designed to increase the acceptance angle of the detector at the detector end of the tube. The other addition that is found in the absorption tube is fully absorbent walls that are placed between the quartz windows and the tube of water. The ac-9 also features a quartz wall that is used to contain the photons within the water sample. With the nature of the properties within SimulO for the objects, modelling this tube is not viable as placing the tube around the water sample ends with all impacting photons being internally reflected which is not what happens in the field. The method used to simulate this tube involves the complex interaction of particles and substances with differing refractive index. The index change between the 'bulk' of the water body and the 'bulk' of the remainder of the simulation environment is enough that upon impacting on the tube edge the photon behaves as if it has impacted upon the quartz tubing, with some photons passing through and escaping.

The attenuation tube is simpler to model, as it does not require the small, fully absorptive walls inside the first quartz window. Instead the interior of the water body cylinder is set to be fully absorbent so that any impact is fully absorbed. This model reflects the setup used by Leymarie, Doxaran and Babin (2010) in a similar set of optical tests.

3.3.1.4   Scripting Simulations

In SimulO simulations are run individually, through the user interface in a simulation window. This window provides a visual interface that shows the variables and data that SimulO records and can output in individual log files as shown in Figure 3.1.

Figure 3.1 - SimulO simulation window

To allow for large amounts of simulation to be run in a single session without requiring user input for each individual simulation SimulO provides a scripting language that can be used to set up large-scale simulations. These large-scale simulations require a single command from the user to begin the simulation session with the scripted requirements then handling the remainder of the session's requirements. In order to set up a simulation session the user requires three main elements. These are:

- Simulation environment

- Simulation input file

- Simulation script file

The simulation environment chosen for ac-9 measurements are the absorption or attenuation tubes as set out in section 3.2.2.3. An incorrect selection here can create results that do not reflect the aim of the simulation session. The input file is set by the user to contain those parameters that they wish to run through the test with a final set of parameters that allows any script to note that it has found the last of the simulation parameters. Each parameter is tab-delineated from the previous in each row with headers at the top of each column allowing for easy visual checks that the parameters will be read to the correct variable by the script.

The script file forms the backbone of the session and is the tool that the user uses to set the session to run without consistent input from the user. It searches for the specified input file and sets up an output file where results for each simulation will be written. These files require full location and filename information. From the input file each row of parameters is taken and passed to variables. These variables are then passed in the water body wizard to establish the nature of the water body. From this point all of the information is passed to the simulation where the photons are simulated. Output variables and properties are defined and the results written to the output file as tab-delineated text. Each simulation was run five times to ensure an adequate number of photons is simulated.

3.3.2 Simulation Input

As Röttgers, McKee and Woźniak (2013) have established a relationship between the 'true' absorption and the measured absorption at 715nm, it is of note that the relationship has been established with a small dataset. As such, it is important that this relationship be examined across a range of water types to establish if the relationship is valid universally or only for the waters that were examined in the study. As a number of tests will be required to test the validity a number of simulations will be conducted to provide data for a range of local water properties. All of these simulations will be carried out at a single wavelength in the near-infrared spectrum (715nm).

The choice of wavelength is important, as it must address the correct spectrum to be able to examine the possible universal nature of the function. 715nm is chosen in particular, as it is the upper limit of the wavelengths that can be used with the ac-9 (WETLabs Inc. 2004, 2005). It also is a wavelength that falls into the near-infrared portion of the electromagnetic spectrum, which has been held as being the source for the zero absorption assumption, used in previous correction methods (Kirk 1992; WETLabs Inc. 2005; Zaneveld, Kitchen & Moore 1994). As this assumption is a possible source of error due to non-zero absorption (Röttgers, McKee & Woźniak 2013) and this wavelength is taken as the reference wavelength where absorption is equal to zero, this is the wavelength that will be tested in the simulations to obtain a correction at 715nm for absorption.

There are four variables that were analysed in the course of the simulations. In each individual simulation set only two of these were varied with the others

held at a constant value. The later simulations used optimal values obtained from previous simulations while the first simulations utilised values that were found to be fairly consistent for inland waters.

The variables that will be evaluated are as follows: the backscatter ratio, backscatter coefficient and the VSF. Each of these will be tested across two sets of simulations while the VSF will only be evaluated if time is able to permit it. All simulation runs will use a minimum of one million photons to ensure that errors in the simulation process are minimised.

3.3.2.1   Constant Values

Due to the complex nature of the simulations there are variables that must be held in a constant state.

The first variable held constant is that of the VSF. The VSF was held as a Fournier-Forand scattering function (Fournier & Forand 1994). The VSF was held as constant throughout the simulation sets to ensure continuity in the scattering directions for the samples.

Across the simulations different variables are held constant. The first simulation set held the backscattering ratio as a constant value. This held the proportion of backscatter constant so that the change in the coefficient can be observed. The second simulation looks at data pairs obtained from the results of the first simulation set while the backscattering ratio was varied.

3.3.2.2   Simulation Set 1

The first simulation set evaluates the effect that varying the scattering coefficient has on the ac-9 calculated values, both absorption and attenuation. The data that was input to SimulO is detailed in Table 3.1.

Table 3.1 - SimulO parameter settings for the simulations examining the effect of absorption and scattering

Parameter	Value
Absorption (m^{-1})	0.01, 0.05, 0.1, 0.15, 0.2, 0.3, 0.4, 0.6, 0.8, 1, 1.2, 1.4, 1.6, 1.8, 2, 2.5, 3, 4
Scattering (m^{-1})	0, 0.1, 0.25, 0.5, 0.75, 1, 1.25, 1.5, 2, 2.5, 3, 3.5, 4, 5, 7, 9, 11, 15
Backscattering ratio	0.015
VSF	Fournier-Forand

3.3.2.3   Simulation Set 2

The second simulation set evaluates varying the backscatter ratio and the effect that this change has on the calculation of the absorption and attenuation coefficients by the ac-9. The backscatter ratio values are shown in Table 3.2.

Table 3.2 - SimulO parameter settings for the simulations examining the effect of absorption and $\frac{b_b}{b}$

Parameter	Value
Absorption (m^{-1})	Determined from results of Section 3.3.2.2 (Appendix E)
Scattering (m^{-1})	Determined from results of Section 3.3.2.2 (Appendix E)
Backscattering ratio	0.005, 0.01, 0.015, 0.02, 0.025, 0.03, 0.035, 0.04, 0.045, 0.05, 0.055, 0.06, 0.065, 0.07, 0.075, 0.08, 0.085, 0.09, 0.095, 0.01
VSF	Fournier-Forand

3.3.3 Simulation Outputs

3.3.3.1   SimulO Output

SimulO output is composed of a two-fold system when scripting large-scale simulations for analysis. For small-scale simulations it can be considered a three-fold system however the smaller number of photons leads too less statistically robust results.

The first output system is touched on in section 3.3.1.4 and is an output file that is generated by the script set by the user. This file only contains the data that the user wishes to save from each individual simulation and does so in an easy to analyse format that allows for analysis through a spreadsheet program. It also allows the user to easily refine the output to the point where only the pertinent information is saved and all other data is discarded. The data that is recorded in this file by default is:

- Number of photons emitted

- Average path length

- Number of un-scattered photons

- Number of single scattered photons

- Number of photons scattered twice

- Number of photons scattered three times

- Number of photons scattered more than three times

- The fate of all photons

- Properties of the water body used for the simulation (a, b, $\frac{b_b}{b}$, VSF)

The second method for saving the data points is the saving of the individual simulations log files. These log files contain data on the entirety of the simulation which can be seen from the simulation window as shown in figure 3.1. The use of these files allows for the saving of all data pertaining to the simulations, allowing the user to choose after the simulations have been completed what data they wish to collect or discard. As each simulation creates an individual log file, large-scale simulation sessions can generate a large number of log files that must be tracked and kept in the same location to ensure that analysis includes all aspects of the session.

The use of these log files also allows for sessions to run across multiple computers and then combined for a single analysis session. This is also possible with the single output file generated by the SimulO script, however this requires file manipulation, which is subject to transfer errors. By saving each individual log file a data dump into a single folder can leave the user with the entirety of the data. A quick check of filenames and the number of files in the folder enables the user to quickly check that all the simulations have been covered in the saved data. There is a number of elements of a log file which can be used in calculations with impacts on the various faces of the simulation environment being the most important as it allows for estimation of the percentage of photons which are 'lost' in the measurement process.

The third element of the output that can be used is for empirical measurement only. It is the tracing system that SimulO offers. This system traces the path that each individual photon travels as it passes from the emitter to its final destination. Figure 3.2 shows an example of this tracing system.
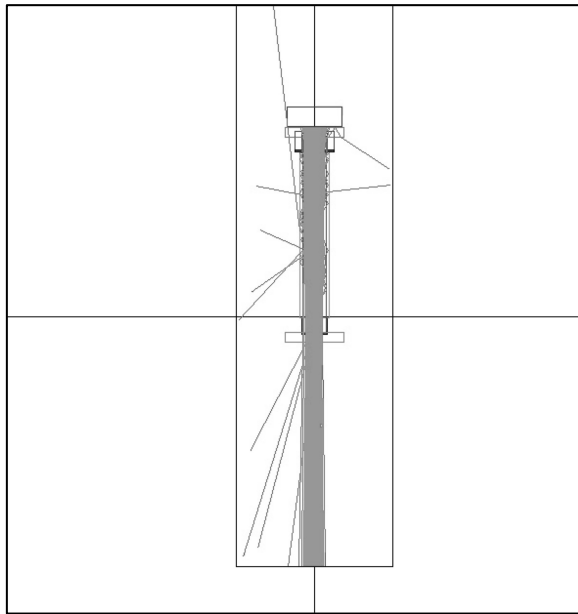
Figure 3.2 – SimulO output with Photon Tracing enabled

This pictographic information allows the user to quickly gauge the percentage of photons that have escaped the environment. Figure 3.2 shows approximately one per cent of the photons escaped the ac-9 tube environment in some manner. This type of analysis is useful for single run simulations where the picture can be saved for later reference.

3.3.3.2   Data Processing

As there are two methods of output of the SimulO results from the simulation sessions, a number of options are available to be used to reduce the simulation data. The two that have been chosen to reduce the data are:

- Reduction of Script Output in Microsoft Excel

- Reduction of SimulO log files in Interactive Data Language (IDL)

By setting the script to record output data and ensuring that the logs have been saved to an appropriate file, both methods can be used to perform checks on both methods of reduction to ensure that consistency. This is important as the simulation data was systematically created across multiple machines and will account for any data entry errors when merging the data.

The reduction of the script output files in Excel first involved the reduction of the data from five records per input set to a single input per record set. By creating an average and standard deviation of the data the variation between the values can be analysed to check the similarity of the results. As the data required has been extracted by the SimulO script there is no requirement to extract data from the file, it can simply be read straight from the file.

From this point the data is called into a second sheet where it is formatted to allow the user to view all the results in one glance. The pure water value for the tube is also attached to this sheet for use in the reductions and as a reference for the IDL reductions.

The log file reduction requires the files to be first loaded into IDL. As the log files contain all the information from each individual simulation, the data that is required must first be extracted. Figure 3.3 provides an example of the extraction code.

```
if temp(0) eq 'Nbr De Photon' then Photons(i) = temp(1)
readf,40,line
readf,40,line
readf,40,line
temp =strsplit(line,'=',/extract,/preserve_null)
if temp(0) eq 'PathLengthAv' then Av_Path_length(i) = temp(1)
readf,40,line
readf,40,line
temp =strsplit(line,'=',/extract,/preserve_null)
if temp(0) eq 'Nbr photons avec 0 diff' then No_scat(i) = temp(1)
readf,40,line
temp =strsplit(line,'=',/extract,/preserve_null)
if temp(0) eq 'Nbr photons avec 1 diff' then One_scat(i) = temp(1)
readf,40,line
temp =strsplit(line,'=',/extract,/preserve_null)
if temp(0) eq 'Nbr photons avec 2 diff' then Two_scat(i) = temp(1)
readf,40,line
```

Figure 3.3 – Example Code to extract data from SimulO Log Files

The data that is extracted from these files is covered in section 3.2.2.5 and is the same as that defined by the SimulO script file. From this point the code averages the extracted data, ensuring that each set of inputs is correctly averaged. At this point spot checks are made between the Excel and IDL data.

With the data reduced to a usable from, the photon counts are converted to the attenuation and absorption coefficients respectively using equation 3.1:

$$x_m(\lambda) = -\frac{1}{L}\ln\left(\frac{P^x_{a_t,b_t}(\lambda)}{P^x_{0,0}(\lambda)}\right) \qquad \text{(Leymarie, Doxaran \& Babin 2010)} \qquad (3.1)$$

Where x is either a or c, $P^x_{a_t,b_t}(\lambda)$ is the probability of detection for the sample of water, $P^x_{0,0}(\lambda)$ is the probability of detection for the pure water sample and L is the average pathlength of the photons. Equation 3.1 is applied to both Excel and IDL data sets, with the IDL data requiring the probability to be calculated where the Excel data is already averaged by the output script.

With the measured absorption and attenuation coefficients calculated the correction values, Ka and Kc are calculated by rearranging equations 2.15 and 2.16.

3.3.3.3   Final Output

There are a number of relationships that will be tested from the processed data. These will be processed graphically to establish relationships between known or measured data and the errors that are measured in the simulations.

Trend analysis will be undertaken to test the universality of the relationship established by Röttgers, McKee and Woźniak (2013) to correct measured absorption to the true absorption value as shown in equation 2.18.

From this point a number of variables are calculated based off the simulated dataset. The variables focused on are:

- The single scattering albedo $\omega = \left(\frac{b_m}{c_m}\right)$

- The multiple scattering albedo $\omega_{ms} = \left(\frac{b_b}{a_m + b_b}\right)$

- Measured absorption ratio

- Measured attenuation ratio

- Measured scattering ratio

- Difference in measured and true values

- K_a and K_c

- Error factor as calculated by $\frac{a_m - a_t}{a_t}$ or $\frac{c_m - c_t}{c_t}$ (Leymarie, Doxaran & Babin 2010)

3.4 Summary

This chapter has described the nature of the programs that are being used in the generation of the experimental data for the project analysis. The simulation environment has been defined within SimulO along with the input values that are required.

The nature of the outputs has been described for both possible output types and the advantages of each have been detailed. The reduction of the outputs to usable data has been shown and the final part of the section covers the data output that has been used in the final analysis.

Chapter 4

Results

4.1 Introduction

The previous chapter described the generation method of the experimental data for the project along with the output types and values that are to be utilised in the analysis process.

This chapter will look at the analysis that was performed on the experimental data with respect to a number of factors. The data for both the Attenuation tube and the Absorption tube will be analysed to determine relationships that are of use to the project.

4.2 Attenuation Tube

This section focuses exclusively on the data generated within the Attenuation tube of the simulated AC-9. It summarises a number of trends that will be discussed further in Chapter 5.

4.2.1 Relationship between C_m and C

Röttgers, McKee and Woźniak (2013) noted that a relationship between the measured and true absorption could be the foundation of a proposed correction method. However a similar analysis using conventional methods has not been created. By defining the true absorption and scattering properties the true attenuation value of the water sample can be calculated using

equation 2.9. The measured attenuation could then be plotted against the true attenuation to note any relationship.

$c = 1.2675c_m$
$R^2 = 0.9913$
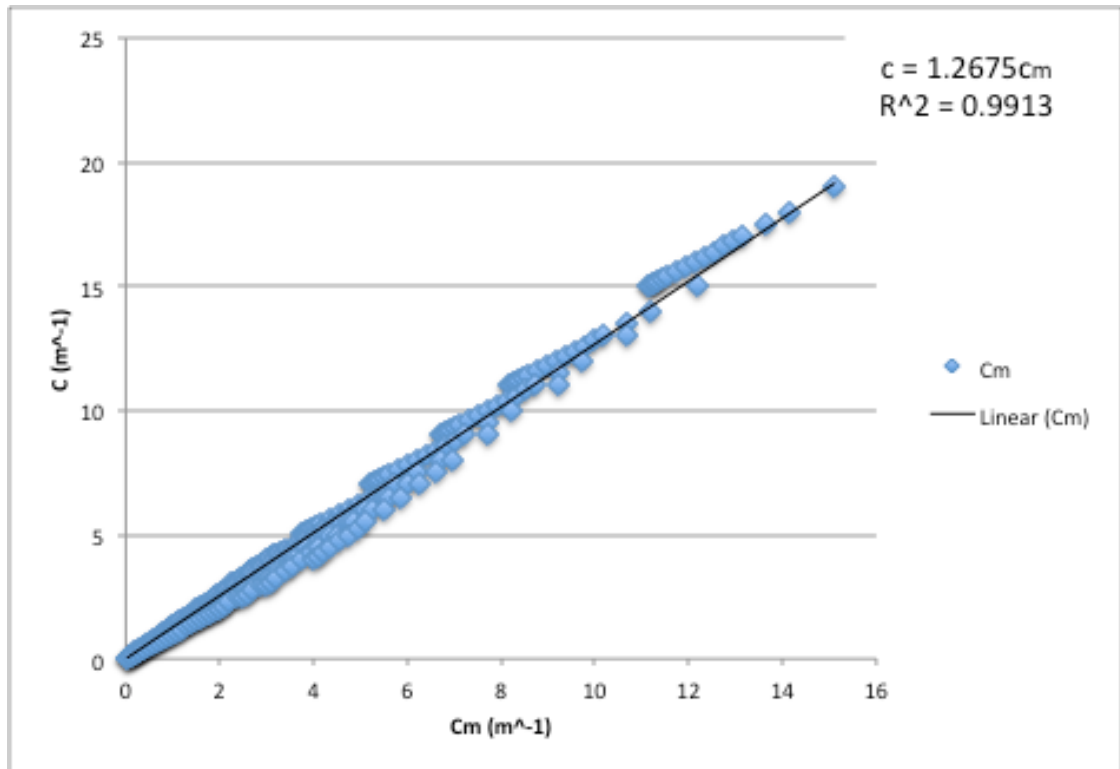
Graph 4.1 –True Attenuation (*c*) as a function of measured attenuation (*c_m*) for a constant backscattering ratio ($\frac{b_b}{b}$).

Graph 4.1 shows how the attenuation measurements changed across the entire simulated data set. It is of note that irrespective of the *a* or *b* value used in the simulations the measured attenuation does not show a large amount of deviation from the fit. The fit indicates through the slope that the attenuation is underestimated through measurement as noted by the literature.
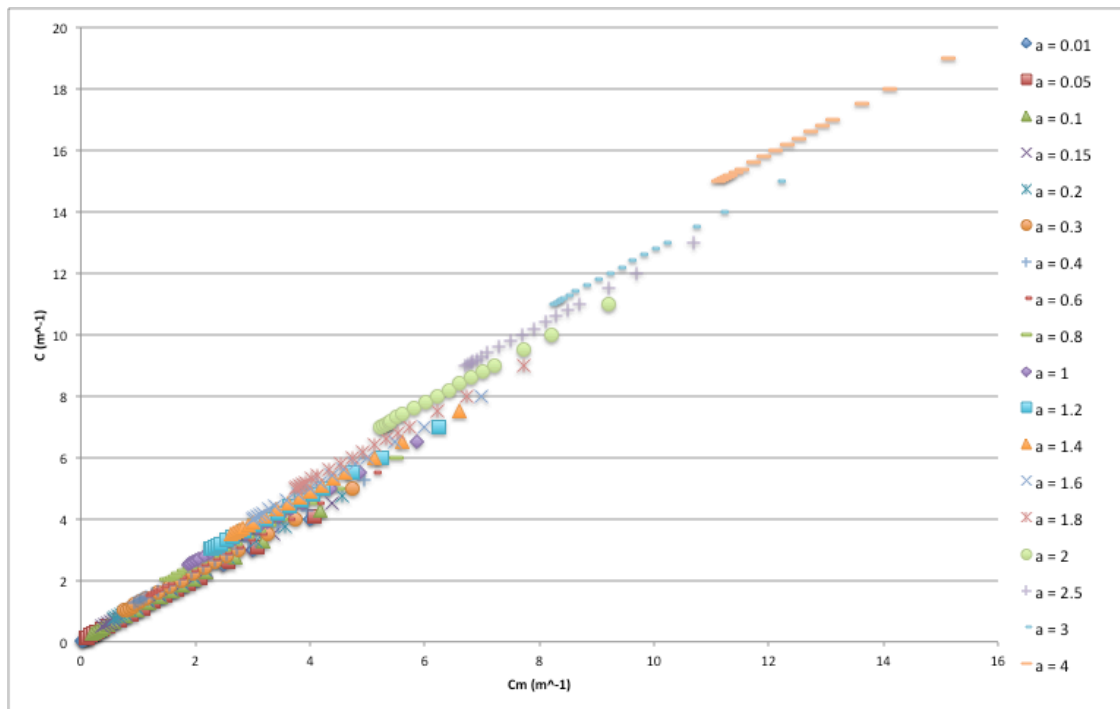
Graph 4.2 – True Attenuation (*c*) as a function of Measured Attenuation (*c~m~*) for constant absorption (*a*)

Trend analysis was also carried out on the relationship between the measured and true attenuation with respect to data series defined by a constant absorption value (Graph 4.2). The analysis provided a graph that provided the same data points but contained interesting data with respect to the y-intercept values for the straight-line fits of each data series. It was noted that as the fixed absorption value increased the y-intercept of the fit also increased, with minimal changes in the slope of the data. Graph 4.3 notes the relationship between the y-intercepts of the linear fits and the absorption coefficients.
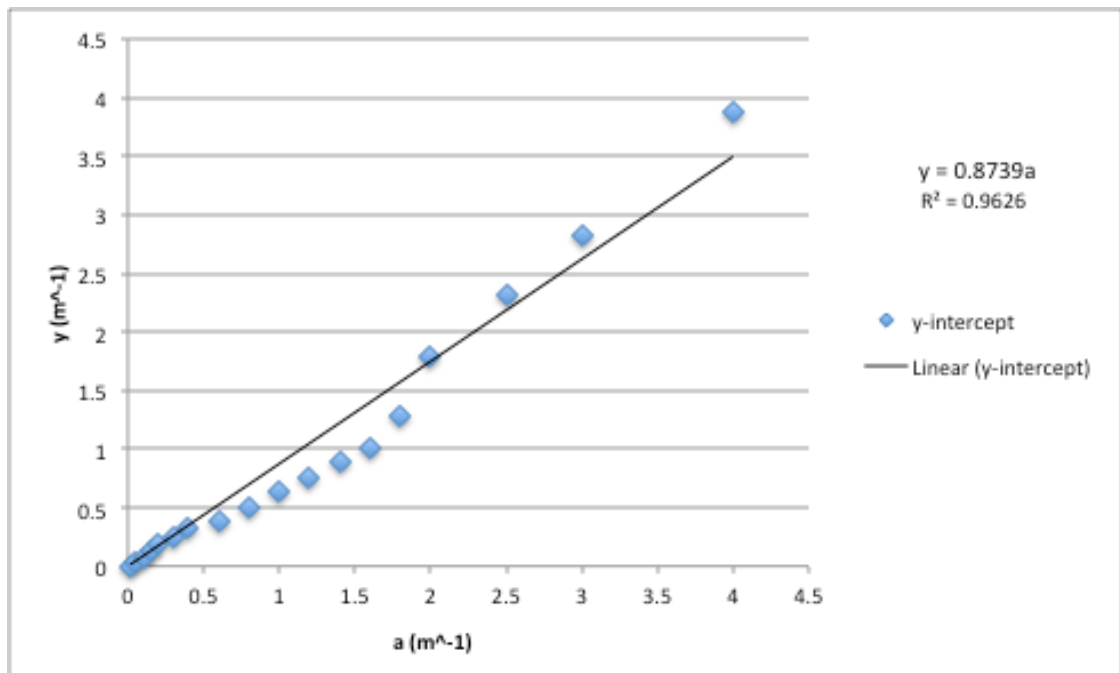
Graph 4.3 – y-intercept values from Graph 4.2 data as a function of absorption

As there is a high correlation between the fit and the y-intercept data it is possible that a correction could be created utilising this data. These graphs show that the effect on a change in the scattering or absorption do not change the overall proportion of the error based on a change in a single variable and appears to be scattering and absorption independent.

Following the analysis for a single $\frac{b_b}{b}$ further analysis was carried out on the data created for varied $\frac{b_b}{b}$ values.
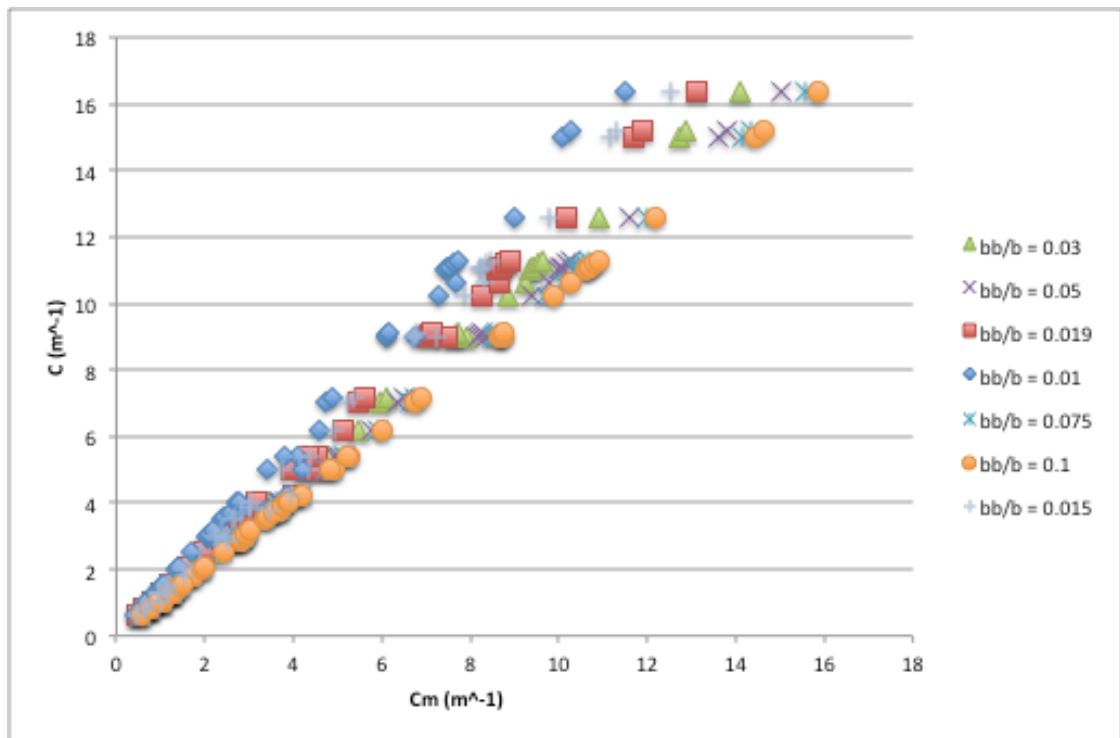
Graph 4.4 – True Attenuation (*c*) as a function of Measured Attenuation (*c_m*)
for varied $\frac{b_b}{b}$

Table 4.1 – Best fit data for Graph 4.4

b_b/b	Slope	y-intercept	R^2
0.01	1.4302	0	0.99227
0.015	1.3114	0	0.99596
0.019	1.254	0	0.99731
0.03	1.1648	0	0.99887
0.05	1.0935	0	0.99963
0.075	1.0551	0	0.99987
0.1	1.0357	0	0.99995

In the case of the changed $\frac{b_b}{b}$ values it was noted that across the entire spectrum of results there is a close correlation to a linear fit and this will be discussed further in Chapter 5. Of interest was that the slope of the best fits across the dataset decreased, indicating that the error in c_m is dependant on the VSF. This can be seen clearly in Graph 4.4 and Table 4.1 where the slope

decreases dramatically across the seven $\frac{b_b}{b}$ values. The relationships that have been noted between the measured and true attenuation values will be discussed further in Chapter 5.

4.2.2 Usage of Error Factor

The usage of the absolute value is one of a number of methods that have been proposed for quantifying the error in *in-situ* measurements. Leymarie, Doxaran and Babin (2010) introduce the concept of a percentage error, however in the case of the data generated for this project the error has been left as an error factor (E_{fc}). The error factor was calculated using the data from Section 3.3.2.3, calculated with Equation 4.1 and is shown in Graph 4.5.

$$E_{fc} = \frac{c_t - c_m}{c_t} \tag{4.1}$$
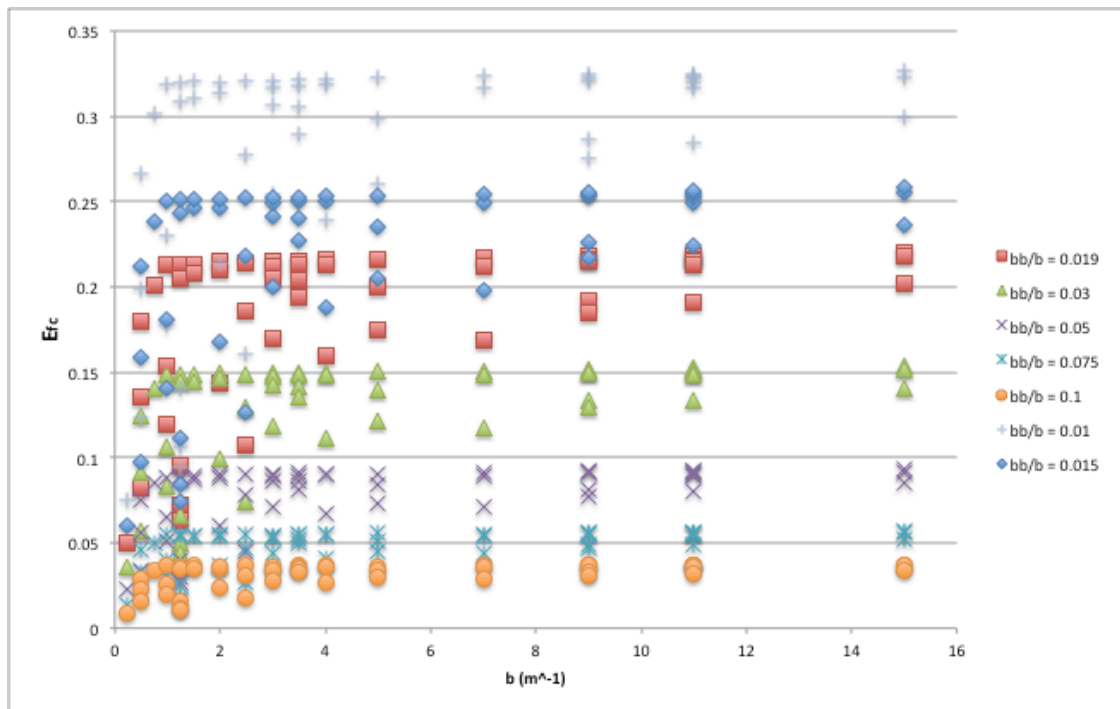
Graph 4.5 – Error factor of Attenuation (E_{fc}) as a function of scattering (b) across multiple $\frac{b_b}{b}$ values

It is interesting to note that the data does not form a distinct relationship between the error factor and the scattering coefficient. It can be seen that for a single value of b there are multiple values of E_{fc}. This indicates that the level of absorption within the sample affects the value of E_{fc} and needs to be accounted for, with higher a values yielding lower E_{fc} values. As such analysis that accounts for changes in both a and b across the samples is required.

4.2.3 Introduction of ω_{ms} and $\frac{b_b}{b}$

As scattering cannot be measured independently and due to the lack of a relationship between E_{fc} and b, the usability of Graph 4.5 is reduced and a different approach to quantifying the error was required. It was noted in section 2.3 that the general method for determining the effect of backscatter is to use the backscattering ratio. In this case the data generation process does not

allow for analysis of the data with respect to $\frac{b_b}{b}$. However, b_b can be seen in equation 2.12 and 2.13 as an input for the calculation of the reflectance. The element of the equation that the backscattering coefficient is part of is the multiple scattering albedo (ω_{ms}) and is a tool that can be used to analyse the error with respect to changes in the backscatter as seen in equation 4.2.

$$\omega_{ms} = \frac{b_b}{b_b + a}$$ (4.2)

Graph 4.6 provides the comparison of the attenuation error factor across seven $\frac{b_b}{b}$ values with respect to the value of ω_{ms}.
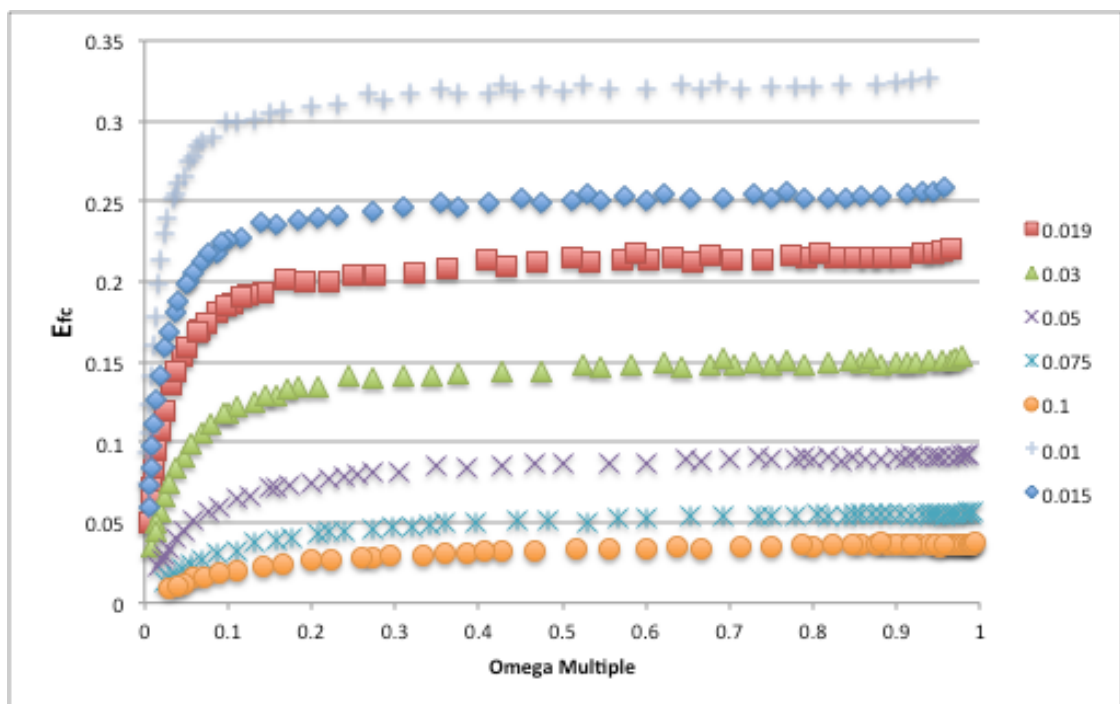
Graph 4.6 – Attenuation Error factor E_{fc} with respect to omega multiple (ω_{ms}) for changing $\frac{b_b}{b}$

It is important to note that Graph 4.6 creates a distinct relationship from the values of E_{fc} seen on Graph 4.5, with no value of ω_{ms} being related to more than one E_{fc} value. This is due to the relationship between b_b and the b with

63

respect to E_{fc}. Graph 4.5 shows changes with respect to a single coefficient variation, that of a. So as a increases, the amount of error in the attenuation tube decreases for a specified b and $\frac{b_b}{b}$. Absorption rich water bodies are characterised by CDOM dominated samples therefore the higher the value of a, the lower the E_{fc} value for constant b and a given $\frac{b_b}{b}$. The lower error is also due to the negligible scattering caused by the CDOM particles, leading to lower values of b than those found in other water types.

The value for ω_{ms} for a single $\frac{b_b}{b}$ utilises a number of changing constants, more in line with the properties of a physical sample. This creates a unique value for each simulation sample that is created. The creation of a ω_{ms} value is affected by the not only changes of the value of b particular to the sample but also the value of a. It can be seen that across the seven tested backscattering ratios that a trend occurs in relation to the value of the error factor. Where the $\frac{b_b}{b}$ value is set to 0.01 E_{fc} is as its greatest and as $\frac{b_b}{b}$ increases to the simulation limit of 0.1 the error reduces to $E_{fc} < 0.05$.

It was also noted that during the creation of the correction method by McKee, Piskozub and Brown (2008) that $\frac{b_b}{b}$ is used as a measure for analysing the error caused by the collection of scattered light in the attenuation tube of the ac-9 as calculated by Equation 4.3:

$$f_c = \frac{c - c_m}{b}$$
(4.3)

$$fc = (7.34E{-}03)/((1.08E{-}2)+b_b/b){-}(2.96E{-}2)$$
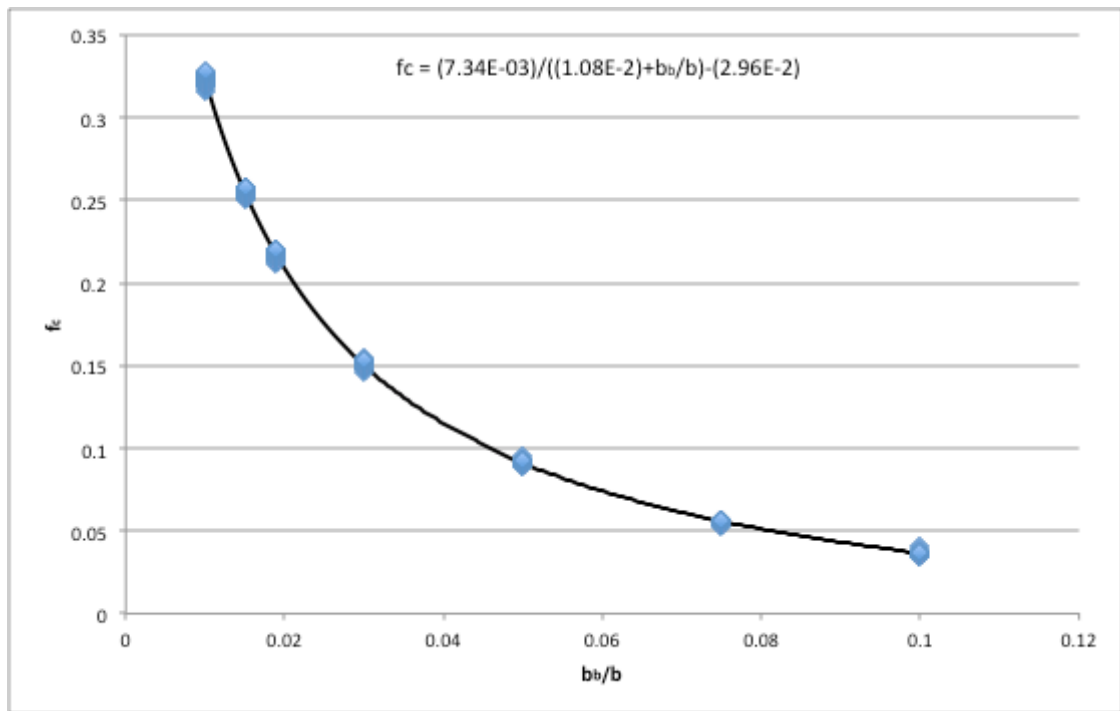
Graph 4.7 – Fraction of scattered light collected by the ac-9 attenuation sensor f_c for varied $\dfrac{b_b}{b}$

Graph 4.7 shows the relationship between $\dfrac{b_b}{b}$ and the fraction of unscattered light from the simulation results The comparison between the simulated results and the measurements made by McKee McKee, Piskozub and Brown (2008) were made to validate the data generated using the inputs from sections 3.3.2.2 and 3.3.2.3.The best fit of the data was carried out using the equation established for this particular data set type (McKee, Piskozub & Brown 2008). Further analysis of the results and evaluation with respect to the results found by McKee, Piskozub and Brown (2008) can be found in section 5.4.1.

4.2.4 Curve Fitting and Analysis

The curves shown in Graph 4.6 show a distinct trend that can be modelled by an equation. The equation used to model each $\frac{b_b}{b}$ curve was Equation 4.4 with L being the curves asymptote and k being the slope of the curve.

$$E_{f_c} = L(1 - e^{-k\omega_m}) \tag{4.4}$$

The fitted curves can be seen in Appendix F and were fitted using a least squares analysis performed in Microsoft Excel. The curves were then combined to a single graph (Graph 4.8) for analysis with respect to the entire dataset.
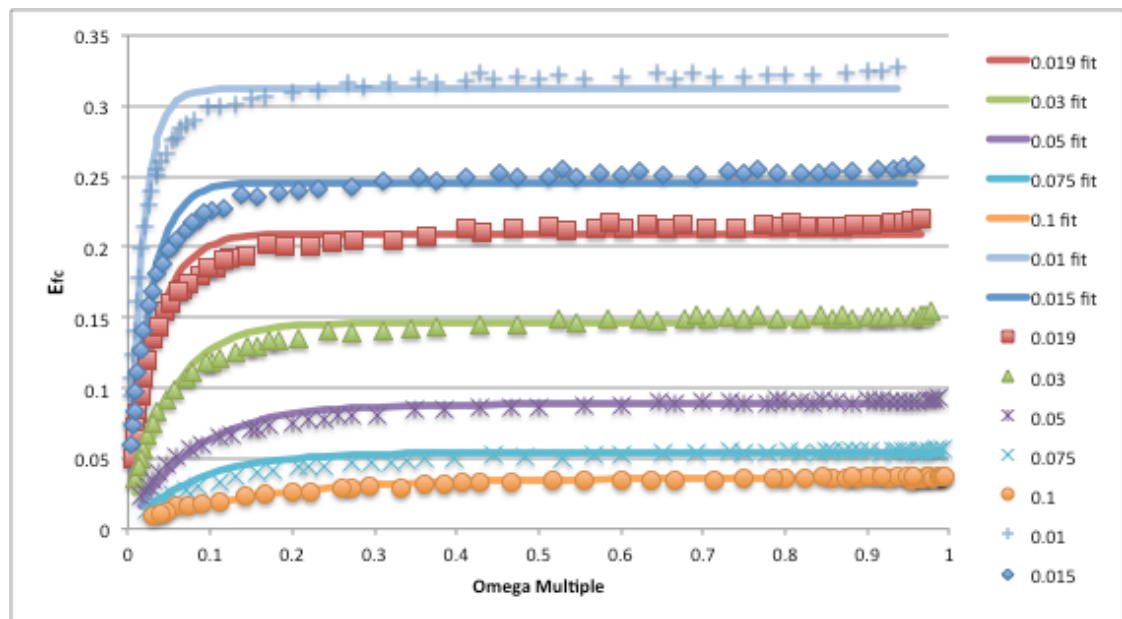
Graph 4.8 – Non-linear fits vs. Simulation Results for the error factor in attenuation (E_{fc}) with respect to ω_{ms} for differing values of $\frac{b_b}{b}$

The curves generated using the fits provided an indication of the error across the majority of the sampled datasets. For low values of ω_{ms} (Absorption dominant samples) the data provided very good fits and for turbid samples ($\omega_{ms} < {\sim}0.3$) the fits provide a good indication of E_{fc}. The 'shoulder' point of the data however, generally indicative of mixed type or absorption dominant water bodies, is an area which shows a distinctive divergence from the data for lower $\frac{b_b}{b}$ values. The divergence is only of significant value for $\frac{b_b}{b} > 0.3$ as the fits for $\frac{b_b}{b} < 0.3$ proved to be accurate for the majority of the data.

4.3   Absorption Tube

This section focuses on the results obtained from the simulated ac-9 absorption tube. It also highlights a number of trends with respect to the large amount of literature available with respect to the absorption error. All of the results are discussed further in chapter 5.

4.3.1 Relationship between A_m and A

The foundation of the correction method proposed by Röttgers, McKee and Woźniak (2013) is the relationship that exists between the measured and true absorption for the 715nm wavelength.

Using the dataset defined by section 3.3.2.2 for a single $\frac{b_b}{b}$, the relationship between a and a_m was plotted as shown in Graph 4.9.
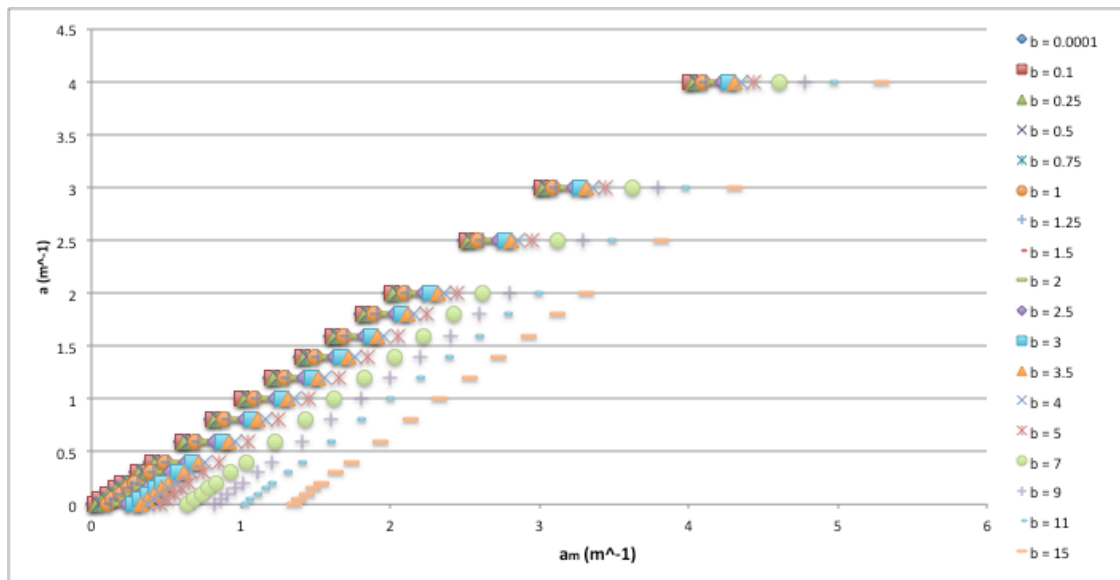
Graph 4.9 – True absorption (*a*) as a function of the measured absorption (*a_m*) for varied scattering values.

The relationship was found to be linear in nature with a slope of almost 1:1 for all of the datasets irrespective of the scattering value used. The correlation between the fit and the data was also high with most cases showing $R^2 = 1$. It was noted that the simulation data provided a change in the y-intercept for the fits where the slope did not change appreciably. It was found that the change in the y-intercept was directly proportional to the value of *b* (Graph 4.10)

68
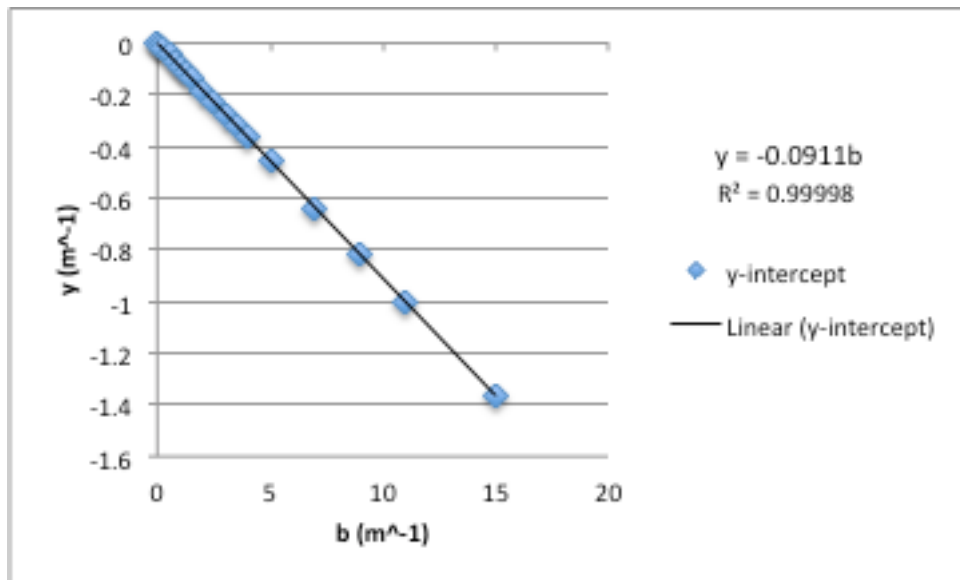
Graph 4.10 – y-intercepts from Graph 4.8 as a function of *b*

Performing the same analysis procedure on the data obtained from simulation set 2 (section 3.3.2.3) provided no useful data, as the data pairs did not allow for creation of an appropriate model to evaluate the relationship. It was also noted that the trends identified incorporated data that, in real-world samples, would not be seen in the field. The simulation input accounted for a wide variety of environments, which leads to data points being established that do not physically occur. This leads to the simulation data fits being skewed due to physically impossible simulation values. This is addressed further in section 4.3.4 and Chapter 5.

4.3.2 Usage of Error Factor

Following the process set out in section 4.2 the absorption was evaluated with respect to the error factor to establish a relationship that can be used to account for the error. The error factor (E_{fa}), calculated from Equation 4.5, was plotted against the scattering coefficient as the use of the other coefficients would have created a circular case and is not related to the real-world cause of the error.

$$E_{fa} = \frac{a_m - a_t}{a_t}$$ (4.5)
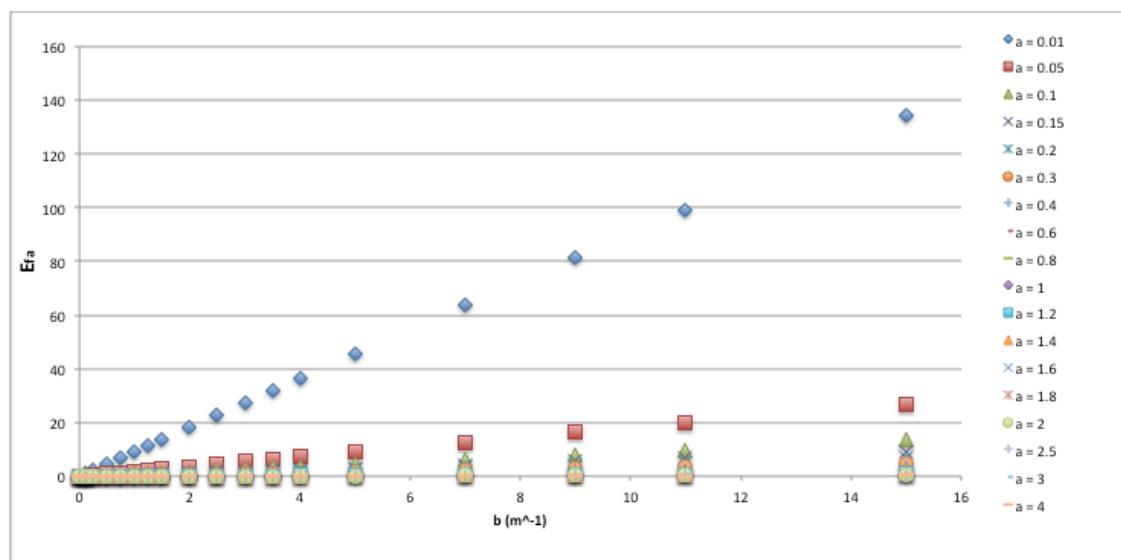
Graph 4.11 – Error factor for absorption (E_{fa}) as a function of b for $\frac{b_b}{b} = 0.015$

The data shown in Graph 4.11 confirmed what the literature had already shown, that the error in absorption for scattering dominated environments is high, while those that are dominated by absorption (high CDOM concentrations) suffer from a smaller error in the measurements. The slope of the error appeared to be a product of the combined properties of scattering

and absorption coefficients. Due to the combination effect exhibited by the data the introduction of another coefficient was required to identify usable trends.

4.3.3 Introduction of ω_{ms} and the $\frac{b_b}{b}$

The reasoning behind the usage of the ω_{ms} has been covered in section 4.2.3. ω_{ms} was again calculated and then plotted against E_{fa} to visually establish a relationship (Graph 4.12).
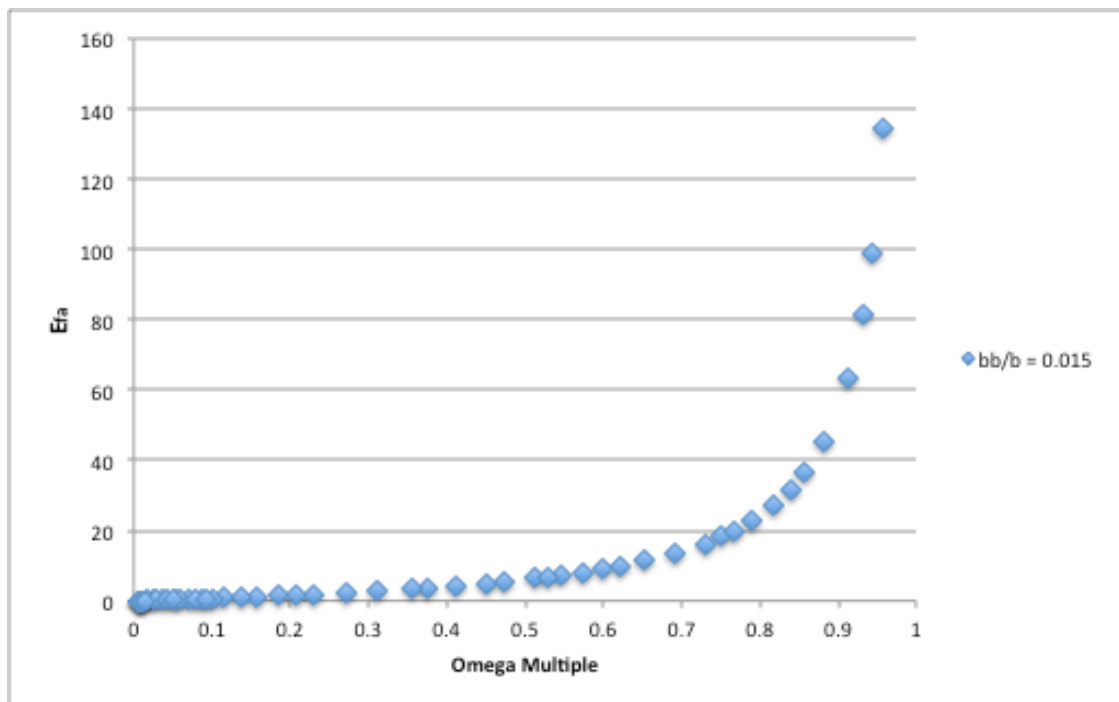
Graph 4.12 – E_{fa} as a function of ω_{ms} for $\frac{b_b}{b} = 0.015$

There was a noticeable trend in the data with the value E_{fa} increasing at a substantial rate as ω_{ms} increased. It was noted that this increase was directly tied to the calculation of the value of ω_{ms}. The calculation accounts for the absorption value as part of the denominator of the equation. As such when the absorption coefficient approached zero, the value of ω_{ms} increased and influence of scattering on the error increased. With the relationship established for a single $\frac{b_b}{b}$ the process was repeated using the second set of simulation data (Section 3.3.2.3).

The introduction of multiple $\frac{b_b}{b}$ values showed a large degree of consistency between E_{fa} and $\frac{b_b}{b}$ for similar values of ω_{ms}. It was also noted that as $\frac{b_b}{b}$ increased the error factor appeared to reduce, against expectations and the literature. Investigation of the data revealed the issue was attached to the method of calculating the value of ω_{ms}.

For a fixed value of ω_{ms} there are two coefficient changes that occurred when $\frac{b_b}{b}$ changed. The increases in the ratio cause an increase in a to ensure the denominator will create the constant value. As such the sample becomes more absorbent and will reduce the error associated with photons becoming lost, as they are more likely to be absorbed. b decreases as the ratio increases due to the ratio being a function of both b_b and b. When combined with the increase in a, the result is a drop in the error factor as shown in Graph 4.13 for a given ω_{ms}.
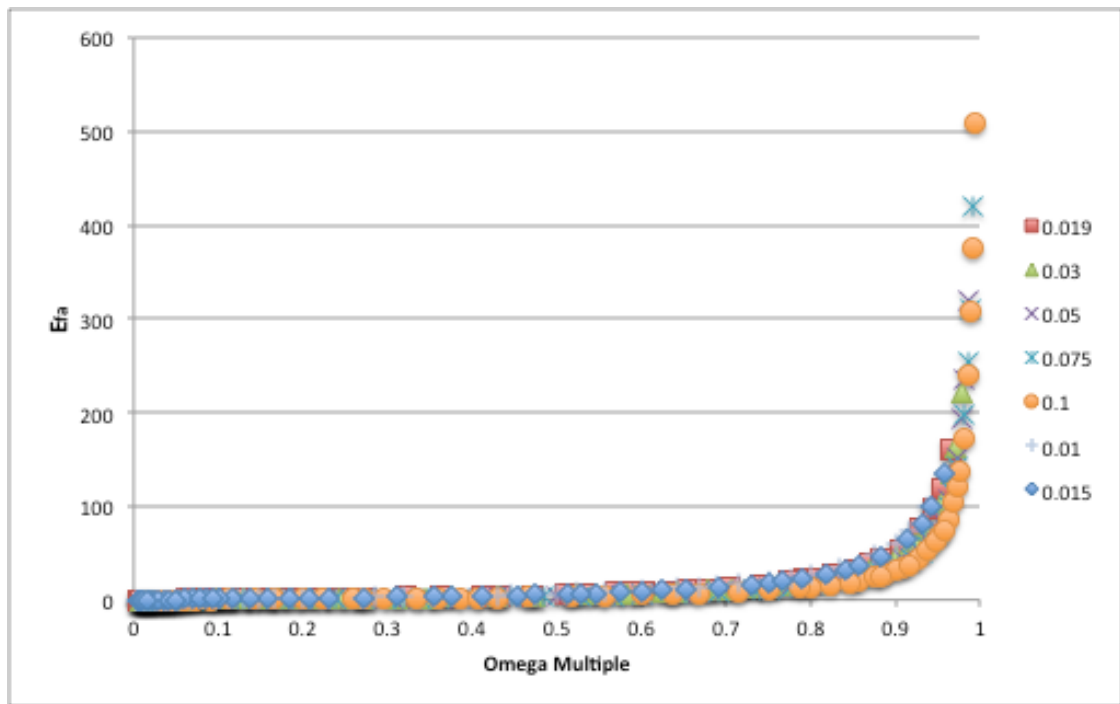
Graph 4.13 – E_{fa} as a function of ω_{ms} for multiple $\frac{b_b}{b}$ values

As has been noted in Section 4.2.3 the study undertaken by McKee, Piskozub and Brown (2008) $\frac{b_b}{b}$ can be used as a measure for the errors associated with the scattered photons not collected in the absorption tube. Equation 4.6 models the un-collected photons error with the data shown in Graph 4.14

$$f_a = \frac{a_m - a}{b}$$ (4.6)

$$f_a = (1.56E\text{-}2) + (5.683)b_b/b - (5.0835E\text{+}1)(b_b/b)\text{\textasciicircum}2 + (4.066E\text{+}2)(b_b/b)\text{\textasciicircum}3 - (1.3832E\text{+}3)(b_b/b)\text{\textasciicircum}4$$
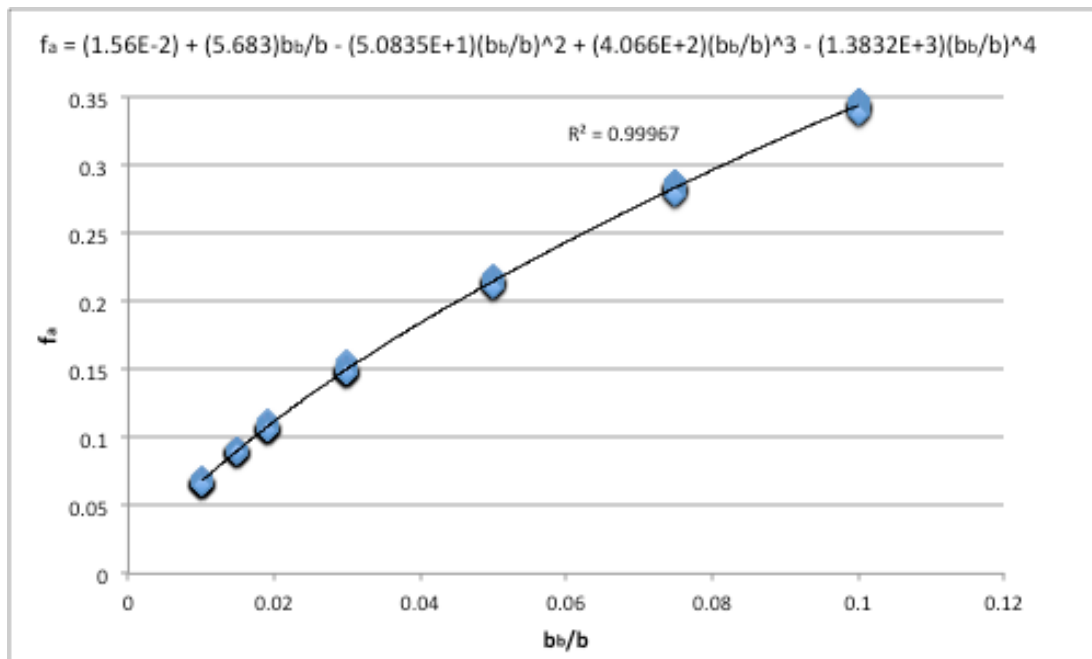
Graph 4.14 - Fraction of scattered light not collected by the ac-9 attenuation sensor f_a for varied $\frac{b_b}{b}$ values

By comparing the data obtained from the simulations with the modelled dataset of McKee, Piskozub and Brown (2008) it was possible to validate the data that was generated through the process detailed in Chapter 3. The best fit of the data points used the equation model proposed by McKee, Piskozub and Brown (2008) with the coefficients adjusted to fit the data. Further analysis of the model and the data can be found in Section 5.4.1.

4.3.4 Usage of ω_{ms}

The usage of the value of ω_{ms} is dependent on the error of the absorption. Optically turbid waters $\omega_{ms} < 0.8$ proved problematic for all non-linear fits. As such a method of diminution was required to identify a cut-off point for the analysis to maintain the data with respect to real-world samples.

As the project is focusing on Australian natural waters for the simulation inputs the data chosen to create the cut-off point was from Campbell, Phinn and Daniel (2011) for the absorption value as it was deemed to be the greater factor in the determination of the appropriate ω_{ms} cut-off point. Using the data, the cut-off absorption value was deemed to be *a = 0.000875*. When combined with $\frac{b_b}{b} = 0.01$ and *b = 0.25* the ω_{ms} cut-off was calculated as 0.7407. Given the nature of the dataset and the calculations this limit extended to 0.75 as the majority of the $\frac{b_b}{b}$ values analysed produced ω_{ms} = 0.75 allowing for simple determination of the upper ω_{ms} limit point.

4.3.5 Curve Fitting and Analysis

With the $\frac{b_b}{b}$ curves limited to a range that could be fitted more easily with a fit equation the curve datasets were processed through the least squares curve fitting applied in Section 4.2.4 to attenuation data.

Equation 4.7 shows the equation that was used as a fit to the absorption data.

$$E_{f_a} = l \times e^{k\omega_{ms}} \tag{4.7}$$

The coefficients obtained from the fitting of the data to the equation were than modelled as a function of the backscattering ratio to obtain a method of determining the curve from Graph 4.15.

Having established the relationship required to chose the correct error curve a plot with the calculated fits was created to visually enable judgment of the fits.
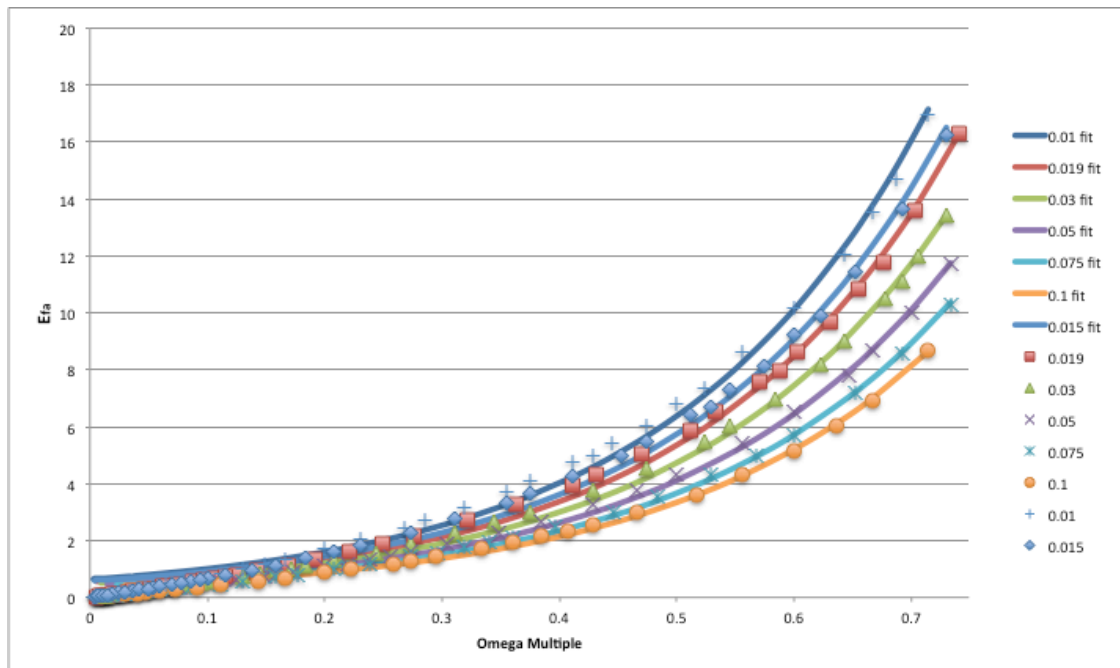
Graph 4.15 – Plot of calculated fit data for error factor for absorption as a function of ω_{ms} for varied $\frac{b_b}{b}$

The fit data closely approximates the simulation results with some overestimation occurring at the lower values of ω_{ms}. The usage of these curves is will be covered further in Chapter 5.

4.4 Scattering

As the simulation parameters set out in section 3.3.2.2 and 3.3.2.3 include the true particulate scattering for each sample trends can be identified with regard to the error that is applied to the scattering coefficient determined from the measured coefficients using Equation 2.14.

As the error on the scattering is created through the error included in measured values using the ac-9, knowing the true value of scattering allows

for the calculation of the error on the scattering coefficient (Δb) from equations 4.8 and 4.9.

$$b_m = (c_m - a_m) \tag{4.8}$$

$$\Delta b = b_m - b_t \tag{4.9}$$

The error forced on the scattering was calculated by using c_m, which is underestimated, and a_m, which is overestimated. By calculating the scattering coefficient the errors were combined into b_m. The calculation of the error experienced on b used the true value of the scattering to obtain the absolute value of the error. As the value of c is underestimated to a greater value than the value of a, the values of Δb were all negative values indicating that the value of the scattering coefficient was also underestimated. To identify a relationship between the scattering error and a measureable quantified value the c_m and a_m values were each tested (Graph 4.16).
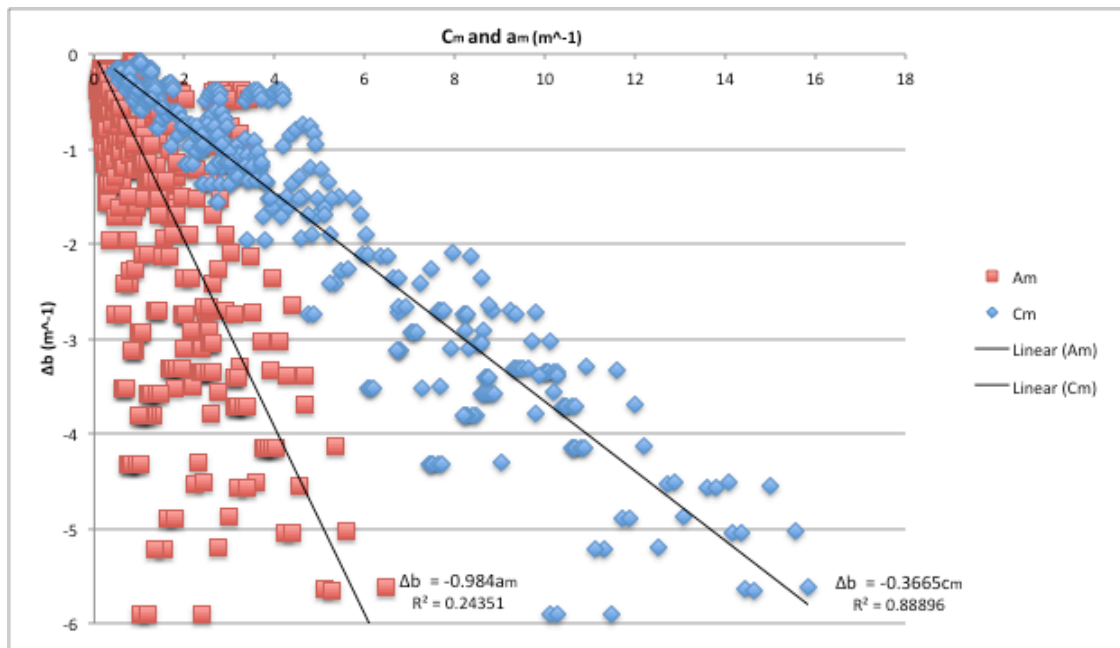
Graph 4.16 – Plot showing the error on the measured scattering coefficient (Δb) as a function of a_m or c_m for all tested $\frac{b_b}{b}$ values.

Linear fit analysis of the two datasets created with Δb as a function of a_m or c_m provided the necessary information to evaluate the better choice of model for the value of Δb. The correlation for the model using c_m value was 400% greater than that of the modelled fit using a_m. As such any calculation involving the estimation of Δb should use the c_m to calculate the value of Δb. It was also noted that the model encompassed the Δb values for the entire simulated $\frac{b_b}{b}$ spectrum.

4.5 Summary

This chapter has shown that a large amount of data was obtained during the processing of the simulation results.

The attenuation tube showed a distinctly linear relationship regardless of the $\frac{b_b}{b}$ value used with the main difference in measurements being due to the magnitude of the change across varied $\frac{b_b}{b}$ coefficients. The error factor E_{fc} showed the greatest use as a correction value as it provided numerous calculation options and could be evaluated as a function of $\frac{b_b}{b}$ or ω_{ms}. However the relationship of c to c_m also proposes options. Usage of ω_{ms} and the E_{fc} provided a good independent fit of the data while analysis following that of McKee, Piskozub and Brown (2008) showed that the simulated values provided a relationship similar to those seen in that study.

The absorption tube provided interesting data trends, with analysis of the relationship between a and a_m providing a linear, almost 1:1 relationship. The usage of the error factor E_{fa} provided further insight into the relationship of scattering and absorption and the error associated. Usage of the $\frac{b_b}{b}$ and ω_{ms} provided a number of interesting relationships in line with the work of McKee, Piskozub and Brown (2008) and the analysis performed on the attenuation tube. The usage of the E_{fa} and ω_{ms} was limited due to the high error values being seen at high ω_m values. It was also noted how the changes in $\frac{b_b}{b}$ were affecting the graphs, creating an un-intuitive system that required further investigation.

Finally an analysis of the error that affects the calculation of the measured scattering coefficient noted that there is a relationship that can be quantified as a function of the measured attenuation.

Chapter 5 will now analyse these results further to note the primary sources that are causing the error in the measurements and the limitations of the models that have been noted in this chapter. It will then take all of the data and combine it in to create a base for the creation of a correction method in the future.

Chapter 5

Discussion

5.1   Introduction

This chapter will take the results detailed in Chapter 4 and provide a greater level of discussion and analysis in relation to correction of the measurement errors.

It will first look at the attenuation measurements and the error associated with them. The primary purpose of the analysis is to identify the sources of the errors affecting the measurements and how these sources cause the error. An analysis of the model for determining the error factor as a function of ω_{ms} will also be undertaken to establish the limitations that the use of such a model would have.

Following this a similar procedure will be undertaken to note the sources of the error on absorption measurements. This will be followed by a discussion on the usage of the error factor as a measure of absorption measurement error and the limitations that must be observed when using the error factor. Following on the limitations of the error factor the limitations of the model found in section 4.3.5 will be discussed.

Having established the primary sources of the error and the affect they have on the measured values a brief analysis of the data will be undertaken with respect to the models proposed by McKee, Piskozub and Brown (2008) and Röttgers, McKee and Woźniak (2013). This analysis will evaluate the data

generated by this study against the trends identified by these studies to validate the measurements taken and determine any relationship to both simulated and real-world datasets.

Finally, all of the data will be analysed to note the limitations of corrections performed using only measurements performed using measured data from the AC-9. Following this discussion, the use of external data will be evaluated with particular attention to the usage of ω_{ms}. All information will then be compiled to produce a correction scheme that can be applied to absorption and attenuation measurements with the limitations also being noted and discussed.

5.2   Attenuation Error

This section will focus on the models of the attenuation error affecting the measurement of the attenuation coefficient. It looks at the sources of the error and notes the limitations of the models generated from the simulated data.

5.2.1 Sources of Error and Model Creation

It is noted in section 2.4 that the error in the ac-9 instrument is related to the photons that are scattered and collected by the sensor as non-scattered photons. As the photons are counted as not being scattered the measured value of the attenuation is reduced when compared to the true value leading to underestimation of the true value.

The simulation data shown in Graph 4.1 shows that this was found to be correct for all values of c. As the true scattering and hence the true attenuation coefficient of the sample increased, the measured attenuation was an

underestimation in for each simulation result. It was noticed that the best fit between the measured and true absorption had a near constant slope of ~1.2675 for the entirety of the samples for a single $\frac{b_b}{b}$. Classifying the data relative to specific values of a caused the slope of the datasets to form an approximate 1:1 slope between the datasets. While the slope remained fairly constant across the data, the y-intercept for the data series increased with the increase in a which caused the underestimation of c by c_m. It was found that across the values of a simulated in the AC-9 that the relationship was closely approximated by a straight line with the y-intercept as a function of a. Combination of Graphs 4.2 and 4.3 could therefore be used to obtain an estimate of the attenuation value with calculation of the 'true' value being obtained through a possible iteration scheme.

Usage of Graph 4.4 and Table 4.1 however shows that the amount of underestimation is also highly dependant of the VSF. The scale of underestimation throughout the sample (slope) changes dependant on the $\frac{b_b}{b}$ value. This indicates that the y-intercepts for the individual data series would change along with the VSF. This does lend itself to correction methods and requires further analysis before a method can be created.

Given that the slope of the datasets is dependant on the VSF, as shown in Table 4.1, it is reasonable to conclude that the major error driver with respect to c_m is the VSF from this small snapshot of the data.

This assumption is upheld further into the analysis as the VSF is incorporated in greater depth to the analysis. The calculation of E_{fc} is entirely dependant on

83

the data that is measured and known to be true. As such if the error is highly dependent on $\frac{b_b}{b}$ then E_{fc}, will produce markedly different values as $\frac{b_b}{b}$ changes. To check all of these assumptions the analysis first looked at E_{fc} as a function of b. It was noted that when analysing this unorganised set of data that there was no definable relationship between E_{fc} and b. This data assumes that the absorption does not play a part in the determination in E_{fc} with respect to b. However there are a number of samples that have returned multiple data points for the same b and $\frac{b_b}{b}$ with differing E_{fc} values. This indicates that the as a increases the value of E_{fc} should decrease. It is through this combination effect of VSF and a that results in the usage of ω_{ms}. By using ω_{ms} as the independent variable in analysis of E_{fc} all of the changes that occur between the measured samples are accommodated into a single measurable value. Final analysis notes that as the media becomes more turbid, E_{fc} steadies at an almost constant value where the change in a and b have no affect on E_{fc}. However as the turbidity of the media lessens and CDOM begins to dominate the samples the value of E_{fc} decreases dramatically. This shows that while the VSF is the primary driver of the magnitude of E_{fc} with the value of a inversely driving the error.

There are two major models that were created through the process of analysing the error. The first is that of the relationship between c and c_m and the other is that of E_{fc} as a function of ω_{ms}. The first to be discussed is that of the relationship between c and c_m. This model provides a simple linear fit to the simulated data that only varies in slope as $\frac{b_b}{b}$ changes. Provided that the

value of $\frac{b_b}{b}$ is known then the slope of the fit can be estimated through the use of Graph 5.1.
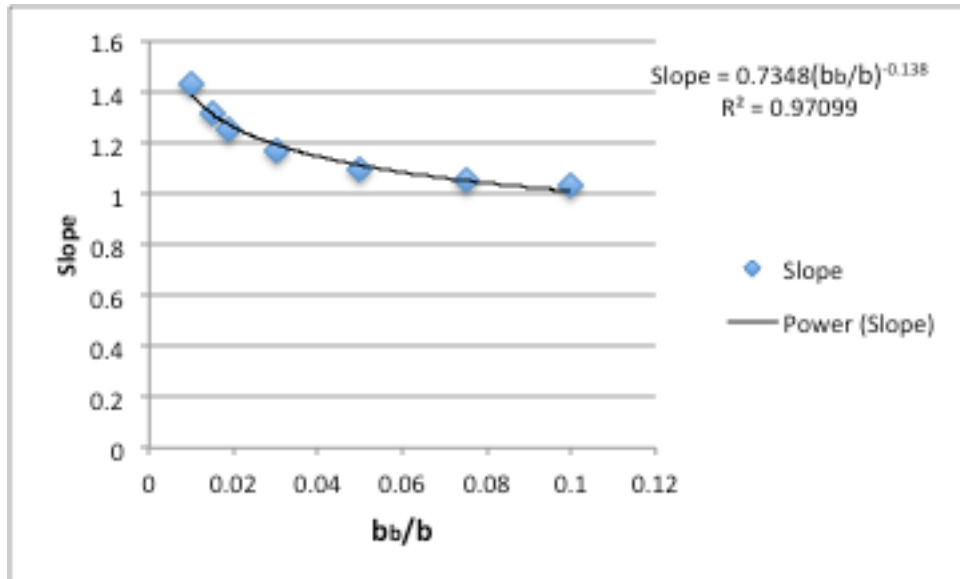
Graph 5.1 – Slope of Graph 4.3 as a function of $\frac{b_b}{b}$

Once the slope of the linear fit has been determined then it is possible to correct c_m to an almost 'true' value of c.

The second model developed through the analysis process was the E_{fc} model. This E_{fc} model uses the error factor of attenuation as a function of ω_{ms}. This accounts for an increased range of error as it works irrespective of the attenuation coefficient. This is because the correction works as a factor of c_m, which is not dependant on the exact value measured, rather than the error itself. The E_{fc} model also accounts for the effect that the absorption has on the error through the calculation of the value of ω_{ms}. Calculation of the correct curve is obtained by producing a non-linear fit on the coefficients L and k as a

function of $\frac{b_b}{b}$ (Appendix F). Using the calculated fit coefficients, the user can then calculate an estimate for any value of $\frac{b_b}{b}$ providing that ω_{ms} is known. The non-linear fits calculated from the interpolation process are shown in Graph 5.2.
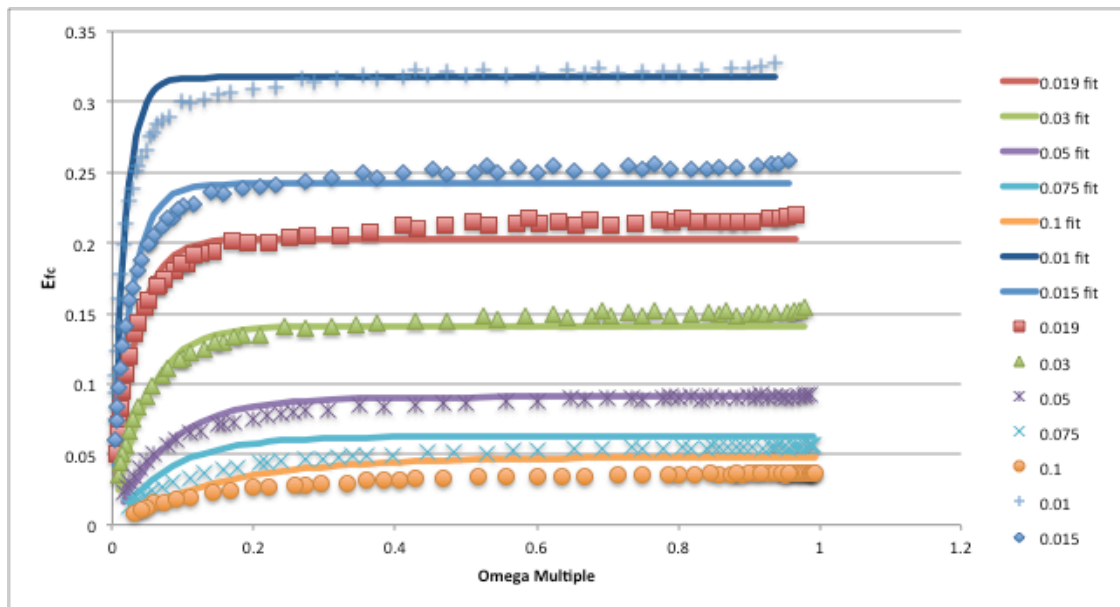
Graph 5.2 – Estimated fits based off coefficient interpolation for given $\frac{b_b}{b}$

5.2.2 Limitations of Models

There are a number of limitations that must be considered in relation to the creation of a correction scheme for attenuation with respect to the models noted in Section 5.2.1. The simulation data used in the creation of the models, while based on real-world data, will not account for all combinations of data points which can occur through different types of water bodies. Scattering dominated and CDOM (absorption) dominated waters are considered,

however the data covers the entire spectrum and as such may be subject to variation between limited sample sizes.

The c to c_m relationship that was established in Chapter 4 and expanded on in section 5.2.1 is limited in respect to the water body types and the range of data the correction can be applied to. It only looks at the attenuation error with respect to the VSF. It was established in section 5.2.1 that the drivers of the error in the attenuation tube are not only the VSF but the absorption coefficient as well. The model only explicitly accounts for the VSF, with the absorption being incorporated into the dataset through the nature of c. This means that levels of absorption outside those tested in the simulations could affect the outcome of a correction based off the c to c_m relationship. A benefit of the model however is that is easy to use and calculations can be made quickly and with a high level of accuracy providing that $\frac{b_b}{b}$ is known.

There are a number of limitations in the E_{fc} method. The first is that the current data curves fitted to the simulation data provide cover only a small number of $\frac{b_b}{b}$ values. If the $\frac{b_b}{b}$ is known to be one of the values tested through the simulation data then the curve can be accurately determined and adjustments made. However in the case that the $\frac{b_b}{b}$ value of the sample is determined to not be one of the range simulated in this study then the determination of the curves becomes more complicated. The coefficients of the fits do not provide a high quality non-linear relationship. This introduces error into the determination of the curve for the particular $\frac{b_b}{b}$ value. The effect caused by the error in coefficient determination can be seen in Graph 5.2 where the fits are

estimated based off the calculations for L and k from $\frac{b_b}{b}$. Where all the data

curves are shown as good estimations in Chapter 4, the fits in Graph 5.2 show

some significant deviation from the data across the majority of the fits. The

lower values of $\frac{b_b}{b}$ show significant overestimation of the simulation E_{fc} values.

As $\frac{b_b}{b}$ increases the quality of the fits increases with overestimation being seen

around the 'shoulder' of the curves and underestimation beginning to be seen

as ω_{ms} increases leading to an overall moderate quality fit. This estimation

error stems from the calculation of the L as no fit calculated for the data points

provided a good estimate of the 'best fit' value of L. As the re-calculated fits do

not provide a good estimate across a number of $\frac{b_b}{b}$ datasets care should be

taken when calculating E_{fc} for high $\frac{b_b}{b}$ values as E_{fc} is likely to be overestimated.

5.3   Absorption Error

This section will provide further investigation into the errors found in the

absorption tube of the ac-9. It will analyse the results from the simulations and

identify the primary drivers that cause the error in the attenuation

measurement. It will also identify the limitations imposed on the error factor

and the model of the error factor.

5.3.1 Sources of Error and Model Creation

Across the numerous bodies of literature, absorption is the measured

coefficient that receives the most attention. As discussed in Section 2.4, it is

noted that the measurement error in the ac-9 absorption tube is caused by

scattered photons being 'lost' and counted as absorbed. This leads to an overestimation of the absorption value that must be corrected for.

Following the relationship established by Röttgers, McKee and Woźniak (2013) for a_m^{715} the relationship between measured and true absorption was established with Graph 4.9. It is noted that a similar trend can be observed in the attenuation tube (Section 5.2) with the slope of the error also remaining constant across the entire data spectrum. As the slope of the data remained constant across all the data further investigation was required to ascertain any possible relationship. The linear fits of the data from Graph 4.9 noted that as the *b* value of the sample increased the y-intercept of the fits decreased in value. Analysis of the y-intercept as a function of *b* is shown in Graph 4.10 and notes that the y-intercept can be modelled as a linear function of *b*. A high strength rating cannot be placed on this analysis due to a number of physical limitations of the water samples. As all suspended particulate matter in a sample contributes to the value of *a* and *b,* with CDOM also contributing to *b*, there are limitations on the combinations of samples that can be classified as physically possible. Samples where the value of *b* is orders of magnitude larger than *a,* therefore are not possible, as the particles inducing the scattering are also contributing a non-negligible amount to the value of *a*. Samples dominated by CDOM however can have large values for *a* combined with the lower values of *b*. As the simulation data from Section 3.3.2.2 accounts for a large range of *a* and *b* values there are a number of regions where the results represent physically impossible scenarios. The inclusion of these scenarios, it is assumed, skews the data fits when the data is combined

into a single data set. It was also noted that the simulation data pairs used for simulation set 2 did not allow for identification of trends across varied $\frac{b_b}{b}$ due to the large number of changing variables in the simulation inputs. As such the usage of the a vs. a_m function cannot be effectively evaluated through the simulation data and is discussed further in Section 5.4.2.

Due to the limitations of the data for simulation set 2, a model was required that allowed for determination of the error with respect to a single variable. The determination of the error factor E_{fa} was deemed an appropriate model and testing was carried out. The major limitations of this model were found towards the end of the analysis when looking at E_{fa} as a function of ω_{ms}. It was noted through the trends found with E_{fa} as a function of b that the error increased with increases in $\frac{b_b}{b}$. It was only fully noted how this error increased through the usage of the E_{fa} vs. ω_{ms} model (Graphs 4.12 & 4.13). The error in these graphs, where ω_{ms} values represented extremely turbid waters ($\omega_{ms} > 0.75$), exponentially increased at a rate exceeding that which could be modelled. Analysis of the data for the data points involved in this section of the model showed that this spike was due to a combination of factors, the major driver being the value of a. In this area the value of a was low (~0.01) and so the calculation of E_{fa} caused the final value to increase. This was also relative to $\frac{b_b}{b}$ and b as they form part of the calculation of ω_{ms} and define the optical characteristics of the water body. As the relationship between a and b in this range was beginning to move into the area of physically unlikely values with E_{fa} also reaching unstable values analysis was required to ensure that the values stayed in the physically possible (Section 4.3.4). As in Section 5.2.1,

interpolation was carried out to identify if any errors would be introduced when performing analysis on $\frac{b_b}{b}$ values outside those tested through simulation (Graph 5.3).
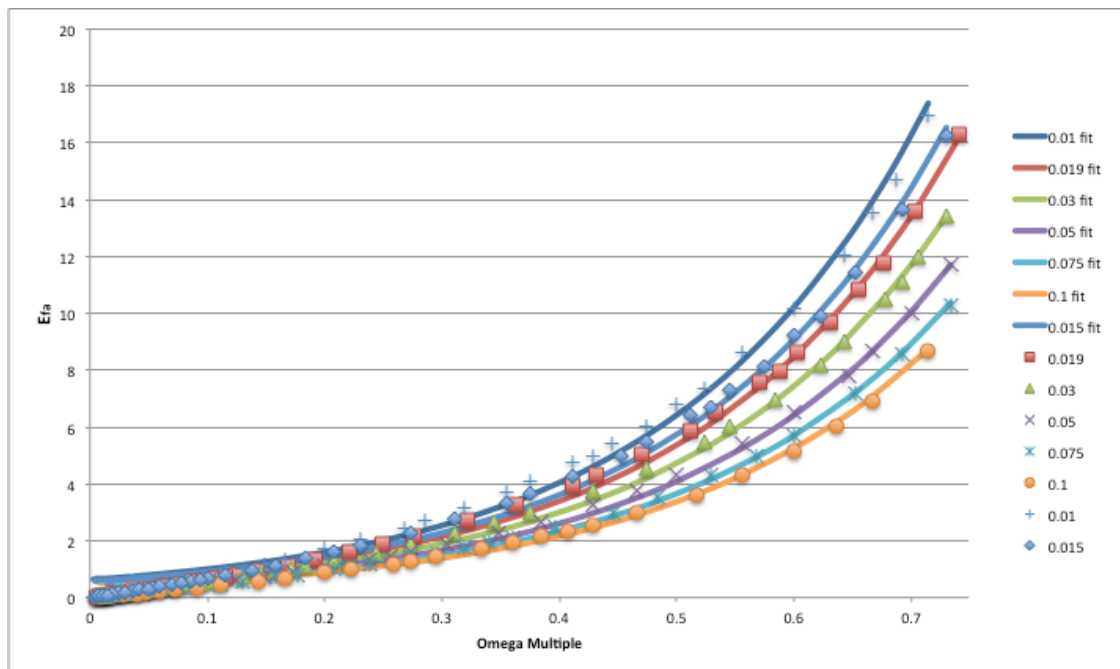
Graph 5.3 – Estimated fits based off coefficient interpolation for given $\frac{b_b}{b}$

Through the process of generating the models and performing the analysis the sources of the error can be defined. The changes seen when comparing the error with respect to differing $\frac{b_b}{b}$ values shows that the amount of backscatter in the sample contributes to the measurement error. It can also be seen, through Graph 4.9, that the coefficient of scattering, of which b_b is an element, forms part of the error as is expected. It is also important to note that for CDOM dominated samples, the error is less than that seen in mixed and scattering dominated waters. As such, it can be noted that the primary drivers of the error

in the absorption tube are backscatter and the VSF, with absorption also affecting the quantity of error.

5.3.2 Limitations of Error Factor and Models

The major limitation that exists in the usage of E_{fa} relates to the magnitude of the error in high scattering environments. This can be seen in Graph 4.13 where E_{fa} reaches extreme levels for turbid waters. Due to this error, there are a number of limitations that must be observed with respect to the model. As the increase is restricted to a specific range of ω_{ms} (0.75 < ω_{ms} < 1) the limitation of usage with respect to the model means that ω_{ms} values above 0.75 cannot provide a reliable estimate of E_{fa}. This is of benefit as it restricts the analysis to turbulent waters, mixed type and CDOM dominated waters.

The models created in chapter 4.3 are subject to a number of limitations that must be considered when using the models for correction. The limitation with respect to the error factor and the values of ω_{ms} has been discussed and therefore any correction where the value of ω_{ms} is greater than the upper limit set out in Section 4.3.4 cannot be reliably applied to the data using the model shown by Graph 4.13. It should also be noted that the non-linear fits generated through the analysis provide slight overestimation of E_{fa} against the simulation data for small values of ω_{ms}. Interpolation of the L and k coefficients for $\frac{b_b}{b}$ outside the values tested does not reduce this error and so limits the usage of the model for obtaining a 'true' value of the absorption. The interpolation process does not provide great difference from the best-fit data through the

interpolation process with the majority of the fit providing values similar to the simulations best-fit results (Graphs 4.15 & 5.3).

Due to the complex interaction between scattering and absorption, the relationship between a and a_m could not be modelled. While a possible correction scheme could be created, the model for the relationship would need to be generated for each separate set of data samples. The simulated data showed that there is no simple linear relationship between data for differing values of a and b for a given $\frac{b_b}{b}$. This is expanded on further in Section 5.4.2.

5.4 Evaluation with respect to current research

5.4.1 McKee's Iterative Correction Scheme

The correction method established by McKee, Piskozub and Brown (2008) looks at the portions of scattered light that contributes to the error through either collection or non-collection by the sensor.
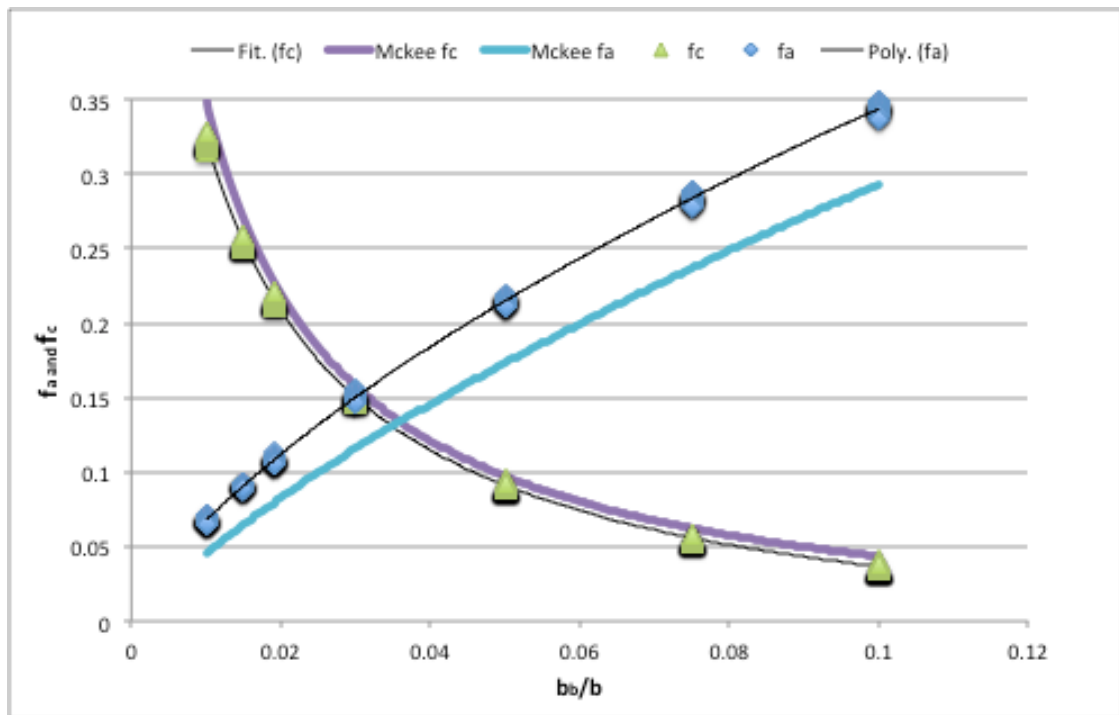
Graph 5.4 – The trends observed for f_a and f_c for all simulation data

Table 5.1 – Best fit Equations for McKee, Piskozub and Brown (2008) and Simulation data

Data	Fit Equation
Simulated f_a	$f_a = (1.56E\text{-}2) + ((5.683)(b_b/b)) - ((5.0835E{+}1)(b_b/b)^2) + ((4.066E{+}2)(b_b/b)^3) - ((1.3832E{+}3)(b_b/b)^4)$
McKee f_a	$f_a = (2.699E\text{-}3) + ((4.636E0)(b_b/b)) - ((3.746E1)(b_b/b)^2) + (3.177E2)(b_b/b)^3) - ((1.166E3)(b_b/b)^4)$
Simulated f_c	$f_c = (7.34E\text{-}03)/((1.08E\text{-}2)+(b_b/b)) - (2.96E\text{-}2)$
McKee f_c	$f_c = (6.809E\text{-}3)/((8.502E\text{-}3)+(b_b/b)) - (1.918E\text{-}2)$

As can be seen from Graph 5.4 and Table 5.1 there is a high degree of correlation between the relationship established by McKee, Piskozub and Brown (2008) and the curves established using the simulation data.

It was noted that there were a number of differences between the analysis for the datasets and the data fits. Most notable were the differences between the coefficients of the fit equations. These differences were small, however they still were enough to warrant further examination of the processes used by

94

McKee in the creation of the dataset used for the model. It was also noted that there appeared to be a distinct difference in the magnitude of the values that could be compared at the $\frac{b_b}{b}$ values tested in this study. Further investigation decided that the values of f_c were similar between the studies as shown in Graph 5.4. The magnitude of the slope for the values of f_a created a steeper slope than that seen in the previous study, which led to lower values at the upper limit of the tested $\frac{b_b}{b}$ range.

The investigation into the difference between the two datasets noted an important difference with regards to the input values tested for the creation of the simulated dataset. The data created for this study utilised a large number of data points tested against seven $\frac{b_b}{b}$ values. The study by McKee, Piskozub and Brown (2008) utilised a single set of data points (*a = 0.006, b = 0.25*) across a large number of $\frac{b_b}{b}$ values ranging from zero to 0.1. As this study had a minimum absorption value of 0.01 and scattering of 0.25 it is put forward that the differences between the study by McKee and this study are due to the differences between the IOPs input into SimulO.

It is unknown how much the differences between the studies would affect the usage of the correction method proposed by McKee, Piskozub and Brown (2008) and improved in McKee et al. (2013), however given that the difference is significant this requires further quantification.

5.4.2 Röttgers Absorption Correction

The method proposed by Röttgers, McKee and Woźniak (2013) as noted in Section 2.6.2 looks at the relationship between the measured and true absorption. The comparison of the simulation data provides a relationship that is distinctly linear in nature which when compared to equation 2.18 in itself does not provide a great level of difference as equation 2.18 closely represents a straight line fit.

The data obtained using the simulation inputs found that the linear relationship for varied scattering and constant absorption closely approximated a 1:1 relationship between the measured and true absorption with linear shifts based on the scattering coefficient. This relationship does not agree with the relationship provided by Röttgers, McKee and Woźniak (2013) and so further analysis as noted in section 4.3.1 was required.

By classifying the simulation data into sample sets bounded by the limits found for absorption and scattering for the in-situ measurement samples, analysis could be undertaken to note any possible trends from the simulation data and the relationship proposed by Röttgers, McKee and Woźniak (2013). Classification of this nature does not account for the differences between the data points of the studies, only allowing for general analysis of the simulation data for the classes and not between the studies.

This classification provided a number of interesting trends to be noted as the backscattering ratio and sample ranges changed. It was also noted that the culture sample set could not be created as a class using the existing simulation data.
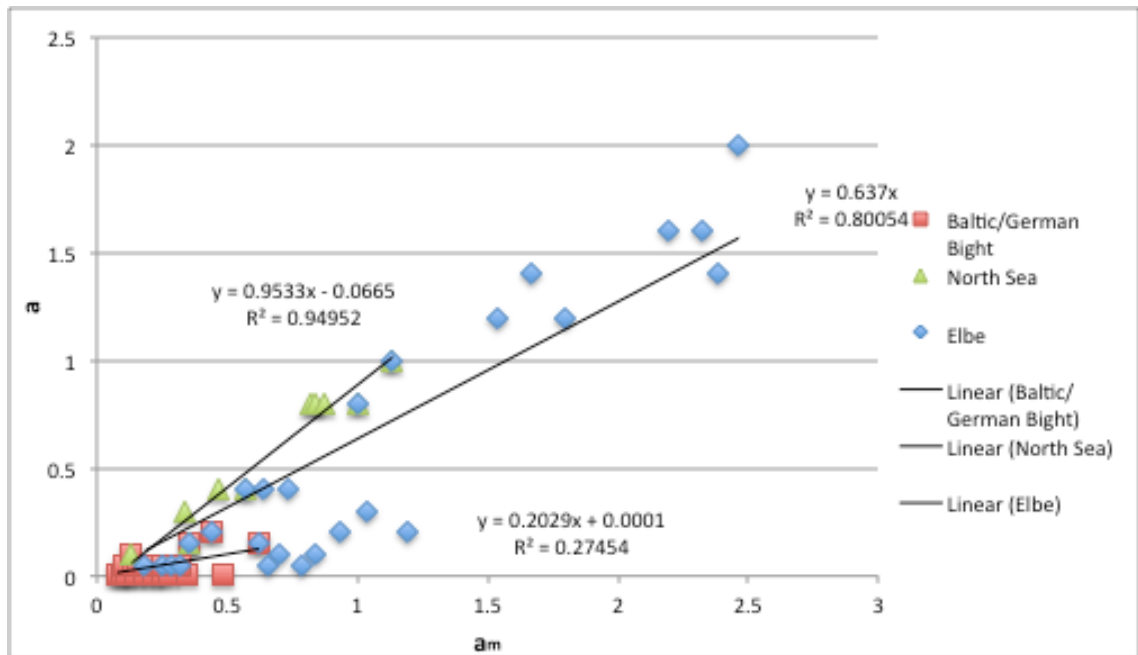
Graph 5.5 – Simulation results for 3 sample sets defined by Röttgers, McKee and Woźniak (2013) for $\frac{b_b}{b} = 0.01$.

It is of note that the relationship between the measured and true absorption varied greatly between the simulation classes. This relationship change is due to the different water body types that the classified samples are a part of with the Elbe classification leading to distinctly turbid water samples.

Of note with the distinction between the classes is that where $\frac{b_b}{b} = 0.01$ the Baltic Sea/German Bight class show a similar trend to the relationship established by Röttgers, McKee and Woźniak (2013) with the slope of the fit being 0.2029. It is only at this $\frac{b_b}{b}$ value for the Baltic/German Bight class that a fit indicates correlation with the established relationship for the majority of the classified simulation data. The fit for the Elbe classified samples at $\frac{b_b}{b} = 0.1$

shows a slope similar to the Röttgers relationship however the low correlation between the slope and data does not indicate that the fit is of high quality.

The majority of the fit data shows slopes that are greater than that seen in the Röttgers study. The major factor between this study and that performed by Röttgers is the range of the data. The data for the Elbe samples in the Röttgers study create a large class range for scattering (*2<b<35*) as opposed to the limited range used for this study (Section 3.3.2.2). The extreme range of the scattering values may have played a role in difference seen between the simulation data and proposed correction.

As already noted the scattering coefficient plays a large role in the error of the absorption alongside the $\frac{b_b}{b}$. The $\frac{b_b}{b}$ value is not defined in the Röttgers study and restricts the analysis as it has already been ascertained that it is a driver of the measurement error. The analysis of the simulation classes notes that the slope of the fit to the data varies greatly with changes in $\frac{b_b}{b}$. The change is in line with the affect of the $\frac{b_b}{b}$ noted by the literature and Section 4.3.2 where the absorption error increases with the increased proportion of backscatter.

As there appears to be no correlation between the work of Röttgers, McKee and Woźniak (2013) and this study no direct conclusions can be made regarding the use of the proposed relationship. It is of note that due to the study by Röttgers, McKee and Woźniak (2013) using *in-situ* measurements there is likely to be little correlation between the simulation parameters in the classified datasets and *in-situ* results. As such, the conclusion drawn from the data is that the correction proposed by Röttgers, McKee and Woźniak (2013)

is valid for the data that it has been generated with. This is supported as the majority of the simulation data shows little correlation with the proposed correction across all elements of the simulations analysis.

5.5   Correction Procedure Creation

5.5.1   Limitations of AC-9 only Corrections

There are a number of limitations inherent in the usage of corrections that only utilise the measurements from the AC-9. The first and smallest of the limitations is the error creep that can occur if the instrument is not calibrated correctly or the base temperature and salinity calibration corrections are not applied to the results. This limitation is purely due to human error and as such cannot be effectively corrected other than through constant monitoring and quality control with regard to the operation of the AC-9.

Further to that, there is the limitation inherent in the measurement nature of the IOPs of the water sample which give rise to the requirement for the correction of the data. The scattering error is prevalent in the measurement of a, c and quantification of the amount of error introduced. The main driver of the error in both tubes of the AC-9 noted by the simulation results and analysis is $\frac{b_b}{b}$. The quantity of the error in the attenuation tube and the slope of the linear relationship for the absorption data is dependant on the magnitude of $\frac{b_b}{b}$.

The quantification of the errors particular to each individual sample is not a function that the AC-9 is able to perform. It's primary purpose is to measure a

and *c* values of a water sample, irrespective of the scattering error and as such can not provide the required information for a single measured wavelength to accurately account for the scattering error.

5.5.2 External Data Requirement

As the AC-9 does not provide enough data to facilitate the required correction of the *a* and *c*, external data is required to provide a link between the coefficients, the error and the nature of the error. McKee et al. (2013) note that the use of external data is time expensive and prohibitive but that it provides greater accuracy in the determination of the correct coefficients. The data created by this study also indicate that the usage of data external to the AC-9 is required to increase the accuracy of determination of a_t, b_t and c_t for the sample.

It is noted in Chapter 4 that the use of ω_{ms} provides a solid link between E_{fa}/E_{fc}, $\frac{b_b}{b}$ and hence the backscatter coefficient. It is also noted in Chapter 2 that the remotely sensed reflectance ($f(\lambda)$) is a function of ω_{ms} and a complex function of IOPs and other factors as represented by Equation 5.2 where $f(\lambda)$ is the complex IOP function.

$$R(\lambda) = f(\lambda) \times \omega_{ms} \tag{5.2}$$

By obtaining remotely sensed reflectance values and an estimation of the value of $f(\lambda)$ it is possible to obtain an estimated value of ω_{ms} by rearranging equation 5.2. The usage of this external data allows the usage of the models from Chapter 4 where the error factor is a function ω_{ms}. As the value of ω_{ms} can

be calculated by Equation 4.2 it is possible to obtain an estimation of the b_b which can then be used with the Iterative correction scheme from McKee, Piskozub and Brown (2008) or the improved method McKee et al. (2013).

5.5.3 Possible Correction Procedure

With the compilation of the simulated dataset prepared by this study and the evaluation with respect to the established and proposed methods completed the creation of a correction procedure was the final task to perform.

The first relationship that was not included in previous analysis is the relationship noted in Section 4.4 with respect to Δb calculated from the measured and true IOPs as a function of the c_m. Across the $\frac{b_b}{b}$ tested by the simulated data it was found there was a linear fit as per Equation 5.3 where Δb is the error in the measured scattering:

$$\Delta b = -0.3665 c_m \qquad (n = 364 \quad R^2 = 0.88896) \tag{5.3}$$

The value of Δb, while affected by $\frac{b_b}{b}$ swung between values as the error in the attenuation decreased and the error in the absorption increased as $\frac{b_b}{b}$ increased. This leant itself to being a candidate for a linear fit as the fits for the varied $\frac{b_b}{b}$ values swung around a single point. Equation 5.4 then allows the calculation of an estimate for b_t based off the estimation of the error calculated in Equation 5.3:

$$b = b_m + \Delta b \tag{5.4}$$

Use of this estimated b is reserved for the calculation of $\frac{b_b}{b}$ after calculation of

b_b through a modified form of equation 4.1 as shown through Equation 5.5:

$$b_b = \frac{\omega_m \times a_m}{1 - \omega_m} \qquad (5.5)$$

With the value of the backscattering ratio estimated it is possible to proceed

with two courses of action. The first is the use of the graphs shown in sections

4.2.4 and 4.3.5 and the associated coefficient calculations (Appendix F &

Appendix G) to calculate the error factor associated with each AC-9

measurement in the 715nm wavelength. The other the implementation of the

Iterative correction method from McKee, Piskozub and Brown (2008) to correct

the data.

The use of a combination of the methods could also be a viable alternative, as

this would provide for accuracy in the backscattering ratio through iteration that

could provide a better estimate for the error factor method. The base theory of

the method is shown in figure 5.2
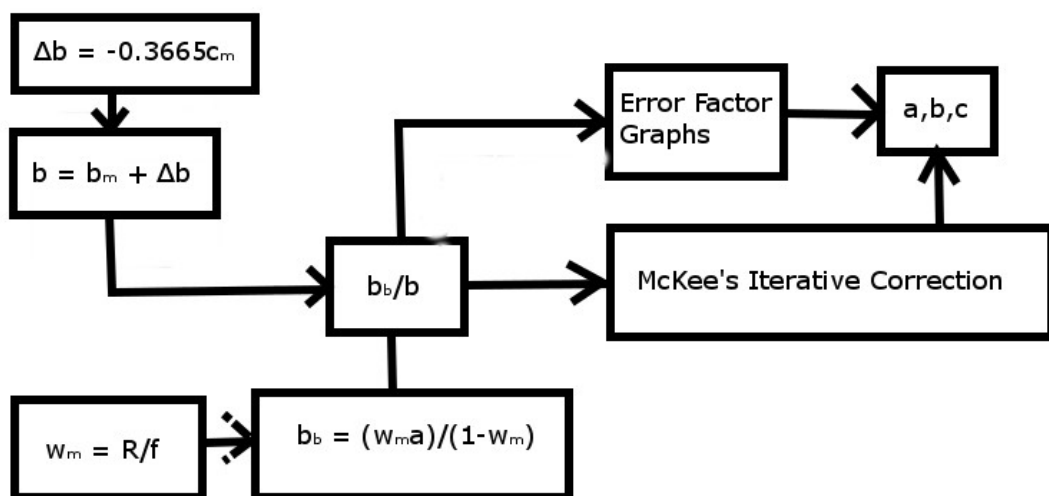
Figure 5.1 – Flow chart detailing correction procedure

5.5.4 Limitations of Correction

There are a number of limitations in the usage of the possible correction procedures discussed above. The first and most important of these limitations is the creation of the scattering error correction. The calculation of the error provides an estimation of the true scattering value and as such introduces error into the calculations. The calculation of ω_{ms} is also worked off estimations to provide and estimation ω_{ms} value. Usage of all measured values in the procedure introduces small amounts of error to the final result. The calculation of all values through the usage of the models requires the assumption that no error is being introduced into the calculations at any stage of the process and this is not correct.

Further simulations and the inclusion of *in-situ* measurements are required to test the validity of the relationships established and noted through the current simulated results. The inclusion of 'real-world' *in-situ* and remotely sensed reflectance data is also required to analyse the effectiveness in the field due to the assumptions used in the creation of the procedure.

5.6   Summary

This chapter has provided insight into the errors that are prevalent in *in-situ* measurements taken with the AC-9 and a base correction procedure for correction of the errors.

It has noted that the major driver in the AC-9 attenuation tube is the proportion of backscatter within the sample of water. As the proportion of backscatter in

the sample increases the amount of error that exists within the sample decreases. It also noted that there are a number of limitations with the models used to analyse and model the trends within the simulated dataset, which lead to overestimation of elements of the simulated results.

The absorption tube is more complex than that of the attenuation tube, showing no indication of a single error driver. Instead it was noted that the error was a combined function of the a, b and $\frac{b_b}{b}$. The model to account for the error factor in the absorption tube was limited due to the nature of the calculation required to obtain the error factor. This led to the reduction in the range of data analysed for the fit and leads to coverage of the error for a given range of ω_{ms}. The fit also systematically showed overestimation of the error for all $\frac{b_b}{b}$ values for small values of ω_{ms}, which also showed the smallest error factor value.

The simulated data set was compared to the relationships and models proposed in the creation of the iterative correction scheme (McKee, Piskozub & Brown 2008) with the simulations providing similar models to those from the iterative correction. Small differences were noted however it was noted that the IOP values simulated for the iterative method varied from those used in this study which would lead to the model differences.

The data was then broken down into classes based on the samples measured for the Absorption Correction scheme proposed by Röttgers, McKee and Woźniak (2013). It was noted that the simulated dataset would not provide the same results as seen by Röttgers, McKee and Woźniak (2013) due to the

difference between the simulations input and the *in-situ* measurements. It was also noted that the IOPs of the *in-situ* measurements did cover a range of scattering values that were not covered by the simulations run for this study which may have effected the simulation results.

The limitations of using only AC-9 data to perform a correction scheme were then noted, including the error drivers that prevented this usage of the data with $\frac{b_b}{b}$ providing the major driver of the error preventing the data from forming a correction method. The requirements of external data were briefly discussed due to the limitations of the AC-9, with the remotely sensed reflectance posed as a possible external data source for usage in the correction procedure.

Finally, the entire dataset and analysed trends were combined and noted as forming part of a larger procedure for the correction of AC-9 measurement data. The procedure uses the remotely sensed reflectance, a_m and c_m to allow for the calculation E_{fa} and E_{fc}. The limitations of the procedure were discussed with the assumption of no introduced error in the process being the major assumption that requires addressing. It was also noted that testing against real-world data is required to test a number of other assumptions in the procedure.

Chapter 6

Conclusion

6.1   Review Project Objectives

Remote sensing has become a major tool for the monitoring of particulate and dissolved matter in water bodies. The process requires accurate knowledge of the inherent optical properties of the water body and the process for determination of the quantified values introduces errors to the measured values.

This project set out to quantify the errors inherent in the measurement of the IOPs and evaluate current methods of correction with respect to simulated data for natural Australian waters, resulting in a combined correction scheme to account for the errors. This was achieved by:

1. Performing a literature review to identify and understand the following:

    i.   The Inherent Optical Properties of waters and how they interact with photons

    ii.   The relationship that exists between IOPs and the remote sensing process

    iii. The WETLabs AC-9 instrument, both its operation and the theory behind its use

    iv.   The pre-existing correction methods in use with AC-9 data

v.   The current research into correction methods to account for assumptions in pre-existing corrections

2. Designing a suite of simulations for an AC-9 instrument modelled in SimulO to generate experimental measurements.

3. Using the Experimental data, identify the primary drivers behind the error that is generated through operation of the AC-9 to measure IOP coefficients.

4. Having identified the primary error drivers, develop a correction scheme that can be implemented to account for the modelled errors.

The results of the project have allowed for the primary drivers of the measurement error to be identified as noted in sections 5.2.1 and 5.3.1 in line with the third research objective. The final element of the discussion from Chapter 5 (Section 5.5) takes the knowledge of the primary error drivers and the models generated to formulate a theoretical procedure for the correction of *in-situ* measurements.

The generated procedure, while theoretical, requires future evaluation to ensure that the procedure generates the results required and expected when used. It also makes use of result data that can be used to further benefit the field currently forming regarding the research of the errors inherent in *in-situ* measurements and the field of water body particulate concentration monitoring.

6.2   Project Conclusions

The results presented in Chapter 4 and the discussion in Chapter 5 note that there are a number of drivers for the AC-9 measurement error. These drivers are noted to be different between the absorption and attenuation tubes and affect the magnitude of the error differently. Several models were created to note the magnitude of the error observed in the simulated AC-9 measurements. The relationships established by the models were used to define the drivers of the error for each tube and how the drivers, where they exist in both tubes, act differently with respect to the magnitude of the error. $\frac{b_b}{b}$ was found to be the primary driver of the error with absorption also contributing in the attenuation tube while a combination of a, b and $\frac{b_b}{b}$ was found to be driving the error in the absorption tube.

The analysis also identified that further data was required to create viable relationships that could be used in further analysis. The extra data that was used was ω_{ms} as it was a measureable value due to its use in the calculation of remotely sensed reflectance and its relationship to b_b. By utilising $\frac{b_b}{b}$ and ω_{ms} in the analysis of the error in the measurements, relationships were established to account for the error attached to the simulated AC-9 results. The relationships established using this data, calculated from the simulation inputs, provided the indication as to the drivers of the error, with best-fit calculations providing a method of correction for the error.

Following the establishment of the models, analysis of the simulations data was undertaken against the data noted by McKee, Piskozub and Brown (2008)

and the trend noted Röttgers, McKee and Woźniak (2013). It was noted that the lack of relationship between the classified simulation results and the study by Röttgers was due to the differences between the *in-situ* measurements and the simulation data. The data calculated using the methods noted in McKee, Piskozub and Brown (2008) provided a high degree of visual correlation between the McKee study and the values calculated using the simulation results. It was noted that the differences between the datasets was due to the difference in the simulated IOPs between the studies, providing a small but measureable difference between the two studies.

With the differences between the simulation results and previous studies noted the correction procedure was proposed. It utilises an estimation of the scattering error to get an estimated scattering coefficient from the measured data. This is then combined with estimation process forming an estimation of ω_{ms} to calculate an estimate for b_b and $\frac{b_b}{b}$. Usage of this procedure can be combined with the base theory from McKee, Piskozub and Brown (2008) or the models from this study to account for the error in attenuation and absorption.

The procedure does not provide a definitive error correction method due to limitations in the creation of the procedure and its assumptions. This procedure is designed to be a base system that can be built on to provide a solid and robust correction method.

6.3   Further Research

Further research into the data presented fall into a number of categories due to the nature of the data and analysis.

The creation of a dataset particular to in-situ measurements from Röttgers, McKee and Woźniak (2013) is required for further testing in relation to the proposed correction method. The dataset utilised in this study did not allow for substantial evaluation against the previous studies data as the particular combinations of *a* and *b* could not be replicated.

Integration of *in-situ* measurements to the evaluation of the correction procedure is also required. As the correction procedure is based off limited simulation data the integration of real-world measurements is required to test the limits of the correction procedure. As the correction procedure also requires the use of remotely sensed reflectance values the inclusion into the database of information for testing would benefit the proposed procedure. The inclusion of this information will also enable more conclusive testing of the limits of the procedure.

As the absorption error is particularly sensitive to the changes of the absorption and scattering coefficients further analysis is required with emphasis on water body types to ascertain if particular ranges of the coefficients produce different relationships where the samples are overly scattering or absorption dominant.

Finally, all of the testing requires further investigation across a greater range of $\frac{b_b}{b}$ values to determine if there are areas where $\frac{b_b}{b}$ fails to maintain the relationships established in this study. Through further analysis particular to the values seen in Australian natural waters and the world a correction method can be established to account for error to a high degree of known accuracy.

List of References

Aas, E, Høkedal, J & Sørensen, K 2005, 'Spectral backscattering coefficient in coastal waters', *International Journal of Remote Sensing*, vol. 26, no. 2, pp. 331-43.

Arst, H & Arst, KIU 2003, *Optical properties and remote sensing of multicomponental water bodies*, Springer.

Barnard, AH, Pegau, WS & Zaneveld, JRV 1998, 'Global relationships of the inherent optical properties of the oceans', *Journal of Geophysical Research: Oceans (1978–2012)*, vol. 103, no. C11, pp. 24955-68, viewed 10 April 2014.

Bukata, RP, Jerome, JH, Kondratyev, AS & Pozdnyakov, DV 1995, *Optical properties and remote sensing of inland and coastal waters*, CRC press.

Campbell, G, Phinn, SR & Daniel, P 2011, 'The specific inherent optical properties of three sub-tropical and tropical water reservoirs in Queensland, Australia', *Hydrobiologia*, vol. 658, no. 1, pp. 233-52.

Fournier, GR & Forand, JL 1994, 'Analytic phase function for ocean water', in Ocean Optics XII: *proceedings of theOcean Optics XII* International Society for Optics and Photonics, pp. 194-201.

Freda, W & Piskozub, J 2007, 'Improved method of Fournier-Forand marine phase function parameterization', *Optics express*, vol. 15, no. 20, pp. 12763-8, viewed 7 April 2014.

Herlevi, A 2002, 'A study of scattering, backscattering and a hyperspectral reflectance model for boreal waters', *Geophysica*, vol. 38, no. 1-2, pp. 113-32.

Kirk, JTO 1992, 'Monte Carlo modeling of the performance of a reflective tube absorption meter', *Applied optics*, vol. 31, no. 30, viewed 20 April 2013.

Leathers, RA, Downes, TV & Davis, CO 2000, 'Analysis of a point-source integrating-cavity absorption meter', *Applied optics*, vol. 39, no. 33, pp. 6118-27.

Lee, Z, Carder, KL, Mobley, CD, Steward, RG & Patch, JS 1999, 'Hyperspectral remote sensing for shallow waters. 2. Deriving bottom depths and water properties by optimization', *Applied optics*, vol. 38, no. 18, pp. 3831-43.

Leymarie, E 2005, User Manual for the 3D Monte Carlo Program SimulO, *ver 1.1*.

Leymarie, E, Doxaran, D & Babin, M 2010, 'Uncertainties associated to measurements of inherent optical properties in natural waters', *Applied optics*, vol. 49, no. 28, pp. 5415-36.

McKee, D, Piskozub, J & Brown, I 2008, 'Scattering error corrections for in situ absorption and attenuation measurements', *Optics express*, vol. 16, no. 24, pp. 19480-92.

McKee, D, Piskozub, J, Röttgers, R & Reynolds, RA 2013, 'Evaluation and Improvement of an Iterative Scattering Correction Scheme for in situ Absorption and Attenuation Measurements', *Journal of Atmospheric & Oceanic Technology*, vol. 30, no. 7, pp. 1527-41, viewed 8 April 2014, EBSCOhost, iih, item: 89306425.

Niederreiter, H 1978, 'Quasi-Monte Carlo methods and pseudo-random numbers', *Bulletin of the American Mathematical Society*, vol. 84, no. 6, pp. 957-1041.

Paavel, B, Arst, H & Herlevi, A 2007, 'Dependence of spectral distribution of inherent optical properties of lake waters on the concentrations of different water constituents', *Nordic Hydrology*, vol. 38, no. 3, pp. 265-85, EBSCOhost, a9h, item: 26152816.

Pegau, WS, Zaneveld, JRV & Voss, KJ 1995, 'Toward closure of the inherent optical properties of natural waters', *Journal of Geophysical Research: Oceans (1978–2012)*, vol. 100, no. C7, pp. 13193-9, viewed 10 April 2014.

Pegau, WS, Gray, D & Zaneveld, JRV 1997, 'Absorption and attenuation of visible and near-infrared light in water: dependence on temperature and salinity', *Applied optics*, vol. 36, no. 24, pp. 6035-46, viewed 10 April 2014.

Piskozub, J & McKee, D 2011, 'Effective scattering phase functions for the multiple scattering regime', *Optics express*, vol. 19, no. 5, pp. 4786-94.

Piskozub, J, Stramski, D, Terrill, E & Melville, WK 2004, 'Influence of forward and multiple light scatter on the measurement of beam attenuation in highly scattering marine environments', *Applied optics*, vol. 43, no. 24, pp. 4723-31.

Röttgers, R, McKee, D & Woźniak, SB 2013, 'Evaluation of scatter corrections for ac-9 absorption measurements in coastal waters', *Methods in Oceanography*.

Stramski, D & Piskozub, J 2003, 'Estimation of scattering error in spectrophotometric measurements of light absorption by aquatic particles from three-dimensional radiative transfer simulations', *Applied optics*, vol. 42, no. 18, pp. 3634-46.

Tzortziou, M, Subramaniam, A, Herman, JR, Gallegos, CL, Neale, PJ & Harding Jr, LW 2007, 'Remote sensing reflectance and inherent optical properties in the mid Chesapeake Bay', *Estuarine, Coastal and Shelf Science*, vol. 72, no. 1–2, pp. 16-32.

Ulloa, O, Sathyendranath, S & Platt, T 1994, 'Effect of the particle-size distribution on the backscattering ratio in seawater', *Applied optics*, vol. 33, no. 30, pp. 7070-7, viewed 10 April 2014.

Voss, KJ & Austin, RW 1993, 'Beam-attenuation measurement error due to small-angle scattering acceptance', *Journal of Atmospheric and Oceanic Technology*, vol. 10, no. 1, pp. 113-21, viewed 10 April 2014.

WET Labs Inc. 2006, *Absorption and Attenuation Meter (ac-9) User's Manual (Revision O)*, Western Environmental Technologies Laboratories (WETLabs), Philomath, OR,<.

WETLabs Inc. 2004, *ac-9 plus Specifications Sheet, Revision G*, <http://www.otronix.com/kr/data/p06/ac9plus_brochure.pdf%3E.

WETLabs Inc. 2005, *ac-9 Protocol Document (Revision J)*, Western Environmental Technologies Laboratories (WETLabs), Philomath, OR,<.

Zaneveld, JRV, Kitchen, JC & Moore, CC 1994, 'Scattering error correction of reflecting-tube absorption meters', in Ocean Optics XII: *proceedings of theOcean Optics XII* International Society for Optics and Photonics, pp. 44-55.

List of Appendices

Appendix A – Project Specification

Appendix B – SimulO Input Script Code

Appendix C – IDL Processing Code

Appendix D – Simulation Set 1 Results

Appendix E – Simulation Set 2 Results

Appendix F – Attenuation Fit Coefficients and Graphs

Appendix G – Absorption Fit Coefficients and Graphs

Appendix H – ω_{ms} Limit Calculation

Appendix I – Röttgers Sample Graphs

Appendix A – Project Specification

University of Southern Queensland

FACULTY OF HEALTH, ENGINEERING AND SCIENCE

SCHOOL OF ENGINEERING AND BUILT ENVIRONMENT

ENG4111/4112 Research Project
Project Specification

FOR: Alex Darton

TOPIC: Quantification of the measurement error associated with *in situ* measurements of water absorption and attenuation using the AC-9 instrument.

SUPERVISORS: Dr Glenn Campbell

PROJECT AIM: The aim of this project is to quantify and establish error bounds on the inherent optical properties obtained from *in situ* measurements using the AC-9 instrument.

PROGRAMME: **Issue A, 15th March 2014**

1. Research the background literature on the absorption and scattering of photons in water and the effect on spectral reflectance.
2. Design simulations using Simul0 software to obtain spectral values for absorption, scattering, volume scatter function and backscatter ratios.
3. Analyse simulation results to identify the primary drivers creating the error.
4. Develop correction regime to allow for the established error
5. Submit dissertation reporting findings

AGREED:

_____ (Student) _____ (Supervisor)
      Date: / / 2014   Date: / / 2014

Examiner/Co-Examiner:_____

Appendix B – SimuIO Input Script

```
MaxPhoton=1E7;

IntervalPhoton=MaxPhoton/20;

Path="C:\Users\u1019481\Documents\";

FileName=Path+"ResultSet1a.txt";

InputFile=Path+"Set1a.txt";

WriteToFile[FileName,"lambda","Sample","a","b","c","FF","Detecteur","NbrPhot
on","DetecPath","N0Diff","N1Diff","N2Diff","N3Diff","N3pDiff"];

wave=0;

RefSample=0;

a=0;

b=0;

c=0;

ff=0;

Irep=0;

Ld:ILig=1;

ReadFloatFromFile[InputFile,@wave,ILig,0];

La:ReadFloatFromFile[InputFile,@RefSample,ILig,1];

ReadFloatFromFile[InputFile,@a,ILig,2];

ReadFloatFromFile[InputFile,@b,ILig,3];

ReadFloatFromFile[InputFile,@ff,ILig,4];

c=a+b

BulkPropertiesWizard["water",wave,a,b,ff];

RunSimul;

WriteToFile[FileName,wave,RefSample,a,b,c,ff,Detecteur/NbrPhoton,NbrPhot
on,DetecPath,N0Diff,N1Diff,N2Diff,N3Diff,N3pDiff];

ILig=ILig+1;

ReadFloatFromFile[InputFile,@wave,ILig,0];

if wave>0 then La;

Irep=Irep+1;

if Irep<5 then La;
```

Appendix C – IDL Processing Code

```
pro Read_Simulo
;fnames = file_search('H:\Simulo\01891', 'FileAFF_backr_650*.txt')
fnames = file_search('F:\Logs', 'Set1*.txt')

File_no = n_elements(fnames)
File_name_short = strarr(File_no)
Photons = dblarr(File_no)
Av_Path_length = dblarr(File_no)
No_scat = dblarr(File_no)
One_scat = dblarr(File_no)
Two_scat = dblarr(File_no)
Three_scat = dblarr(File_no)
Three_plus_scat = dblarr(File_no)
BoiteImp = dblarr(File_no)
MasqueInAbs = dblarr(File_no)
QuartzImp = dblarr(File_no)
MasqueOutAbs = dblarr(File_no)
Detect_total = dblarr(File_no)
Detect= dblarr(File_no)
wl = fltarr(File_no)
A = fltarr(File_no)
B = fltarr(File_no)
C = fltarr(File_no)
bb = fltarr(File_no)

for i = 0, File_no-1 do begin
    line = ''
    ; DO SOMETHING ABOUT SAVING THE FILENAME
    temp =strsplit(fnames(i),'\',/extract,/preserve_null)
    x = n_elements(temp)
    File_name_short(i) = temp(x-1)
    openr, 40,fnames(i)
    for j = 0, 3 do begin
          readf,40,line
    endfor
    temp =strsplit(line,'=',/extract,/preserve_null)
    if temp(0) eq 'Photons_count' then Photons(i) = temp(1)
```

Figure C.1 – IDL code for processing Simulation Set 1 Absorption tube results part 1

118

```
readf,40,line
readf,40,line
readf,40,line
temp =strsplit(line,'=',/extract,/preserve_null)
if temp(0) eq 'Average_pathLength' then Av_Path_length(i) = temp(1)
readf,40,line
readf,40,line
temp =strsplit(line,'=',/extract,/preserve_null)
if temp(0) eq 'Photon_count_with_0_ScattEvent' then No_scat(i) = temp(1)
readf,40,line
temp =strsplit(line,'=',/extract,/preserve_null)
if temp(0) eq 'Photon_count_with_1_ScattEvent' then One_scat(i) = temp(1)
readf,40,line
temp =strsplit(line,'=',/extract,/preserve_null)
if temp(0) eq 'Photon_count_with_2_ScattEvent' then Two_scat(i) = temp(1)
readf,40,line
temp =strsplit(line,'=',/extract,/preserve_null)
if temp(0) eq 'Photon_count_with_3_ScattEvent' then Three_scat(i) = temp(1)
readf,40,line
temp =strsplit(line,'=',/extract,/preserve_null)
if temp(0) eq 'Photon_count_withMore_3_ScattEvent' then Three_plus_scat(i) = temp(1)
for j = 14, 19 do begin
     readf,40,line
endfor
temp =strsplit(line,'=',/extract,/preserve_null)
if temp(0) eq 'Boite Abs Cylinder_Internal' then BoiteImp(i) = temp(1)
for j = 20, 48 do begin
     readf,40,line
endfor
temp =strsplit(line,'=',/extract,/preserve_null)
if temp(0) eq 'MasqueIn Abs Cylinder_Internal' then MasqueInAbs(i) = temp(1)
for j = 49, 85 do begin
     readf,40,line
endfor
temp =strsplit(line,'=',/extract,/preserve_null)
if temp(0) eq 'TubeQuartz Imp Cylinder_Internal' then QuartzImp(i) = temp(1)
for j = 86, 114 do begin
```

Figure C.2 – IDL code for processing Simulation Set 1 Absorption tube results part 2

```
        readf,40,line
    endfor
    temp =strsplit(line,'=',/extract,/preserve_null)
    if temp(0) eq 'MasqueOut Abs Cylinder_Internal' then MasqueOutAbs(i) = temp(1)
    for j = 115, 237 do begin
        readf,40,line
    endfor
    temp =strsplit(line,'=',/extract,/preserve_null)
    if temp(0) eq 'Detec Imp Disc_Inf_External' then Detect_total(i) = temp(1)
    for j = 238, 256 do begin
        readf,40,line
    endfor
    temp =strsplit(line,'=',/extract,/preserve_null)
    if temp(0) eq 'Detec Imp<60 Disc_Inf_External' then Detect(i) = temp(1)

    for j = 257, 423 do begin
        readf,40,line
    endfor
    temp =strsplit(line,';',/extract,/preserve_null)
    if temp(0) eq 'BulkInfo=(BTDIFFUSION' then begin
        wl(i) = float(temp(5))
        a(i) = float(temp(6))
        b(i) = float(temp(7))
        c(i)= float(temp(6)) + float(temp(7))
        if c(i) gt 49.0 then stop
    endif
    readf,40,line
    temp =strsplit(line,';',/extract,/preserve_null)
    if temp(0) eq 'ScatteringFct=(Eau + Fournier-Forand' then bb(i) = temp(1)
    close,40
endfor
stop
index = sort(a)
File_name_short = File_name_short(index)
Photons = Photons(index)
Av_Path_length = Av_Path_length(index)
```

Figure C.3 – IDL code for processing Simulation Set 1 Absorption tube results part 3

```
No_scat = No_scat(index)
One_scat = One_scat(index)
Two_scat = Two_scat(index)
Three_scat = Three_scat(index)
Three_plus_scat = Three_plus_scat(index)
BoiteImp = BoiteImp(index)
MasqueInAbs = MasqueInAbs (index)
QuartzImp = QuartzImp(index)
MasqueOutAbs = MasqueOutAbs(index)
Detect_total = Detect_total(index)
Detect= Detect(index)
wl = wl(index)
A = A(index)
B = B(index)
C = C(index)
bb = bb(index)


means = fltarr(File_no/5,18)
stdevs = fltarr(File_no/5,18)
a_vals = a(uniq(a))
temp = b(sort(b))
b_vals = temp(uniq(temp))
count = 0
for i = 0, N_elements(a_vals)-1 do begin
For j = 0, N_elements(b_vals)-1 do begin
means(count,0) = a_vals(i)
means(count,1) = b_vals(j)
stdevs(count,0) = a_vals(i)
stdevs(count,1) = b_vals(j)
index = where((a eq a_vals(i)) and (b eq b_vals(j)))
means(count,2) = mean(Photons(index))
means(count,3) = mean(Av_Path_length(index))
means(count,4) = mean(No_scat(index))
means(count,5) = mean(One_scat(index))
means(count,6) = mean(Two_scat(index))
means(count,7) = mean(Three_scat(index))
```

Figure C.4 – IDL code for processing Simulation Set 1 Absorption tube results part 4

```
means(count,7) = mean(Three_scat(index))
means(count,8) = mean(Three_plus_scat(index))
means(count,9) = mean(BoiteImp(index))
means(count,10) = mean(MasqueInAbs(index))
means(count,11) = mean(MasqueOutAbs(index))
means(count,12) = mean(QuartzImp(index))
means(count,13) = mean(MasqueOutAbs(index))
means(count,14) = mean(Detect_total(index))
means(count,15) = mean(wl(index))
means(count,16) = mean(C(index))
means(count,17) = mean(bb(index))
stdevs(count,2) = stdev(Photons(index))
stdevs(count,3) = stdev(Av_Path_length(index))
stdevs(count,4) = stdev(No_scat(index))
stdevs(count,5) = stdev(One_scat(index))
stdevs(count,6) = stdev(Two_scat(index))
stdevs(count,7) = stdev(Three_scat(index))
stdevs(count,8) = stdev(Three_plus_scat(index))
stdevs(count,9) = stdev(BoiteImp(index))
stdevs(count,10) = stdev(MasqueInAbs(index))
stdevs(count,11) = stdev(MasqueOutAbs(index))
stdevs(count,12) = stdev(QuartzImp(index))
stdevs(count,13) = stdev(MasqueOutAbs(index))
stdevs(count,14) = stdev(Detect_total(index))
stdevs(count,15) = stdev(wl(index))
stdevs(count,16) = stdev(C(index))
stdevs(count,17) = stdev(bb(index))
count = count+1
endfor
endfor

save, Photons,Av_Path_length,No_scat,One_scat,Two_scat,Three_scat,Three_plus_scat,BoiteImp, ...
MasqueInAbs,QuartzImp,MasqueOutAbs,Detect_total,Detect,wl,A,B,C,bb,File_name_short,means,stdevs, filename = 'c:\Simulo_output.sav'


end
```

Figure C.5 – IDL code for processing Simulation Set 1 Absorption tube results part 5

122

```
pro Read_Simulo_a_c
;fnames = file_search('H:\Simulo\01891', 'FileAFF_backr_650*.txt')
;fnames = file_search('C:\Users\u1019481\Documents\a1cLogs', 'Set1*.txt')
fnames = file_search('C:\Users\campbelg\Desktop\Thesis - C-Tube', 'Set1*.txt')
File_no = n_elements(fnames)
File_name_short = strarr(File_no)
Photons = dblarr(File_no)
Av_Path_length = dblarr(File_no)
No_scat = dblarr(File_no)
One_scat = dblarr(File_no)
Two_scat = dblarr(File_no)
Three_scat = dblarr(File_no)
Three_plus_scat = dblarr(File_no)
BoiteImp = dblarr(File_no)
MasqueInAbs = dblarr(File_no)
QuartzImp = dblarr(File_no)
MasqueOutAbs = dblarr(File_no)
Detect_total = dblarr(File_no)
Detect= dblarr(File_no)
wl = fltarr(File_no)
A = fltarr(File_no)
B = fltarr(File_no)
C = fltarr(File_no)
bb = fltarr(File_no)

for i = 0, File_no-1 do begin
    line = ''
    ; DO SOMETHING ABOUT SAVING THE FILENAME
    temp =strsplit(fnames(i),'\',/extract,/preserve_null)
    x = n_elements(temp)
    File_name_short(i) = temp(x-1)
    openr, 40,fnames(i)
    for j = 0, 3 do begin
        readf,40,line
    endfor
    temp =strsplit(line,'=',/extract,/preserve_null)
    if temp(0) eq 'Photons_count' then Photons(i) = temp(1)
```

Figure C.6 – IDL code for processing Simulation Set 1 Attenuation tube results part 1

123

```
readf,40,line
readf,40,line
readf,40,line
temp =strsplit(line,'=',/extract,/preserve_null)
if temp(0) eq 'Average_pathLength' then Av_Path_length(i) = temp(1)
readf,40,line
readf,40,line
temp =strsplit(line,'=',/extract,/preserve_null)
if temp(0) eq 'Photon_count_with_0_ScattEvent' then No_scat(i) = temp(1)
readf,40,line
temp =strsplit(line,'=',/extract,/preserve_null)
if temp(0) eq 'Photon_count_with_1_ScattEvent' then One_scat(i) = temp(1)
readf,40,line
temp =strsplit(line,'=',/extract,/preserve_null)
if temp(0) eq 'Photon_count_with_2_ScattEvent' then Two_scat(i) = temp(1)
readf,40,line
temp =strsplit(line,'=',/extract,/preserve_null)
if temp(0) eq 'Photon_count_with_3_ScattEvent' then Three_scat(i) = temp(1)
readf,40,line
temp =strsplit(line,'=',/extract,/preserve_null)
if temp(0) eq 'Photon_count_withMore_3_ScattEvent' then Three_plus_scat(i) = temp(1)
for j = 14, 26 do begin
      readf,40,line
endfor
temp =strsplit(line,'=',/extract,/preserve_null)
if temp(0) eq 'Boite Abs Cylinder_Internal' then BoiteImp(i) = temp(1)
for j = 27, 127 do begin
      readf,40,line
endfor
;   temp =strsplit(line,'=',/extract,/preserve_null)
;   if temp(0) eq 'MasqueIn Abs Cylinder_Internal' then MasqueInAbs(i) = temp(1)
;   for j = 49, 85 do begin
;         readf,40,line
;   endfor
;   temp =strsplit(line,'=',/extract,/preserve_null)
;   if temp(0) eq 'TubeQuartz Imp Cylinder_Internal' then QuartzImp(i) = temp(1)
;   for j = 86, 114 do begin
```

Figure C.7 – IDL code for processing Simulation Set 1 Attenuation tube results part 2

124

```
;          readf,40,line
;     endfor
;     temp =strsplit(line,'=',/extract,/preserve_null)
;     if temp(0) eq 'MasqueOut Abs Cylinder_Internal' then MasqueOutAbs(i) = temp(1)
;     for j = 115, 237 do begin
;          readf,40,line
;     endfor

     temp =strsplit(line,'=',/extract,/preserve_null)
     if temp(0) eq 'Detec Imp Disc_Inf_External' then Detect_total(i) = temp(1)
     for j = 127, 145 do begin
          readf,40,line
     endfor
     temp =strsplit(line,'=',/extract,/preserve_null)
     if temp(0) eq 'Detec Imp<1.2 Disc_Inf_External' then Detect(i) = temp(1)

     for j = 146, 202 do begin
          readf,40,line
     endfor
     temp =strsplit(line,';',/extract,/preserve_null)
     if temp(0) eq 'BulkInfo=(BTDIFFUSION' then begin
          wl(i) = float(temp(5))
          a(i) = float(temp(6))
          b(i) = float(temp(7))
          c(i)= float(temp(6)) + float(temp(7))
          if c(i) gt 49.0 then stop
     endif
     readf,40,line
     temp =strsplit(line,';',/extract,/preserve_null)
     if temp(0) eq 'ScatteringFct=(Eau + Fournier-Forand' then bb(i) = temp(1)
     close,40
 endfor
;stop
index = sort(a)
stop
File_name_short = File_name_short(index)
Photons = Photons(index)
```

Figure C.8 – IDL code for processing Simulation Set 1 Attenuation tube results part 3

125

```
Av_Path_length = Av_Path_length(index)
No_scat = No_scat(index)
One_scat = One_scat(index)
Two_scat = Two_scat(index)
Three_scat = Three_scat(index)
Three_plus_scat = Three_plus_scat(index)
BoiteImp = BoiteImp(index)
;MasqueInAbs = MasqueInAbs (index)
;QuartzImp = QuartzImp(index)
;MasqueOutAbs = MasqueOutAbs(index)
Detect_total = Detect_total(index)
Detect= Detect(index)
wl = wl(index)
A = A(index)
B = B(index)
C = C(index)
bb = bb(index)

stop
means = fltarr(File_no/5,15)
stdevs = fltarr(File_no/5,15)
a_vals = a(uniq(a))
temp = b(sort(b))
b_vals = temp(uniq(temp))
count = 0
for i = 0, N_elements(a_vals)-1 do begin
For j = 0, N_elements(b_vals)-1 do begin
means(count,0) = a_vals(i)
means(count,1) = b_vals(j)
stdevs(count,0) = a_vals(i)
stdevs(count,1) = b_vals(j)
index = where((a eq a_vals(i)) and (b eq b_vals(j)))
stop
means(count,2) = mean(Photons(index))
means(count,3) = mean(Av_Path_length(index))
means(count,4) = mean(No_scat(index))
means(count,5) = mean(One_scat(index))
```

Figure C.9 – IDL code for processing Simulation Set 1 Attenuation tube results part 4

```
means(count,6) = mean(Two_scat(index))
means(count,7) = mean(Three_scat(index))
means(count,8) = mean(Three_plus_scat(index))
means(count,9) = mean(BoiteImp(index))
;means(count,10) = mean(MasqueInAbs(index))
;means(count,11) = mean(MasqueOutAbs(index))
;means(count,12) = mean(QuartzImp(index))
;means(count,13) = mean(MasqueOutAbs(index))
means(count,10) = mean(Detect_total(index))
means(count,11) = mean(wl(index))
means(count,12) = mean(C(index))
means(count,13) = mean(bb(index))
means(count,14) = mean(Detect(index))
stdevs(count,2) = stdev(Photons(index))
stdevs(count,3) = stdev(Av_Path_length(index))
stdevs(count,4) = stdev(No_scat(index))
stdevs(count,5) = stdev(One_scat(index))
stdevs(count,6) = stdev(Two_scat(index))
stdevs(count,7) = stdev(Three_scat(index))
stdevs(count,8) = stdev(Three_plus_scat(index))
stdevs(count,9) = stdev(BoiteImp(index))
;stdevs(count,10) = stdev(MasqueInAbs(index))
;stdevs(count,11) = stdev(MasqueOutAbs(index))
;stdevs(count,12) = stdev(QuartzImp(index))
;stdevs(count,13) = stdev(MasqueOutAbs(index))
stdevs(count,10) = stdev(Detect_total(index))
stdevs(count,11) = stdev(wl(index))
stdevs(count,12) = stdev(C(index))
stdevs(count,13) = stdev(bb(index))
stdevs(count,14) = stdev(Detect(index))
count = count+1
endfor
endfor


reducedC = fltarr(File_no/5,1)
Kc = fltarr(File_no/5,1)


for i=0, 322 do begin
  purewater = 0.836897976
  reducedC(i,0) = -alog((means(i,14)/means(i,2))/purewater)/0.1
endfor
for i=0, 322 do begin
  Kc(i,0) = ABS((means(i,0)-reducedC(i,0))/means(i,1))
endfor

save, Photons,Av_Path_length,No_scat,One_scat,Two_scat,Three_scat,Three_plus_scat,BoiteImp,...
Detect_total,Detect,wl,A,B,C,bb,File_name_short,means,stdevs,reducedC,Kc,...
filename = 'C:\Users\campbelg\Desktop\Thesis - C-Tube\Simulo_output_a_c.sav'
stop
end
```

Figure C.10 – IDL code for processing Simulation Set 1 Attenuation tube results part 5

```
pro Read_Simulo_a_2
;fnames = file_search('H:\Simulo\01891', 'FileAFF_backr_650*.txt')
fnames = file_search('C:\Users\u1019481\Documents\Logs 2a', 'Set2*.txt')

File_no = n_elements(fnames)
File_name_short = strarr(File_no)
Photons = dblarr(File_no)
Av_Path_length = dblarr(File_no)
No_scat = dblarr(File_no)
One_scat = dblarr(File_no)
Two_scat = dblarr(File_no)
Three_scat = dblarr(File_no)
Three_plus_scat = dblarr(File_no)
BoiteImp = dblarr(File_no)
MasqueInAbs = dblarr(File_no)
QuartzImp = dblarr(File_no)
MasqueOutAbs = dblarr(File_no)
Detect_total = dblarr(File_no)
Detect= dblarr(File_no)
wl = fltarr(File_no)
A = fltarr(File_no)
B = fltarr(File_no)
C = fltarr(File_no)
bb = fltarr(File_no)

for i = 0, File_no-1 do begin
    line = ''
    ; DO SOMETHING ABOUT SAVING THE FILENAME
    temp =strsplit(fnames(i),'\',/extract,/preserve_null)
    x = n_elements(temp)
    File_name_short(i) = temp(x-1)
    openr, 40,fnames(i)
    for j = 0, 3 do begin
         readf,40,line
    endfor
    temp =strsplit(line,'=',/extract,/preserve_null)
    if temp(0) eq 'Nbr De Photon' then Photons(i) = temp(1)
```

Figure C.11 – IDL code for processing Simulation Set 2 Absorption tube results part 1

```
readf,40,line
readf,40,line
readf,40,line
temp =strsplit(line,'=',/extract,/preserve_null)
if temp(0) eq 'PathLengthAv' then Av_Path_length(i) = temp(1)
readf,40,line
readf,40,line
temp =strsplit(line,'=',/extract,/preserve_null)
if temp(0) eq 'Nbr photons avec 0 diff' then No_scat(i) = temp(1)
readf,40,line
temp =strsplit(line,'=',/extract,/preserve_null)
if temp(0) eq 'Nbr photons avec 1 diff' then One_scat(i) = temp(1)
readf,40,line
temp =strsplit(line,'=',/extract,/preserve_null)
if temp(0) eq 'Nbr photons avec 2 diff' then Two_scat(i) = temp(1)
readf,40,line
temp =strsplit(line,'=',/extract,/preserve_null)
if temp(0) eq 'Nbr photons avec 3 diff' then Three_scat(i) = temp(1)
readf,40,line
temp =strsplit(line,'=',/extract,/preserve_null)
if temp(0) eq 'Nbr photons avec plus de 3 diff' then Three_plus_scat(i) = temp(1)
for j = 14, 19 do begin
      readf,40,line
endfor
temp =strsplit(line,'=',/extract,/preserve_null)
Result = STRMATCH( temp(0), 'Boite Abs Cylindre Int*rieur')
if result then BoiteImp(i) = temp(1)
for j = 20, 48 do begin
      readf,40,line
endfor
temp =strsplit(line,'=',/extract,/preserve_null)
Result = STRMATCH( temp(0), 'MasqueIn Abs Cylindre Int*rieur')
if result then MasqueInAbs(i) = temp(1)
for j = 49, 85 do begin
      readf,40,line
endfor
temp =strsplit(line,'=',/extract,/preserve_null)
```

Figure C.12 – IDL code for processing Simulation Set 2 Absorption tube results part 2

```
Result = STRMATCH( temp(0), 'TubeQuartz Imp Cylindre Int*rieur')
if result then QuartzImp(i) = temp(1)
for j = 86, 114 do begin
      readf,40,line
endfor
temp =strsplit(line,'=',/extract,/preserve_null)
Result = STRMATCH( temp(0), 'MasqueOut Abs Cylindre Int*rieur')
if result then MasqueOutAbs(i) = temp(1)
for j = 115, 237 do begin
      readf,40,line
endfor
temp =strsplit(line,'=',/extract,/preserve_null)
Result = STRMATCH( temp(0), 'Detec Imp Disque Inf Ext*rieur')
;if temp(0) eq 'Detec Imp Disque Inf Extérieur' then Detect_total(i) = temp(1)
if result then Detect_total(i) = temp(1)
for j = 238, 256 do begin
      readf,40,line
endfor
temp =strsplit(line,'=',/extract,/preserve_null)
    Result = STRMATCH( temp(0), 'Detec Imp<60 Disque Inf Ext*rieur')
if result then Detect(i) = temp(1)

for j = 257, 423 do begin
      readf,40,line
endfor
temp =strsplit(line,';',/extract,/preserve_null)
if temp(0) eq 'BulkInfo=(BTDIFFUSION' then begin
      wl(i) = float(temp(5))
      a(i) = float(temp(6))
      b(i) = float(temp(7))
      c(i)= float(temp(6)) + float(temp(7))
      if c(i) gt 49.0 then stop
endif
readf,40,line
temp =strsplit(line,';',/extract,/preserve_null)
if temp(0) eq 'ScatteringFct=(Eau + Fournier-Forand' then bb(i) = temp(1)
close,40
```

Figure C.13 – IDL code for processing Simulation Set 2 Absorption tube results part 3

```
endfor
;stop
index = sort(bb)
File_name_short = File_name_short(index)
Photons = Photons(index)
Av_Path_length = Av_Path_length(index)
No_scat = No_scat(index)
One_scat = One_scat(index)
Two_scat = Two_scat(index)
Three_scat = Three_scat(index)
Three_plus_scat = Three_plus_scat(index)
BoiteImp = BoiteImp(index)
MasqueInAbs = MasqueInAbs (index)
QuartzImp = QuartzImp(index)
MasqueOutAbs = MasqueOutAbs(index)
Detect_total = Detect_total(index)
Detect= Detect(index)
wl = wl(index)
A = A(index)
B = B(index)
C = C(index)
bb = bb(index)

;stop
means = fltarr(File_no/5,19)
stdevs = fltarr(File_no/5,19)
bb_vals = bb(uniq(bb))
temp = b(sort(b))
b_vals = temp(uniq(temp))

count = 0
for i = 0, N_elements(bb_vals)-1 do begin
For j = 0, N_elements(b_vals)-1 do begin
;stop
index = where((bb eq bb_vals(i)) and (b eq b_vals(j)))
temp = a(index)
temp = temp(sort(temp))
```

Figure C.14 – IDL code for processing Simulation Set 2 Absorption tube results part 4

```
a_vals = temp(uniq(temp))
;stop
For k = 0, N_elements(a_vals)-1 do begin
  index2 = where(a(index) eq a_vals(k))
means(count,0) = bb_vals(i)
means(count,1) = b_vals(j)
stdevs(count,0) = bb_vals(i)
stdevs(count,1) = b_vals(j)
means(count,2) = mean(Photons(index(index2)))
means(count,3) = mean(Av_Path_length(index(index2)))
means(count,4) = mean(No_scat(index(index2)))
means(count,5) = mean(One_scat(index(index2)))
means(count,6) = mean(Two_scat(index(index2)))
means(count,7) = mean(Three_scat(index(index2)))
means(count,8) = mean(Three_plus_scat(index(index2)))
means(count,9) = mean(BoiteImp(index(index2)))
means(count,10) = mean(MasqueInAbs(index(index2)))
means(count,11) = mean(MasqueOutAbs(index(index2)))
means(count,12) = mean(QuartzImp(index(index2)))
means(count,13) = mean(MasqueOutAbs(index(index2)))
means(count,14) = mean(Detect_total(index(index2)))
means(count,15) = mean(wl(index(index2)))
means(count,16) = mean(C(index(index2)))
means(count,17) = mean(a(index(index2)))
means(count,18) = mean(Detect(index(index2)))
stdevs(count,2) = stdev(Photons(index(index2)))
stdevs(count,3) = stdev(Av_Path_length(index(index2)))
stdevs(count,4) = stdev(No_scat(index(index2)))
stdevs(count,5) = stdev(One_scat(index(index2)))
stdevs(count,6) = stdev(Two_scat(index(index2)))
stdevs(count,7) = stdev(Three_scat(index(index2)))
stdevs(count,8) = stdev(Three_plus_scat(index(index2)))
stdevs(count,9) = stdev(BoiteImp(index(index2)))
stdevs(count,10) = stdev(MasqueInAbs(index(index2)))
stdevs(count,11) = stdev(MasqueOutAbs(index(index2)))
stdevs(count,12) = stdev(QuartzImp(index(index2)))
stdevs(count,13) = stdev(MasqueOutAbs(index(index2)))
```

Figure C.15 – IDL code for processing Simulation Set 2 Absorption tube results part 5

```
stdevs(count,14) = stdev(Detect_total(index(index2)))
stdevs(count,15) = stdev(wl(index(index2)))
stdevs(count,16) = stdev(C(index(index2)))
stdevs(count,17) = stdev(a(index(index2)))
stdevs(count,18) = stdev(Detect(index(index2)))
count = count+1
endfor
endfor
endfor


reducedA = fltarr(File_no/5,1)
Ka = fltarr(File_no/5,1)
;stop
for i=0, (File_no/5)-1 do begin
  purewater = 0.836897976
  reducedA(i,0) = -alog((means(i,18)/means(i,2))/purewater)/0.1
endfor
for i=0, (File_no/5)-1 do begin
  Ka(i,0) = ABS((means(i,17)-reducedA(i,0))/means(i,1))
  ;Think I'm getting the same problem here
  ;Except I'm getting ~0.4 for the correction value
endfor
meansA = means
stop
save, Photons,Av_Path_length,No_scat,One_scat,Two_scat,Three_scat,Three_plus_scat,...
BoiteImp,MasqueInAbs,QuartzImp,MasqueOutAbs,Detect_total,Detect,wl,A,B,C,bb,File_name_short,...
means,stdevs,reducedA,Ka, filename = 'C:\Users\u1019481\Documents\IDL\Simulo_output_a.sav'
save, meansA, reducedA, Ka, filename = 'C:\Users\u1019481\Documents\IDL\A_means.sav'
end
```

Figure C.16 – IDL code for processing Simulation Set 2 Absorption tube results part 6

```
pro Read_Simulo_a_c_2
;fnames = file_search('H:\Simulo\01891', 'FileAFF_backr_650*.txt')
fnames = file_search('C:\Users\u1019481\Documents\Logs 2c', 'Set2*.txt')
;fnames = file_search('C:\Users\campbelg\Desktop\Thesis - C-Tube 2\Logs Set 1 c-tube', 'Set1*.txt')
File_no = n_elements(fnames)
File_name_short = strarr(File_no)
Photons = dblarr(File_no)
Av_Path_length = dblarr(File_no)
No_scat = dblarr(File_no)
One_scat = dblarr(File_no)
Two_scat = dblarr(File_no)
Three_scat = dblarr(File_no)
Three_plus_scat = dblarr(File_no)
BoiteImp = dblarr(File_no)
MasqueInAbs = dblarr(File_no)
QuartzImp = dblarr(File_no)
MasqueOutAbs = dblarr(File_no)
Detect_total = dblarr(File_no)
Detect= dblarr(File_no)
wl = fltarr(File_no)
A = fltarr(File_no)
B = fltarr(File_no)
C = fltarr(File_no)
bb = fltarr(File_no)
;stop
for i = 0, File_no-1 do begin
    line = ''
    ; DO SOMETHING ABOUT SAVING THE FILENAME
    temp =strsplit(fnames(i),'\',/extract,/preserve_null)
    x = n_elements(temp)
    File_name_short(i) = temp(x-1)
    openr, 40,fnames(i)
    for j = 0, 3 do begin
        readf,40,line
    endfor
    temp =strsplit(line,'=',/extract,/preserve_null)
    if temp(0) eq 'Nbr De Photon' then Photons(i) = temp(1)
```

Figure C.17 – IDL code for processing Simulation Set 2 Attenuation tube results part 1

```
     readf,40,line
     readf,40,line
     readf,40,line
     temp =strsplit(line,'=',/extract,/preserve_null)
     if temp(0) eq 'PathLengthAv' then Av_Path_length(i) = temp(1)
     readf,40,line
     readf,40,line
     temp =strsplit(line,'=',/extract,/preserve_null)
     if temp(0) eq 'Nbr photons avec 0 diff' then No_scat(i) = temp(1)
     readf,40,line
     temp =strsplit(line,'=',/extract,/preserve_null)
     if temp(0) eq 'Nbr photons avec 1 diff' then One_scat(i) = temp(1)
     readf,40,line
     temp =strsplit(line,'=',/extract,/preserve_null)
     if temp(0) eq 'Nbr photons avec 2 diff' then Two_scat(i) = temp(1)
     readf,40,line
     temp =strsplit(line,'=',/extract,/preserve_null)
     if temp(0) eq 'Nbr photons avec 3 diff' then Three_scat(i) = temp(1)
     readf,40,line
     temp =strsplit(line,'=',/extract,/preserve_null)
     if temp(0) eq 'Nbr photons avec plus de 3 diff' then Three_plus_scat(i) = temp(1)
     for j = 14, 26 do begin
          readf,40,line
     endfor
     temp =strsplit(line,'=',/extract,/preserve_null)
     Result = STRMATCH( temp(0), 'Boite Abs Cylindre Int*rieur')
     if result then BoiteImp(i) = temp(1)
;     if temp(0) eq 'Boite Abs Cylindre Intérieur' then print, 'bob'; BoiteImp(i) = temp(1)
     for j = 27, 127 do begin
          readf,40,line
     endfor
;     temp =strsplit(line,'=',/extract,/preserve_null)
;     if temp(0) eq 'MasqueIn Abs Cylinder_Internal' then MasqueInAbs(i) = temp(1)
;     for j = 49, 85 do begin
;          readf,40,line
;     endfor
;     temp =strsplit(line,'=',/extract,/preserve_null)
```

Figure C.18 – IDL code for processing Simulation Set 2 Attenuation tube results part 2

135

```
;     if temp(0) eq 'TubeQuartz Imp Cylinder_Internal' then QuartzImp(i) = temp(1)
;     for j = 86, 114 do begin
;         readf,40,line
;     endfor
;     temp =strsplit(line,'=',/extract,/preserve_null)
;     if temp(0) eq 'MasqueOut Abs Cylinder_Internal' then MasqueOutAbs(i) = temp(1)
;     for j = 115, 237 do begin
;         readf,40,line
;     endfor

    temp =strsplit(line,'=',/extract,/preserve_null)
    Result = STRMATCH( temp(0), 'Detec Imp Disque Inf Ext*rieur')
    ;if temp(0) eq 'Detec Imp Disque Inf Extérieur' then Detect_total(i) = temp(1)
    if result then Detect_total(i) = temp(1)
    for j = 127, 145 do begin
        readf,40,line
    endfor
    temp =strsplit(line,'=',/extract,/preserve_null)
        Result = STRMATCH( temp(0), 'Detec Imp<1.2 Disque Inf Ext*rieur')
    if result then Detect(i) = temp(1)
;    if temp(0) eq 'Detec Imp<1.2 Disque Inf Extérieur' then Detect(i) = temp(1)

    for j = 146, 202 do begin
        readf,40,line
    endfor
    temp =strsplit(line,';',/extract,/preserve_null)
    if temp(0) eq 'BulkInfo=(BTDIFFUSION' then begin
        wl(i) = float(temp(5))
        a(i) = float(temp(6))
        b(i) = float(temp(7))
        c(i)= float(temp(6)) + float(temp(7))
        if c(i) gt 49.0 then stop
    endif
    readf,40,line
    temp =strsplit(line,';',/extract,/preserve_null)
    if temp(0) eq 'ScatteringFct=(Eau + Fournier-Forand' then bb(i) = temp(1)
    close,40
```

Figure C.19 – IDL code for processing Simulation Set 2 Attenuation tube results part 3

```
endfor
;stop
index = sort(bb)
File_name_short = File_name_short(index)
Photons = Photons(index)
Av_Path_length = Av_Path_length(index)
No_scat = No_scat(index)
One_scat = One_scat(index)
Two_scat = Two_scat(index)
Three_scat = Three_scat(index)
Three_plus_scat = Three_plus_scat(index)
BoiteImp = BoiteImp(index)
;MasqueInAbs = MasqueInAbs (index)
;QuartzImp = QuartzImp(index)
;MasqueOutAbs = MasqueOutAbs(index)
Detect_total = Detect_total(index)
Detect= Detect(index)
wl = wl(index)
A = A(index)
B = B(index)
C = C(index)
bb = bb(index)

;stop
means = fltarr(File_no/5,15)
stdevs = fltarr(File_no/5,15)
bb_vals = bb(uniq(bb))
temp = b(sort(b))
b_vals = temp(uniq(temp))
count = 0
for i = 0, N_elements(bb_vals)-1 do begin
For j = 0, N_elements(b_vals)-1 do begin
index = where((bb eq bb_vals(i)) and (b eq b_vals(j)))
;stop
temp = a(index)
temp = temp(sort(temp))
a_vals = temp(uniq(temp))
```

Figure C.20 – IDL code for processing Simulation Set 2 Attenuation tube results part 4

```
;stop
For k = 0, N_elements(a_vals)-1 do begin
means(count,0) = bb_vals(i)
means(count,1) = b_vals(j)
stdevs(count,0) = bb_vals(i)
stdevs(count,1) = b_vals(j)
   index2 = where(a(index) eq a_vals(k))
means(count,2) = mean(Photons(index(index2)))
means(count,3) = mean(Av_Path_length(index(index2)))
means(count,4) = mean(No_scat(index(index2)))
means(count,5) = mean(One_scat(index(index2)))
means(count,6) = mean(Two_scat(index(index2)))
means(count,7) = mean(Three_scat(index(index2)))
means(count,8) = mean(Three_plus_scat(index(index2)))
means(count,9) = mean(BoiteImp(index(index2)))
;means(count,10) = mean(MasqueInAbs(index(index2)))
;means(count,11) = mean(MasqueOutAbs(index(index2)))
;means(count,12) = mean(QuartzImp(index(index2)))
;means(count,13) = mean(MasqueOutAbs(index(index2)))
means(count,10) = mean(Detect_total(index(index2)))
means(count,11) = mean(wl(index(index2)))
means(count,12) = mean(C(index(index2)))
means(count,13) = mean(a(index(index2)))
means(count,14) = mean(Detect(index(index2)))
stdevs(count,2) = stdev(Photons(index(index2)))
stdevs(count,3) = stdev(Av_Path_length(index(index2)))
stdevs(count,4) = stdev(No_scat(index(index2)))
stdevs(count,5) = stdev(One_scat(index(index2)))
stdevs(count,6) = stdev(Two_scat(index(index2)))
stdevs(count,7) = stdev(Three_scat(index(index2)))
stdevs(count,8) = stdev(Three_plus_scat(index(index2)))
stdevs(count,9) = stdev(BoiteImp(index(index2)))
;stdevs(count,10) = stdev(MasqueInAbs(index(index2)))
;stdevs(count,11) = stdev(MasqueOutAbs(index(index2)))
;stdevs(count,12) = stdev(QuartzImp(index(index2)))
;stdevs(count,13) = stdev(MasqueOutAbs(index(index2)))
stdevs(count,10) = stdev(Detect_total(index(index2)))
```

Figure C.21 – IDL code for processing Simulation Set 2 Attenuation tube results part 5

```
stdevs(count,11) = stdev(wl(index(index2)))
stdevs(count,12) = stdev(C(index(index2)))
stdevs(count,13) = stdev(a(index(index2)))
stdevs(count,14) = stdev(Detect(index(index2)))
count = count+1
endfor
endfor
endfor


reducedC = fltarr(File_no/5)
Kc = fltarr(File_no/5)

for i=0, (File_no/5)-1 do begin
  purewater = 0.82717888 ;correct value from c-tube simulations
  reducedC(i) = -alog((means(i,14)/means(i,2))/purewater)/0.1
endfor
for i=0, (File_no/5)-1 do begin
  Kc(i) = ABS((reducedC(i)-means(i,12))/means(i,1))
  ;I think this is better. Just not sure if it's outputting correctly
  ;getting 0.25 for Kc now, had to reduce Bb to 0.015 though
endfor
meansC = means

save, Photons,Av_Path_length,No_scat,One_scat,Two_scat,Three_scat,Three_plus_scat,BoiteImp,...
Detect_total,Detect,wl,A,B,C,bb,File_name_short,means,stdevs,reducedC,Kc,...
filename = 'C:\Users\u1019481\Documents\IDL\Simulo_output_a_c.sav'
save, meansC, reducedC, Kc, filename = 'C:\Users\u1019481\Documents\IDL\C_means.sav'
stop
end
```

Figure C.22 – IDL code for processing Simulation Set 2 Attenuation tube results part 6

Appendix D – Simulation Set 1 Results

0.01	0.05	0.1	0.15	0.2	0.3
0.01	0.05	0.1	0.15	0.2	0.3
0.01	0.05	0.1	0.15	0.2	0.3
0.01	0.05	0.1	0.15	0.2	0.3
0.01	0.05	0.1	0.15	0.2	0.3
0.01	0.05	0.1	0.15	0.2	0.3
0.01	0.05	0.1	0.15	0.2	0.3
0.01	0.05	0.1	0.15	0.2	0.3
0.01	0.05	0.1	0.15	0.2	0.3
0.01	0.05	0.1	0.15	0.2	0.3
0.01	0.05	0.1	0.15	0.2	0.3
0.01	0.05	0.1	0.15	0.2	0.3
0.01	0.05	0.1	0.15	0.2	0.3
0.01	0.05	0.1	0.15	0.2	0.3
0.01	0.05	0.1	0.15	0.2	0.3
0.01	0.05	0.1	0.15	0.2	0.3
0.01	0.05	0.1	0.15	0.2	0.3
0.01	0.05	0.1	0.15	0.2	0.3

Figure D.1 – Absorption Values for Series 1-6

0.4	0.6	0.8	1	1.2	1.4
0.4	0.6	0.8	1	1.2	1.4
0.4	0.6	0.8	1	1.2	1.4
0.4	0.6	0.8	1	1.2	1.4
0.4	0.6	0.8	1	1.2	1.4
0.4	0.6	0.8	1	1.2	1.4
0.4	0.6	0.8	1	1.2	1.4
0.4	0.6	0.8	1	1.2	1.4
0.4	0.6	0.8	1	1.2	1.4
0.4	0.6	0.8	1	1.2	1.4
0.4	0.6	0.8	1	1.2	1.4
0.4	0.6	0.8	1	1.2	1.4
0.4	0.6	0.8	1	1.2	1.4
0.4	0.6	0.8	1	1.2	1.4
0.4	0.6	0.8	1	1.2	1.4
0.4	0.6	0.8	1	1.2	1.4
0.4	0.6	0.8	1	1.2	1.4
0.4	0.6	0.8	1	1.2	1.4

Figure D.2 – Absorption Values for Series 7-12

1.6	1.8	2	2.5	3	4
1.6	1.8	2	2.5	3	4
1.6	1.8	2	2.5	3	4
1.6	1.8	2	2.5	3	4
1.6	1.8	2	2.5	3	4
1.6	1.8	2	2.5	3	4
1.6	1.8	2	2.5	3	4
1.6	1.8	2	2.5	3	4
1.6	1.8	2	2.5	3	4
1.6	1.8	2	2.5	3	4
1.6	1.8	2	2.5	3	4
1.6	1.8	2	2.5	3	4
1.6	1.8	2	2.5	3	4
1.6	1.8	2	2.5	3	4
1.6	1.8	2	2.5	3	4
1.6	1.8	2	2.5	3	4
1.6	1.8	2	2.5	3	4
1.6	1.8	2	2.5	3	4

Figure D.3 – Absorption Values for series 13-18

0.0001
0.1
0.25
0.5
0.75
1
1.25
1.5
2
2.5
3
3.5
4
5
7
9
11
15

Figure D.4 – Scattering Values for Series 1-18

0.009596	0.048751	0.099382	0.150636	0.200856	0.299801
0.08372	0.126027	0.173341	0.224657	0.274831	0.374429
0.19739	0.236732	0.286827	0.337099	0.387644	0.486
0.383676	0.424193	0.472987	0.523722	0.572805	0.672866
0.571519	0.60952	0.659503	0.712078	0.75976	0.859266
0.757268	0.795854	0.847823	0.898382	0.946365	1.047733
0.943336	0.984119	1.034499	1.084375	1.134215	1.234684
1.130301	1.168369	1.220509	1.269973	1.323143	1.422843
1.504167	1.544475	1.593782	1.645505	1.6948	1.793342
1.877483	1.916935	1.966627	2.01623	2.069129	2.16843
2.250034	2.291092	2.339226	2.390972	2.440284	2.542047
2.624099	2.66209	2.712433	2.761934	2.811636	2.914333
2.994353	3.036875	3.085212	3.134866	3.183455	3.284945
3.742224	3.77827	3.828786	3.879866	3.929883	4.02851
5.225912	5.267313	5.316269	5.366833	5.413058	5.512268
6.707614	6.748796	6.799041	6.845445	6.899422	6.995332
8.189987	8.225289	8.27857	8.32719	8.375926	8.47821
11.134943	11.177529	11.224462	11.272573	11.325432	11.426435

Figure D.5 – Cm for series 1-6

0.39894	0.599645	0.799429	0.998371	1.19955	1.399802
0.474297	0.674909	0.87482	1.075477	1.273332	1.475111
0.587546	0.787321	0.986815	1.185586	1.385208	1.588457
0.773734	0.973094	1.173243	1.374254	1.575298	1.774431
0.960063	1.161319	1.360327	1.560274	1.75966	1.961434
1.14706	1.347079	1.546428	1.748247	1.949206	2.147494
1.333722	1.535554	1.734064	1.93421	2.132283	2.332639
1.5193	1.720265	1.920853	2.120487	2.321398	2.519297
1.894125	2.094296	2.294113	2.495567	2.69393	2.894605
2.267591	2.466331	2.666133	2.867874	3.067191	3.265098
2.639827	2.838843	3.039828	3.239329	3.440983	3.640159
3.013782	3.212466	3.412138	3.612093	3.812974	4.010007
3.385813	3.58375	3.785738	3.987105	4.186949	4.386904
4.131402	4.32833	4.528758	4.730865	4.928613	5.130558
5.614561	5.816124	6.015777	6.212146	6.415246	6.616035
7.098104	7.300465	7.497671	7.698829	7.894541	8.099646
8.579197	8.77622	8.976798	9.177583	9.376396	9.575461
11.523528	11.724467	11.924234	12.12439	12.329954	12.525169

Figure D.6 – Cm for series 7-12

1.599714	1.799392	2.002115	2.501184	3.001483	3.999429
1.67458	1.873389	2.076105	2.575148	3.075921	4.076193
1.786652	1.986349	2.18723	2.686937	3.188029	4.187295
1.974006	2.175104	2.375356	2.873285	3.372766	4.374748
2.161287	2.361075	2.561044	3.059786	3.560173	4.562106
2.348984	2.548041	2.745645	3.248793	3.748681	4.748576
2.533931	2.73358	2.934282	3.435702	3.936418	4.931147
2.720934	2.920534	3.120595	3.619191	4.121093	5.119451
3.095046	3.294935	3.493459	3.995138	4.493756	5.493266
3.467263	3.668893	3.867249	4.365765	4.868176	5.868595
3.841061	4.042274	4.240982	4.739964	5.240285	6.241024
4.211949	4.413109	4.612545	5.112715	5.613954	6.613036
4.585461	4.784728	4.984845	5.484869	5.983388	6.986156
5.331404	5.529634	5.73021	6.231647	6.729367	7.730427
6.81429	7.017993	7.21425	7.718211	8.214036	9.214797
8.296652	8.501602	8.697626	9.199016	9.701096	10.698523
9.777865	9.977808	10.176332	10.679685	11.17773	12.17966
12.723676	12.925154	13.12608	13.622936	14.123292	15.121294

Figure D.7 – Cm for series 13-18

0.010201	0.049776	0.099846	0.149508	0.199964	0.301737
0.018844	0.059319	0.109594	0.159299	0.208336	0.309307
0.032652	0.073747	0.123375	0.173236	0.223284	0.324316
0.054842	0.095226	0.145848	0.196595	0.245776	0.346234
0.079011	0.118346	0.169523	0.219614	0.268575	0.369039
0.102405	0.142057	0.191897	0.242005	0.291092	0.392703
0.124326	0.164715	0.21549	0.26481	0.315029	0.414618
0.146594	0.189058	0.237029	0.286447	0.338043	0.438829
0.193216	0.232734	0.282174	0.33344	0.384296	0.483452
0.238736	0.278387	0.328706	0.378704	0.428402	0.528223
0.283407	0.323977	0.373691	0.424854	0.475142	0.573126
0.328056	0.370244	0.418944	0.470401	0.51847	0.61832
0.374599	0.414333	0.464178	0.514615	0.564197	0.664369
0.465528	0.504996	0.555095	0.604426	0.654869	0.753696
0.646738	0.687073	0.735609	0.785049	0.833757	0.933394
0.82524	0.863613	0.913676	0.963521	1.014681	1.11139
1.001418	1.041574	1.090231	1.139952	1.191502	1.289205
1.354531	1.39357	1.443858	1.491108	1.541502	1.638807

Figure D.8 – a$_m$ for series 1-6

0.399515	0.601791	0.801395	1.00236	1.202225	1.401699
0.408414	0.611147	0.810477	1.010176	1.21104	1.41156
0.423486	0.624204	0.821792	1.024742	1.223771	1.425635
0.446421	0.647486	0.846448	1.04677	1.247185	1.446412
0.468798	0.669313	0.869716	1.069813	1.269886	1.469781
0.492262	0.693063	0.892503	1.092274	1.292544	1.493585
0.514228	0.713519	0.91514	1.115075	1.314506	1.51514
0.537158	0.73748	0.937977	1.138451	1.339036	1.536636
0.581941	0.783299	0.982121	1.182376	1.38185	1.581781
0.628602	0.826777	1.028426	1.228182	1.426382	1.628106
0.673339	0.873739	1.074046	1.271199	1.473043	1.671839
0.718171	0.919481	1.115916	1.317565	1.518333	1.717553
0.763369	0.964333	1.163201	1.362671	1.561727	1.761083
0.854702	1.053002	1.252824	1.452111	1.652417	1.851036
1.033233	1.232629	1.431312	1.627954	1.828402	2.027549
1.211442	1.409821	1.607394	1.805947	2.004144	2.202859
1.389025	1.587758	1.784444	1.981555	2.179587	2.377428
1.739184	1.937278	2.136404	2.331404	2.529341	2.727007

Figure D.9 – a$_m$ for series 7-12

1.604553	1.804041	2.000852	2.504404	3.00318	4.006068
1.612551	1.812696	2.012894	2.51338	3.013706	4.01322
1.625686	1.82494	2.024353	2.525348	3.028693	4.029649
1.647353	1.847112	2.048006	2.549211	3.048426	4.048664
1.669683	1.870678	2.071098	2.57206	3.071871	4.072423
1.69203	1.893382	2.093741	2.59224	3.092113	4.09328
1.713717	1.916424	2.115778	2.615579	3.114886	4.113281
1.737689	1.938623	2.137367	2.636809	3.135183	4.135163
1.781268	1.9841	2.183005	2.681451	3.180882	4.178026
1.82656	2.027455	2.224598	2.724122	3.225104	4.22447
1.872085	2.072963	2.271594	2.770685	3.270928	4.265826
1.915688	2.115028	2.314781	2.814838	3.313733	4.309451
1.960427	2.16018	2.358762	2.857805	3.356048	4.352773
2.049106	2.247524	2.447789	2.945763	3.444576	4.439188
2.22748	2.424481	2.623802	3.120682	3.618964	4.611587
2.401795	2.601261	2.798714	3.295459	3.791092	4.782213
2.577287	2.773917	2.972996	3.467257	3.959701	4.954433
2.924067	3.120807	3.318836	3.814182	4.303844	5.294468

Figure D.10 – a$_m$ for series 13-18

0.049883	0.026933	0.00717	0.003574	0.003776	0.000996
0.238912	0.159818	0.133295	0.101371	0.083896	0.063927
0.240806	0.210894	0.180494	0.157253	0.13857	0.116364
0.247694	0.228739	0.211689	0.194273	0.181707	0.158918
0.248002	0.2381	0.224115	0.208803	0.200253	0.181652
0.25023	0.242044	0.229252	0.218798	0.211363	0.194051
0.25132	0.242986	0.233704	0.225446	0.217783	0.20343
0.251457	0.246213	0.237182	0.230319	0.22168	0.209531
0.251658	0.246597	0.241056	0.234649	0.229636	0.220286
0.251999	0.248261	0.243605	0.239158	0.233656	0.225561
0.252481	0.248822	0.245411	0.240961	0.237411	0.229683
0.252393	0.250116	0.246546	0.243306	0.240098	0.23307
0.253279	0.250154	0.247509	0.244611	0.242034	0.236059
0.253049	0.251828	0.249258	0.246628	0.244253	0.239904
0.254506	0.252863	0.25123	0.249394	0.248186	0.244895
0.255537	0.254277	0.252853	0.251864	0.250063	0.247814
0.256132	0.25563	0.254183	0.253167	0.252149	0.249716
0.258165	0.257307	0.256658	0.255936	0.254906	0.253174

Figure D.11 – Attenuation Error Factor for series 1-6

0.002898	0.000758	0.000838	0.001729	0.000458	0.000213
0.051405	0.035844	0.027977	0.022294	0.020514	0.016593
0.096083	0.07374	0.060176	0.051531	0.044684	0.037299
0.140296	0.115369	0.097506	0.083831	0.073354	0.066089
0.165163	0.139763	0.12237	0.108415	0.09761	0.087705
0.180672	0.158076	0.140873	0.125877	0.113997	0.105211
0.191684	0.169971	0.154115	0.140351	0.12968	0.119759
0.200368	0.180826	0.164847	0.151805	0.140223	0.131277
0.210781	0.194501	0.180674	0.168144	0.158147	0.148646
0.218072	0.204409	0.192081	0.180608	0.17103	0.162795
0.22358	0.211433	0.200045	0.190168	0.180718	0.172691
0.227236	0.216472	0.20648	0.197313	0.188729	0.181631
0.230497	0.220924	0.211305	0.202579	0.194817	0.18761
0.234925	0.227084	0.21918	0.211523	0.205062	0.19835
0.241276	0.234721	0.228747	0.223482	0.217653	0.212377
0.244882	0.239535	0.234932	0.230117	0.226025	0.221188
0.247439	0.243429	0.239254	0.235201	0.231443	0.227785
0.251719	0.248432	0.245302	0.242226	0.238892	0.23627

Figure D.12 – Attenuation Error Factor for Series 7-12

0.000241	0.000393	0.001007	0.000434	0.000461	0.000168
0.014953	0.014006	0.011379	0.009559	0.007767	0.005806
0.034242	0.031049	0.027898	0.022932	0.019068	0.014754
0.059997	0.054303	0.049858	0.042238	0.036353	0.027834
0.080304	0.074088	0.068711	0.058528	0.05062	0.039557
0.096545	0.089985	0.084785	0.071773	0.06283	0.050285
0.110901	0.103744	0.097144	0.083813	0.073784	0.060734
0.122279	0.11499	0.108402	0.095202	0.084202	0.069191
0.140265	0.132912	0.126635	0.112191	0.101249	0.084456
0.154326	0.146769	0.140611	0.126847	0.114877	0.097139
0.164987	0.15786	0.151804	0.138188	0.126619	0.108425
0.174128	0.167338	0.161355	0.147881	0.136315	0.118262
0.181168	0.175047	0.169192	0.156174	0.14523	0.126731
0.192211	0.186818	0.181399	0.169114	0.158829	0.141064
0.207641	0.202501	0.198417	0.187557	0.178596	0.162291
0.217297	0.212815	0.209307	0.200086	0.191575	0.177037
0.223979	0.220484	0.217205	0.208912	0.201591	0.188023
0.233514	0.230646	0.227878	0.221547	0.215373	0.204142

Figure D.13 – Attenuation Error factor for Series 13-18

0.020117	0.884447	2.265163	4.484214	6.901091	9.240538
0.004477	0.18639	0.474942	0.904515	1.366928	1.841137
0.001542	0.095944	0.233748	0.458482	0.695229	0.918968
0.00328	0.061993	0.154907	0.310635	0.464094	0.613369
0.00018	0.04168	0.11642	0.228878	0.342875	0.455458
0.005789	0.031022	0.081055	0.154113	0.230129	0.309011
0.001211	0.021035	0.058714	0.116052	0.171994	0.230654
0.002984	0.018578	0.040339	0.079143	0.115522	0.155105
0.001744	0.013096	0.02724	0.05806	0.087144	0.115628
0.00236	0.010176	0.024742	0.04677	0.069813	0.092274
0.001854	0.0092	0.019809	0.039321	0.058239	0.07712
0.001214	0.008257	0.018311	0.033151	0.049843	0.066846
0.002845	0.007844	0.016054	0.029595	0.043552	0.057519
0.002245	0.007054	0.013856	0.026174	0.039266	0.051879
0.000426	0.006447	0.012177	0.024003	0.035549	0.046871
0.001762	0.005352	0.010139	0.019684	0.028824	0.036896
0.00106	0.004569	0.009564	0.016142	0.023957	0.030704
0.001517	0.003305	0.007412	0.012166	0.018106	0.02332

Figure D.14 – Absorption Error Factor for Series 1-6

146

11.432591	13.6594	18.321596	22.873583	27.340729	31.805624
2.294295	2.781158	3.65469	4.567744	5.479543	6.404882
1.154895	1.370285	1.821742	2.28706	2.736912	3.189442
0.765401	0.909648	1.222931	1.524695	1.832362	2.136004
0.575146	0.690217	0.921482	1.142012	1.375709	1.592348
0.38206	0.462762	0.611505	0.760743	0.910421	1.061066
0.285569	0.342895	0.454851	0.571505	0.683347	0.795427
0.189198	0.229134	0.305498	0.377961	0.456231	0.532468
0.143925	0.172471	0.227652	0.285532	0.342558	0.394895
0.115075	0.138451	0.182376	0.228182	0.271199	0.317565
0.095422	0.115863	0.151541	0.188652	0.227536	0.265277
0.082243	0.097597	0.129844	0.162933	0.194171	0.226824
0.071073	0.086056	0.113293	0.1416	0.170053	0.197305
0.06468	0.077013	0.102278	0.126364	0.151646	0.175016
0.057889	0.068684	0.091502	0.112299	0.135797	0.157391
0.046231	0.054724	0.07258	0.089649	0.108274	0.125935
0.038295	0.045061	0.060294	0.075035	0.090309	0.104578
0.02832	0.033791	0.044506	0.056117	0.066456	0.077363

Figure D.15 – Absorption Error for series 7-12

36.459888	45.552814	63.673759	81.523979	99.141754	134.453125
7.286654	9.099924	12.74145	16.272253	19.831476	26.871393
3.641776	4.550945	6.356092	8.136757	9.902306	13.438575
2.430764	3.029504	4.233659	5.423471	6.599677	8.940722
1.820984	2.274346	3.168785	4.073403	4.95751	6.707512
1.214564	1.51232	2.111312	2.704635	3.297348	4.46269
0.908422	1.136755	1.583084	2.028605	2.472563	3.34796
0.607222	0.755003	1.054381	1.349702	1.646263	2.228797
0.454002	0.56603	0.78914	1.009242	1.230555	1.670505
0.362671	0.452111	0.627954	0.805947	0.981555	1.331404
0.301439	0.377014	0.523668	0.67012	0.816322	1.107785
0.257916	0.322169	0.448249	0.573471	0.698163	0.947862
0.225267	0.280691	0.392175	0.501122	0.610804	0.827542
0.2001	0.248624	0.346934	0.445145	0.541065	0.733782
0.179381	0.223894	0.311901	0.399357	0.486498	0.659418
0.143122	0.178305	0.248273	0.318184	0.386903	0.525673
0.118683	0.148192	0.206321	0.263697	0.3199	0.434615
0.088193	0.109797	0.152897	0.195553	0.238608	0.323617

Figure D.16 – Absorption Error for Series 13-18

0.00014998	2.99991E-05	1.49998E-05	9.9999E-06	7.49994E-06	4.99998E-06
0.13043478	0.029126214	0.014778325	0.00990099	0.007444169	0.004975124
0.27272727	0.069767442	0.036144578	0.02439024	0.018404908	0.012345679
0.42857143	0.130434783	0.069767442	0.04761905	0.036144578	0.024390244
0.52941176	0.183673469	0.101123596	0.06976744	0.053254438	0.036144578
0.6	0.230769231	0.130434783	0.09090909	0.069767442	0.047619048
0.65217391	0.272727273	0.157894737	0.11111111	0.085714286	0.058823529
0.69230769	0.310344828	0.183673469	0.13043478	0.101123596	0.069767442
0.75	0.375	0.230769231	0.16666667	0.130434783	0.090909091
0.78947368	0.428571429	0.272727273	0.2	0.157894737	0.111111111
0.81818182	0.473684211	0.310344828	0.23076923	0.183673469	0.130434783
0.84	0.512195122	0.344262295	0.25925926	0.207920792	0.14893617
0.85714286	0.545454545	0.375	0.28571429	0.230769231	0.166666667
0.88235294	0.6	0.428571429	0.33333333	0.272727273	0.2
0.91304348	0.677419355	0.512195122	0.41176471	0.344262295	0.259259259
0.93103448	0.72972973	0.574468085	0.47368421	0.402985075	0.310344828
0.94285714	0.76744186	0.622641509	0.52380952	0.452054795	0.35483871
0.95744681	0.818181818	0.692307692	0.6	0.529411765	0.428571429

Figure D.17 - ω_{ms} values for Series 1-6

3.74999E-06	2.49999E-06	1.875E-06	1.5E-06	1.25E-06	1.07143E-06
0.00373599	0.002493766	0.00187149	0.00149775	0.00124844	0.001070282
0.009287926	0.00621118	0.00466563	0.00373599	0.00311526	0.002671416
0.018404908	0.012345679	0.00928793	0.00744417	0.00621118	0.005328597
0.027355623	0.018404908	0.01386749	0.01112485	0.00928793	0.007971656
0.036144578	0.024390244	0.01840491	0.01477833	0.01234568	0.010600707
0.044776119	0.03030303	0.02290076	0.01840491	0.01538462	0.013215859
0.053254438	0.036144578	0.02735562	0.02200489	0.01840491	0.015817223
0.069767442	0.047619048	0.03614458	0.02912621	0.02439024	0.020979021
0.085714286	0.058823529	0.04477612	0.03614458	0.03030303	0.026086957
0.101123596	0.069767442	0.05325444	0.0430622	0.03614458	0.031141869
0.116022099	0.08045977	0.06158358	0.04988124	0.04191617	0.036144578
0.130434783	0.090909091	0.06976744	0.05660377	0.04761905	0.04109589
0.157894737	0.111111111	0.08571429	0.06976744	0.05882353	0.050847458
0.207920792	0.14893617	0.1160221	0.09502262	0.08045977	0.069767442
0.252336449	0.183673469	0.14438503	0.11894273	0.1011236	0.087947883
0.292035398	0.215686275	0.17098446	0.1416309	0.12087912	0.10543131
0.36	0.272727273	0.2195122	0.18367347	0.15789474	0.138461538

Figure D.18 – ω_{ms} values for Series 7-12

9.37499E-07	8.33333E-07	7.49999E-07	6E-07	5E-07	3.75E-07
0.000936622	0.000832639	0.000749438	0.00059964	0.00049975	0.00037486
0.00233827	0.002079002	0.001871491	0.00149775	0.00124844	0.00093662
0.00466563	0.004149378	0.00373599	0.00299103	0.00249377	0.00187149
0.006982157	0.00621118	0.005593536	0.00447984	0.00373599	0.00280461
0.009287926	0.008264463	0.007444169	0.00596421	0.00497512	0.00373599
0.011583012	0.010309278	0.009287926	0.00744417	0.00621118	0.00466563
0.013867488	0.012345679	0.011124845	0.00891972	0.00744417	0.00559354
0.018404908	0.016393443	0.014778325	0.01185771	0.00990099	0.00744417
0.022900763	0.020408163	0.018404908	0.01477833	0.01234568	0.00928793
0.027355623	0.024390244	0.02200489	0.01768173	0.01477833	0.01112485
0.031770045	0.028340081	0.025578563	0.02056807	0.01719902	0.01295497
0.036144578	0.032258065	0.029126214	0.0234375	0.01960784	0.01477833
0.044776119	0.04	0.036144578	0.02912621	0.02439024	0.01840491
0.061583578	0.05511811	0.049881235	0.0403071	0.03381643	0.02557856
0.077809798	0.069767442	0.06323185	0.0512334	0.0430622	0.03264813
0.093484419	0.083969466	0.076212471	0.0619137	0.0521327	0.03961585
0.123287671	0.111111111	0.101123596	0.08256881	0.06976744	0.05325444

Figure D.19 – ω_{ms} values for Series 13-18

Appendix E – Simulation Set 2 Inputs and Results

a	b
0.01	1
0.01	1.25
0.01	1.5
0.01	2
0.01	2.5
0.01	3
0.01	3.5
0.01	4
0.01	5
0.01	7
0.01	9
0.01	11
0.01	15
0.05	0.75
0.05	1.25
0.05	1.5
0.05	2
0.05	3
0.05	3.5
0.05	4
0.05	9
0.05	11
0.1	0.5
0.1	9
0.1	11
0.15	3
0.15	7
0.2	3.5
0.2	11
0.2	15
0.3	0.5
0.3	11
0.4	1
0.4	2.5
0.4	3.5
0.4	5
0.8	0.25
0.8	0.5
0.8	1
0.8	3
1	2
1.2	5
1.2	9
1.4	4
1.4	15
1.6	1.25
1.6	9
1.6	11
2	7
2.5	1.25
2.5	2.5
3	1.25

Figure E.1 – Data pairs for Absorption and scattering used in Simulation Set 2

Table E.1 – Backscatter ratio value order for results processing

b_b/b							
0.01	0.019	0.03	0.05	0.075	0.1		0.015

a	b
0.8	0.25
0.8	0.5
0.3	0.5
0.1	0.5
0.05	0.75
0.8	1
0.4	1
0.01	1
3	1.25
2.5	1.25
1.6	1.25
0.05	1.25
0.01	1.25
0.05	1.5
0.01	1.5
1	2
0.05	2
0.01	2
2.5	2.5
0.4	2.5
0.01	2.5
0.8	3
0.15	3
0.05	3
0.01	3
0.4	3.5
0.2	3.5
0.05	3.5
0.01	3.5
1.4	4
0.05	4
0.01	4
1.2	5
0.4	5
0.01	5
2	7
0.15	7
0.01	7
1.6	9
1.2	9
0.1	9
0.05	9
0.01	9
1.6	11
0.3	11
0.2	11
0.1	11
0.05	11
0.01	11
1.4	15
0.2	15
0.01	15

Figure E.2 – Data point order for b_b/b = 0.015 data set extracted from Simulation set 1

0.817586	0.82828	0.839059	0.854753	0.872051	0.887265	0.821792
0.133578	0.153638	0.174977	0.208716	0.242803	0.273966	0.846448
0.335438	0.3547	0.375865	0.408636	0.442334	0.473159	0.346234
0.835025	0.855289	0.877198	0.908654	0.944212	0.973997	0.145848
0.101276	0.131694	0.162626	0.212235	0.264567	0.307781	0.118346
0.077751	0.118363	0.16038	0.227207	0.294882	0.356168	0.892503
0.468567	0.508668	0.552047	0.617041	0.685417	0.746003	0.492262
0.86891	0.909994	0.951598	1.017262	1.08548	1.146833	0.102405
0.096162	0.146021	0.198336	0.2811	0.36866	0.443228	3.114886
0.134928	0.185849	0.238059	0.320945	0.408182	0.483445	2.615579
1.68596	1.735804	1.788922	1.869667	1.956638	2.033032	1.713717
2.587471	2.636719	2.689044	2.772684	2.854467	2.93221	0.164715
3.087059	3.136825	3.18756	3.270055	3.354751	3.429492	0.124326
0.111613	0.173251	0.236849	0.334053	0.436393	0.528952	0.189058
0.152679	0.212994	0.276662	0.374933	0.47827	0.569364	0.146594
0.145563	0.226445	0.312308	0.441646	0.581586	0.701438	1.182376
0.186002	0.266106	0.352148	0.482769	0.620955	0.741615	0.232734
1.135731	1.21647	1.300884	1.431292	1.56866	1.689491	0.193216
0.179508	0.280783	0.387028	0.549953	0.72288	0.874231	2.724122
0.568607	0.671463	0.775898	0.937378	1.111857	1.264071	0.628602
2.667246	2.768047	2.87247	3.035645	3.2088	3.359371	0.238736
0.213158	0.33583	0.461749	0.657691	0.864148	1.045838	1.074046
0.253936	0.376552	0.501295	0.697784	0.90464	1.086628	0.424854
0.353424	0.475119	0.599867	0.79583	1.006336	1.185063	0.323977
1.002545	1.125075	1.25157	1.445267	1.652904	1.833073	0.283407
0.247206	0.389783	0.536618	0.764951	1.005877	1.217952	0.718171
0.287438	0.428841	0.575775	0.804273	1.04452	1.258273	0.51847
0.437203	0.579524	0.727126	0.953345	1.194578	1.405117	0.370244
0.636778	0.779346	0.925422	1.154181	1.394028	1.605057	0.328056
0.280356	0.444365	0.612309	0.872706	1.146447	1.387314	1.761083
0.321118	0.481999	0.650554	0.910907	1.187455	1.429276	0.414333
1.668913	1.827889	1.997683	2.255797	2.531989	2.774037	0.374599
0.348646	0.550002	0.762742	1.085178	1.429427	1.730293	1.652417
0.73778	0.941011	1.149457	1.474504	1.817774	2.11757	0.854702
1.534744	1.737655	1.945788	2.267848	2.612668	2.915069	0.465528
0.481712	0.764716	1.057823	1.51111	1.991081	2.412087	2.623802
0.622219	0.902855	1.196329	1.650778	2.131025	2.550426	0.785049
2.463701	2.742022	3.0335	3.482998	3.963768	4.385888	0.646738
0.613097	0.976378	1.353088	1.935345	2.549118	3.087668	2.401795
0.653712	1.016276	1.391594	1.974865	2.589062	3.126989	2.004144
0.703119	1.066433	1.442615	2.023707	2.640259	3.176652	0.913676
1.796597	2.158208	2.531402	3.112088	3.726976	4.265059	0.863613
2.194623	2.55508	2.925511	3.507489	4.123812	4.662599	0.82524
0.747173	1.187933	1.649495	2.357359	3.10511	3.759595	2.577287
0.785267	1.228879	1.68657	2.395481	3.145846	3.801325	1.289205
0.837285	1.277335	1.736034	2.444292	3.195411	3.849513	1.191502
0.9362	1.37633	1.83591	2.544251	3.294548	3.950041	1.090231
1.033676	1.475174	1.934835	2.641953	3.390753	4.046526	1.041574
2.321301	2.761513	3.218244	3.92504	4.676287	5.33175	1.001418
1.008005	1.607217	2.230579	3.19305	4.209498	5.095799	2.727007
1.194752	1.795017	2.417091	3.380455	4.397987	5.284689	1.541502
2.380784	2.97877	3.59974	4.560281	5.5768	6.460359	1.354531

Figure E.3 – a_m results for all simulations

0.971124	0.997183	1.012728	1.026167	1.036071	1.040879	0.986815
0.440345	0.491851	0.525187	0.555022	0.572168	0.582584	1.173243
0.64094	0.69178	0.726823	0.755066	0.773912	0.78156	0.672866
1.139321	1.193105	1.225916	1.255449	1.273104	1.279708	0.472987
0.559015	0.639505	0.687163	0.731597	0.759788	0.772584	0.60952
0.687518	0.794972	0.860082	0.920682	0.954503	0.97302	1.546428
1.07827	1.184284	1.250875	1.309022	1.344694	1.363309	1.14706
1.479157	1.584771	1.649551	1.708491	1.745225	1.764964	0.757268
0.857576	0.991456	1.072582	1.147087	1.190729	1.214462	3.936418
0.898045	1.033252	1.112512	1.186366	1.230259	1.254668	3.435702
2.447887	2.579283	2.661535	2.73601	2.780534	2.804781	2.533931
3.350454	3.480984	3.561107	3.637208	3.682829	3.704122	0.984119
3.850034	3.980294	4.061656	4.137323	4.182557	4.203836	0.943336
1.025954	1.187509	1.285216	1.374789	1.427849	1.454777	1.168369
1.068006	1.227409	1.326067	1.415218	1.466957	1.495547	1.130301
1.366956	1.578658	1.70992	1.828681	1.89966	1.93952	2.495567
1.406873	1.619073	1.750402	1.868472	1.938563	1.976925	1.544475
2.357884	2.569711	2.702307	2.820465	2.888334	2.927411	1.504167
1.705516	1.971579	2.137197	2.283431	2.372508	2.418603	4.365765
2.094366	2.36107	2.525058	2.672829	2.762952	2.809124	2.267591
4.194704	4.462783	4.627516	4.774454	4.864769	4.908854	1.877483
2.04372	2.363401	2.558546	2.737233	2.846002	2.90059	3.039828
2.082734	2.402228	2.600754	2.777919	2.886029	2.940473	2.390972
2.183029	2.50502	2.700487	2.878319	2.983457	3.041967	2.291092
2.83328	3.154293	3.350168	3.529197	3.633237	3.692634	2.250034
2.381195	2.755939	2.983325	3.191087	3.316008	3.381679	3.013782
2.422354	2.793006	3.022842	3.232395	3.356433	3.422045	2.811636
2.569798	2.945532	3.176222	3.381167	3.506473	3.571898	2.66209
2.770156	3.144299	3.373139	3.583935	3.706992	3.772303	2.624099
2.718648	3.145266	3.408678	3.647165	3.787823	3.863083	4.386904
2.759655	3.185624	3.447867	3.686362	3.827971	3.904005	3.036875
4.109198	4.53772	4.800857	5.038481	5.178926	5.256404	2.994353
3.394605	3.929702	4.255587	4.557279	4.731739	4.827666	4.928613
3.784567	4.31809	4.645909	4.944789	5.123794	5.215925	4.131402
4.583422	5.117528	5.445838	5.746729	5.922363	6.016529	3.742224
4.742978	5.486164	5.95274	6.37012	6.622553	6.753905	7.21425
4.882465	5.63073	6.089959	6.509373	6.76025	6.892353	5.366833
6.737832	7.479534	7.940076	8.357658	8.607376	8.744477	5.225912
6.087485	7.047883	7.646027	8.183033	8.503998	8.679401	8.296652
6.124988	7.089937	7.68273	8.223583	8.547462	8.715471	7.894541
6.177463	7.140774	7.734571	8.273088	8.597134	8.766747	6.799041
7.276681	8.239215	8.833675	9.373521	9.69563	9.867793	6.748796
7.680648	8.636358	9.229758	9.777168	10.100222	10.267605	6.707614
7.43105	8.604983	9.331947	9.996622	10.393534	10.606265	9.777865
7.470207	8.641874	9.370586	10.035218	10.431596	10.641288	8.47821
7.518291	8.696012	9.420364	10.084867	10.481064	10.693641	8.375926
7.61982	8.792305	9.524643	10.187694	10.579208	10.78817	8.27857
7.717196	8.892355	9.623415	10.287132	10.681807	10.893608	8.225289
9.01785	10.193292	10.923428	11.587	11.982583	12.192489	8.189987
10.096794	11.708066	12.699242	13.616242	14.157373	14.45218	12.525169
10.287825	11.891887	12.893792	13.810521	14.349482	14.6346	11.325432
11.482247	13.095065	14.089879	15.008329	15.547699	15.837709	11.134943

Figure E.4 – c_m results for all simulations

0.021983	0.03535	0.048823	0.068441	0.090064	0.109081	0.02724
0.335783	0.536381	0.749768	1.087164	1.428028	1.739657	0.05806
0.118128	0.182332	0.252883	0.362121	0.474445	0.577198	0.154113
0.043781	0.069111	0.096498	0.135818	0.180264	0.217496	0.458482
1.025527	1.633875	2.252525	3.244696	4.291333	5.155628	1.366928
6.775116	10.836328	15.037951	21.720686	28.48822	34.616829	0.115628
0.171416	0.271669	0.380117	0.542602	0.713543	0.865008	0.230654
0.086138	0.137493	0.189497	0.271577	0.35685	0.433541	9.240538
8.616211	13.602123	18.833633	27.110014	35.866024	43.322773	0.038295
1.698569	2.716976	3.761177	5.418895	7.163646	8.668905	0.046231
0.053725	0.084878	0.118076	0.168542	0.222899	0.270645	0.071073
0.034988	0.054688	0.075618	0.109074	0.141787	0.172884	2.294295
0.02902	0.045608	0.06252	0.090018	0.11825	0.143164	11.432591
10.161336	16.325129	22.684912	32.405277	42.639259	51.895191	2.781158
2.053588	3.259881	4.533242	6.498661	8.565401	10.387275	13.6594
13.556278	21.644468	30.230774	43.164589	57.158619	69.143814	0.182376
2.720037	4.322121	6.04295	8.655381	11.419091	13.832294	3.65469
0.135731	0.21647	0.300884	0.431292	0.56866	0.689491	18.321596
16.950771	27.07832	37.702835	53.995266	71.288017	86.423103	0.089649
0.421518	0.678658	0.939745	1.343444	1.779642	2.160177	0.571505
0.066898	0.107219	0.148988	0.214258	0.28352	0.343749	22.873583
20.315784	32.583035	45.174908	64.769081	85.414818	103.583801	0.342558
4.07873	6.53104	9.025899	12.955671	17.092798	20.732569	1.832362
1.356158	2.167462	2.999114	4.305532	5.708908	6.900423	5.479543
0.253181	0.406343	0.564462	0.806583	1.06613	1.291341	27.340729
23.72057	37.978336	52.66185	75.49511	99.587685	120.795204	0.795427
4.748758	7.57682	10.515491	15.08546	19.890394	24.165451	1.592348
1.186016	1.897622	2.63563	3.766724	4.972889	6.025582	6.404882
0.591946	0.948365	1.313554	1.885453	2.48507	3.012643	31.805624
27.035595	43.436485	60.23093	86.270645	113.644676	137.731445	0.257916
5.422368	8.639981	12.01107	17.21814	22.749107	27.58552	7.286654
0.192081	0.305635	0.426916	0.611284	0.808563	0.981455	36.459888
33.864559	54.000175	75.274246	107.517815	141.942749	172.029312	0.377014
0.84445	1.352528	1.873641	2.686261	3.544436	4.293925	1.136755
0.278953	0.448046	0.62149	0.889874	1.177223	1.429224	45.552814
47.1712	75.471626	104.782295	150.111023	198.108124	240.208725	0.311901
3.148124	5.019033	6.975527	10.005187	13.20683	16.002836	4.233659
0.23185	0.371011	0.51675	0.741499	0.981884	1.192944	63.673759
60.309704	96.637802	134.308853	192.534485	253.911758	307.766815	0.501122
12.074233	19.325518	26.831888	38.497311	50.781246	61.539787	0.67012
6.031191	9.664326	13.426152	19.23707	25.402594	30.766525	8.136757
0.497164	0.798506	1.109502	1.593407	2.105813	2.554216	16.272253
0.37164	0.596925	0.828445	1.192181	1.577383	1.914124	81.523979
73.717285	117.793327	163.949524	234.735901	309.511047	374.959534	0.610804
14.705335	23.577576	32.7314	46.909618	61.91692	75.026505	3.297348
7.372846	11.773347	16.360338	23.442919	30.954113	37.495132	4.95751
3.681	5.881648	8.179551	11.721253	15.472737	18.750206	9.902306
2.445587	3.917246	5.449449	7.806511	10.30251	12.48842	19.831476
0.450813	0.725946	1.011403	1.45315	1.92268	2.332344	99.141754
99.800545	159.721725	222.057922	318.304993	419.949768	508.579926	0.947862
4.973759	7.975082	11.085455	15.902275	20.989937	25.423445	6.707512
0.70056	1.127693	1.571242	2.257343	2.983428	3.614542	134.453125

Figure E.5 – Absorption Error Factor for all simulations

0.07512	0.050302	0.035497	0.022698	0.013265	0.008686	0.060176
0.266092	0.180248	0.124688	0.074963	0.046387	0.029027	0.097506
0.198826	0.135275	0.091472	0.056167	0.03261	0.02305	0.158918
0.123599	0.082227	0.056988	0.03427	0.020689	0.01561	0.211689
0.301231	0.200618	0.141046	0.085503	0.050266	0.03427	0.2381
0.319289	0.212899	0.148433	0.088434	0.054947	0.036614	0.140873
0.229807	0.154083	0.106518	0.064984	0.039504	0.026208	0.180672
0.178246	0.119572	0.083583	0.050838	0.030431	0.019464	0.25023
0.319384	0.21313	0.148745	0.089614	0.054977	0.036141	0.073784
0.309196	0.205191	0.144222	0.087411	0.053647	0.034871	0.083813
0.141092	0.094988	0.066128	0.039996	0.024374	0.015866	0.110901
0.106546	0.071738	0.050371	0.030078	0.017912	0.012234	0.242986
0.09411	0.06346	0.044316	0.026512	0.015869	0.010862	0.25132
0.32056	0.21357	0.148863	0.089543	0.054404	0.036572	0.246213
0.310964	0.208123	0.144473	0.086956	0.053576	0.035131	0.251457
0.319923	0.214598	0.149293	0.090208	0.054896	0.035065	0.168144
0.313721	0.210208	0.146145	0.08855	0.054359	0.035646	0.246597
0.214039	0.14343	0.099231	0.059845	0.037222	0.024196	0.251658
0.320512	0.21451	0.148527	0.090267	0.054778	0.036413	0.126847
0.277805	0.185838	0.12929	0.078335	0.047258	0.031337	0.218072
0.161059	0.107443	0.074497	0.045109	0.027046	0.018229	0.251999
0.321023	0.214817	0.149985	0.09062	0.054485	0.036349	0.200045
0.317136	0.212384	0.147294	0.089207	0.053761	0.03591	0.240961
0.306975	0.204756	0.142703	0.086248	0.052871	0.034296	0.248822
0.2544	0.169923	0.118377	0.071264	0.043885	0.028254	0.252481
0.321597	0.214832	0.15005	0.090858	0.055268	0.036559	0.227236
0.317647	0.213238	0.148495	0.089466	0.054526	0.036044	0.240098
0.30546	0.20391	0.141562	0.086171	0.052305	0.034622	0.250116
0.289704	0.19377	0.135093	0.081042	0.049489	0.032743	0.252393
0.322033	0.215644	0.149956	0.090483	0.055406	0.036638	0.18761
0.318604	0.213426	0.148675	0.089787	0.054822	0.036048	0.250154
0.239037	0.159682	0.110952	0.066948	0.04094	0.026592	0.253279
0.322434	0.215628	0.150582	0.090363	0.055541	0.036394	0.205062
0.299154	0.200354	0.139646	0.084298	0.051149	0.034088	0.234925
0.260738	0.174592	0.121639	0.073108	0.04478	0.029592	0.253049
0.323398	0.21738	0.150822	0.091281	0.055271	0.036533	0.198417
0.317138	0.212485	0.148258	0.089598	0.054511	0.036035	0.249394
0.251352	0.168941	0.117769	0.071371	0.043625	0.028391	0.254506
0.324363	0.217771	0.151384	0.091783	0.05616	0.036692	0.217297
0.323206	0.216582	0.15108	0.091317	0.055529	0.036965	0.226025
0.321158	0.2153	0.150047	0.090869	0.05526	0.036621	0.252853
0.2866	0.192234	0.133953	0.081027	0.049448	0.032569	0.254277
0.275411	0.185249	0.129268	0.077626	0.047149	0.031358	0.255537
0.325064	0.218439	0.152412	0.092042	0.055992	0.03667	0.223979
0.323963	0.21793	0.151983	0.091835	0.055964	0.036988	0.249716
0.322677	0.216576	0.151319	0.091453	0.05576	0.036609	0.252149
0.319659	0.214973	0.149585	0.090384	0.055428	0.036771	0.254183
0.317062	0.213066	0.14837	0.089634	0.054707	0.035964	0.25563
0.284298	0.191009	0.133061	0.080397	0.049001	0.032342	0.256132
0.327329	0.219982	0.153948	0.092855	0.056804	0.037163	0.23627
0.323169	0.217639	0.151724	0.091413	0.055955	0.037197	0.254906
0.299863	0.20152	0.140861	0.084858	0.05197	0.034286	0.258165

Figure E.6 – Attenuation Error Factor for all simulations

0.00311526	0.00590245	0.00928793	0.01538462	0.02290076	0.03030303	0.00466563
0.04761905	0.08675799	0.13043478	0.2	0.27272727	0.33333333	0.00928793
0.01639344	0.03069467	0.04761905	0.07692308	0.11111111	0.14285714	0.02439024
0.00621118	0.01173564	0.01840491	0.03030303	0.04477612	0.05882353	0.06976744
0.13043478	0.22178988	0.31034483	0.42857143	0.52941176	0.6	0.18367347
0.5	0.65517241	0.75	0.83333333	0.88235294	0.90909091	0.01840491
0.02439024	0.04534606	0.06976744	0.11111111	0.15789474	0.2	0.03614458
0.01234568	0.02319902	0.03614458	0.05882353	0.08571429	0.11111111	0.6
0.55555556	0.7037037	0.78947368	0.86206897	0.90361446	0.92592593	0.00621118
0.2	0.3220339	0.42857143	0.55555556	0.65217391	0.71428571	0.00744417
0.00775194	0.01462664	0.02290076	0.03759398	0.05535055	0.07246377	0.01158301
0.00497512	0.0094106	0.01477833	0.02439024	0.03614458	0.04761905	0.27272727
0.00414938	0.00785449	0.01234568	0.02040816	0.03030303	0.04	0.65217391
0.6	0.74025974	0.81818182	0.88235294	0.91836735	0.9375	0.31034483
0.23076923	0.36305732	0.47368421	0.6	0.69230769	0.75	0.69230769
0.66666667	0.79166667	0.85714286	0.90909091	0.9375	0.95238095	0.02912621
0.28571429	0.43181818	0.54545455	0.66666667	0.75	0.8	0.375
0.01960784	0.03660886	0.05660377	0.09090909	0.13043478	0.16666667	0.75
0.71428571	0.82608696	0.88235294	0.92592593	0.94936709	0.96153846	0.01477833
0.05882353	0.10614525	0.15789474	0.23809524	0.31914894	0.38461538	0.08571429
0.00990099	0.01864573	0.02912621	0.04761905	0.06976744	0.09090909	0.78947368
0.75	0.85074627	0.9	0.9375	0.95744681	0.96774194	0.05325444
0.375	0.53271028	0.64285714	0.75	0.81818182	0.85714286	0.23076923
0.16666667	0.27536232	0.375	0.5	0.6	0.66666667	0.47368421
0.03614458	0.06651109	0.1011236	0.15789474	0.2195122	0.27272727	0.81818182
0.77777778	0.86928105	0.91304348	0.94594595	0.96330275	0.97222222	0.1160221
0.41176471	0.57081545	0.67741935	0.77777778	0.84	0.875	0.20792079
0.14893617	0.24953096	0.3442623	0.46666667	0.56756757	0.63636364	0.51219512
0.08045977	0.14255091	0.20792079	0.30434783	0.39622642	0.46666667	0.84
0.8	0.88372093	0.92307692	0.95238095	0.96774194	0.97560976	0.04109589
0.44444444	0.6031746	0.70588235	0.8	0.85714286	0.88888889	0.54545455
0.02777778	0.05149051	0.07894737	0.125	0.17647059	0.22222222	0.85714286
0.83333333	0.9047619	0.9375	0.96153846	0.97402597	0.98039216	0.05882353
0.11111111	0.19191919	0.27272727	0.38461538	0.48387097	0.55555556	0.15789474
0.04	0.07335907	0.11111111	0.17241379	0.23809524	0.29411765	0.88235294
0.875	0.93006993	0.95454545	0.97222222	0.98130841	0.98591549	0.04988124
0.31818182	0.46996466	0.58333333	0.7	0.77777778	0.82352941	0.41176471
0.03381643	0.06235349	0.09502262	0.14893617	0.20792079	0.25925926	0.91304348
0.9	0.94475138	0.96428571	0.97826087	0.98540146	0.98901099	0.0778098
0.64285714	0.77375566	0.84375	0.9	0.93103448	0.94736842	0.1011236
0.47368421	0.63099631	0.72972973	0.81818182	0.87096774	0.9	0.57446809
0.06976744	0.12472648	0.18367347	0.27272727	0.36	0.42857143	0.72972973
0.05325444	0.09655562	0.14438503	0.2195122	0.2967033	0.36	0.93103448
0.91666667	0.9543379	0.97058824	0.98214286	0.98802395	0.99099099	0.09348442
0.6875	0.80694981	0.86842105	0.91666667	0.94285714	0.95652174	0.35483871
0.52380952	0.6763754	0.76744186	0.84615385	0.89189189	0.91666667	0.45205479
0.35483871	0.51100244	0.62264151	0.73333333	0.80487805	0.84615385	0.62264151
0.26829268	0.41060904	0.52380952	0.64705882	0.73333333	0.78571429	0.76744186
0.06432749	0.11553344	0.17098446	0.25581395	0.34020619	0.40740741	0.94285714
0.9375	0.96610169	0.97826087	0.98684211	0.99118943	0.99337748	0.13846154
0.42857143	0.58762887	0.69230769	0.78947368	0.8490566	0.88235294	0.52941176
0.09677419	0.16913947	0.24324324	0.34883721	0.44554455	0.51724138	0.95744681

Figure E.7 - ω_{ms} values for all simulations

0.153538	0.168903	0.173669	0.171414	0.16402	0.153614	0.165023
0.306767	0.338213	0.35021	0.346306	0.329365	0.308618	0.326795
0.305502	0.33708	0.350958	0.34643	0.331578	0.308401	0.326632
0.304296	0.337816	0.348718	0.346795	0.328892	0.305711	0.327139
0.457739	0.507811	0.524537	0.519362	0.495221	0.464803	0.491174
0.609767	0.676609	0.699702	0.693475	0.659621	0.616852	0.653925
0.609703	0.675616	0.698828	0.691981	0.659277	0.617306	0.654798
0.610247	0.674777	0.697953	0.691229	0.659745	0.618131	0.654863
0.761414	0.845435	0.874246	0.865987	0.822069	0.771234	0.821532
0.763117	0.847403	0.874453	0.865421	0.822077	0.771223	0.820123
0.761927	0.843479	0.872613	0.866343	0.823896	0.771749	0.820214
0.762983	0.844265	0.872063	0.864524	0.828362	0.771912	0.819404
0.762975	0.843469	0.874096	0.867268	0.827806	0.774344	0.81901
0.914341	1.014258	1.048367	1.040736	0.991456	0.925825	0.979311
0.915327	1.014415	1.049405	1.040285	0.988687	0.926183	0.983707
1.221393	1.352213	1.397612	1.387035	1.318074	1.238082	1.313191
1.220871	1.352967	1.398254	1.385703	1.317608	1.23531	1.311741
1.222153	1.353241	1.401423	1.389173	1.319674	1.23792	1.310951
1.526008	1.690796	1.750169	1.733478	1.649628	1.544372	1.641643
1.525759	1.689607	1.74916	1.735451	1.651095	1.545053	1.638989
1.527458	1.694736	1.755046	1.738809	1.655969	1.549483	1.638747
1.830562	2.027571	2.096797	2.079542	1.981854	1.854752	1.965782
1.828798	2.025676	2.099459	2.080135	1.981389	1.853845	1.966118
1.829605	2.029901	2.10062	2.082489	1.977121	1.856904	1.967115
1.830735	2.029218	2.098598	2.08393	1.980333	1.859561	1.966627
2.133989	2.366156	2.446707	2.426136	2.310131	2.163727	2.295611
2.134916	2.364165	2.447067	2.428122	2.311913	2.163772	2.293166
2.132595	2.366008	2.449096	2.427822	2.311895	2.166781	2.291846
2.133378	2.364953	2.447717	2.429754	2.312964	2.167246	2.296043
2.438292	2.700901	2.796369	2.774459	2.641376	2.475769	2.625821
2.438537	2.703625	2.797313	2.775455	2.640516	2.474729	2.622542
2.440285	2.709831	2.803174	2.782684	2.646937	2.482367	2.619754
3.045959	3.3797	3.492845	3.472101	3.302312	3.097373	3.276196
3.046787	3.377079	3.496452	3.470285	3.30602	3.098355	3.2767
3.048678	3.379873	3.50005	3.478881	3.309695	3.10146	3.276696
4.261266	4.721448	4.894917	4.85901	4.631472	4.341818	4.590448
4.260246	4.727875	4.89363	4.858595	4.629225	4.341927	4.581784
4.274131	4.737512	4.906576	4.87466	4.643608	4.358589	4.579174
5.474388	6.071505	6.292939	6.247688	5.95488	5.591733	5.894857
5.471276	6.073661	6.291136	6.248718	5.9584	5.588482	5.890397
5.474344	6.074341	6.291956	6.249381	5.956875	5.590095	5.885365
5.480084	6.081007	6.302273	6.261433	5.968654	5.602734	5.885183
5.486025	6.081278	6.304247	6.269679	5.97641	5.605006	5.882374
6.683877	7.41705	7.682452	7.639263	7.288424	6.84667	7.200578
6.68494	7.412995	7.684016	7.639737	7.28575	6.839963	7.189005
6.681006	7.418677	7.68433	7.640575	7.285653	6.844128	7.184424
6.68362	7.415975	7.688733	7.643443	7.28466	6.838129	7.188339
6.68352	7.417181	7.68858	7.645179	7.291054	6.847082	7.183715
6.696549	7.431779	7.705184	7.66196	7.306296	6.860739	7.188569
9.088789	10.100849	10.468663	10.423192	9.947875	9.356381	9.798162
9.093073	10.09687	10.476701	10.430066	9.951495	9.349911	9.78393
9.101463	10.116295	10.490139	10.448048	9.970899	9.37735	9.780412

Figure E.8 – b_m values for all simulations

-0.096462	-0.081097	-0.076331	-0.078586	-0.08598	-0.096386	-0.084977
-0.193233	-0.161787	-0.14979	-0.153694	-0.170635	-0.191382	-0.173205
-0.194498	-0.16292	-0.149042	-0.15357	-0.168422	-0.191599	-0.173368
-0.195704	-0.162184	-0.151282	-0.153205	-0.171108	-0.194289	-0.172861
-0.292261	-0.242189	-0.225463	-0.230638	-0.254779	-0.285197	-0.258826
-0.390233	-0.323391	-0.300298	-0.306525	-0.340379	-0.383148	-0.346075
-0.390297	-0.324384	-0.301172	-0.308019	-0.340723	-0.382694	-0.345202
-0.389753	-0.325223	-0.302047	-0.308771	-0.340255	-0.381869	-0.345137
-0.488586	-0.404565	-0.375754	-0.384013	-0.427931	-0.478766	-0.428468
-0.486883	-0.402597	-0.375547	-0.384579	-0.427923	-0.478777	-0.429877
-0.488073	-0.406521	-0.377387	-0.383657	-0.426104	-0.478251	-0.429786
-0.487017	-0.405735	-0.377937	-0.385476	-0.421638	-0.478088	-0.430596
-0.487025	-0.406531	-0.375904	-0.382732	-0.422194	-0.475656	-0.43099
-0.585659	-0.485742	-0.451633	-0.459264	-0.508544	-0.574175	-0.520689
-0.584673	-0.485585	-0.450595	-0.459715	-0.511313	-0.573817	-0.516293
-0.778607	-0.647787	-0.602388	-0.612965	-0.681926	-0.761918	-0.686809
-0.779129	-0.647033	-0.601746	-0.614297	-0.682392	-0.76469	-0.688259
-0.777847	-0.646759	-0.598577	-0.610827	-0.680326	-0.76208	-0.689049
-0.973992	-0.809204	-0.749831	-0.766522	-0.850372	-0.955628	-0.858357
-0.974241	-0.810393	-0.75084	-0.764549	-0.848905	-0.954947	-0.861011
-0.972542	-0.805264	-0.744954	-0.761191	-0.844031	-0.950517	-0.861253
-1.169438	-0.972429	-0.903203	-0.920458	-1.018146	-1.145248	-1.034218
-1.171202	-0.974324	-0.900541	-0.919865	-1.018611	-1.146155	-1.033882
-1.170395	-0.970099	-0.89938	-0.917511	-1.022879	-1.143096	-1.032885
-1.169265	-0.970782	-0.901402	-0.91607	-1.019667	-1.140439	-1.033373
-1.366011	-1.133844	-1.053293	-1.073864	-1.189869	-1.336273	-1.204389
-1.365084	-1.135835	-1.052933	-1.071878	-1.188087	-1.336228	-1.206834
-1.367405	-1.133992	-1.050904	-1.072178	-1.188105	-1.333219	-1.208154
-1.366622	-1.135047	-1.052283	-1.070246	-1.187036	-1.332754	-1.203957
-1.561708	-1.299099	-1.203631	-1.225541	-1.358624	-1.524231	-1.374179
-1.561463	-1.296375	-1.202687	-1.224545	-1.359484	-1.525271	-1.377458
-1.559715	-1.290169	-1.196826	-1.217316	-1.353063	-1.517633	-1.380246
-1.954041	-1.6203	-1.507155	-1.527899	-1.697688	-1.902627	-1.723804
-1.953213	-1.622921	-1.503548	-1.529715	-1.69398	-1.901645	-1.7233
-1.951322	-1.620127	-1.49995	-1.521119	-1.690305	-1.89854	-1.723304
-2.738734	-2.278552	-2.105083	-2.14099	-2.368528	-2.658182	-2.409552
-2.739754	-2.272125	-2.10637	-2.141405	-2.370775	-2.658073	-2.418216
-2.725869	-2.262488	-2.093424	-2.12534	-2.356392	-2.641411	-2.420826
-3.525612	-2.928495	-2.707061	-2.752312	-3.04512	-3.408267	-3.105143
-3.528724	-2.926339	-2.708864	-2.751282	-3.0416	-3.411518	-3.109603
-3.525656	-2.925659	-2.708044	-2.750619	-3.043125	-3.409905	-3.114635
-3.519916	-2.918993	-2.697727	-2.738567	-3.031346	-3.397266	-3.114817
-3.513975	-2.918722	-2.695753	-2.730321	-3.02359	-3.394994	-3.117626
-4.316123	-3.58295	-3.317548	-3.360737	-3.711576	-4.15333	-3.799422
-4.31506	-3.587005	-3.315984	-3.360263	-3.71425	-4.160037	-3.810995
-4.318994	-3.581323	-3.31567	-3.359425	-3.714347	-4.155872	-3.815576
-4.31638	-3.584025	-3.311267	-3.356557	-3.71534	-4.161871	-3.811661
-4.31648	-3.582819	-3.31142	-3.354821	-3.708946	-4.152918	-3.816285
-4.303451	-3.568221	-3.294816	-3.33804	-3.693704	-4.139261	-3.811431
-5.911211	-4.899151	-4.531337	-4.576808	-5.052125	-5.643619	-5.201838
-5.906927	-4.90313	-4.523299	-4.569934	-5.048505	-5.650089	-5.21607
-5.898537	-4.883705	-4.509861	-4.551952	-5.029101	-5.62265	-5.219588

Figure E.9 - Δb values for all simulations

Appendix F – Attenuation Fit Graphs
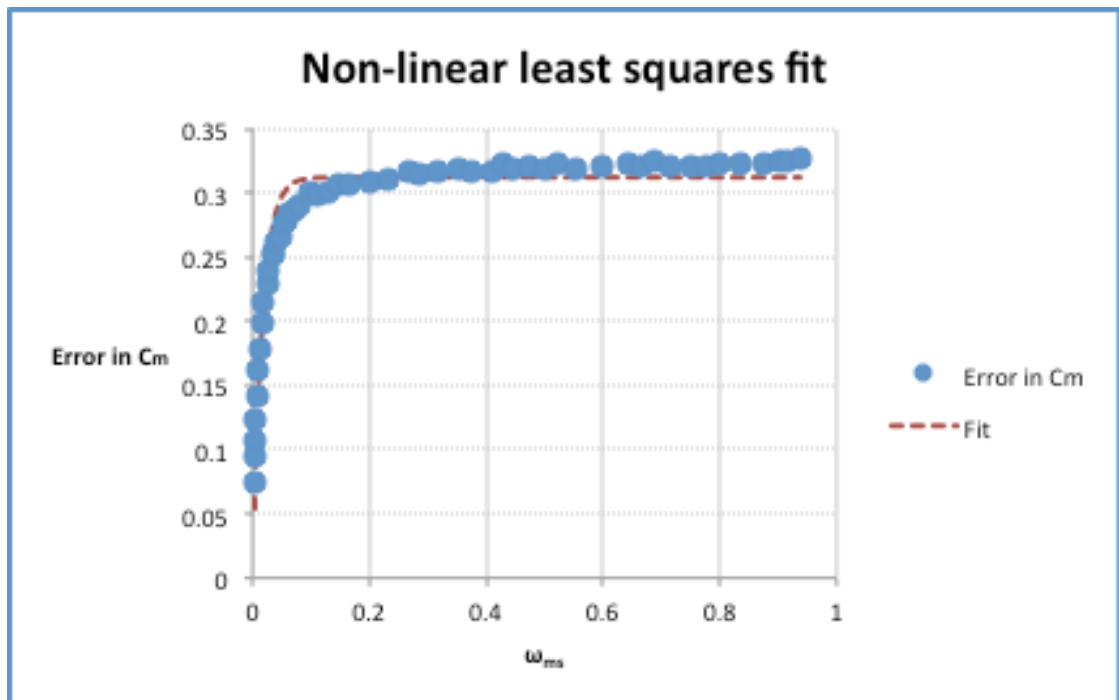
Graph F.1 – Non-linear least squares fit for b_b/b = 0.01
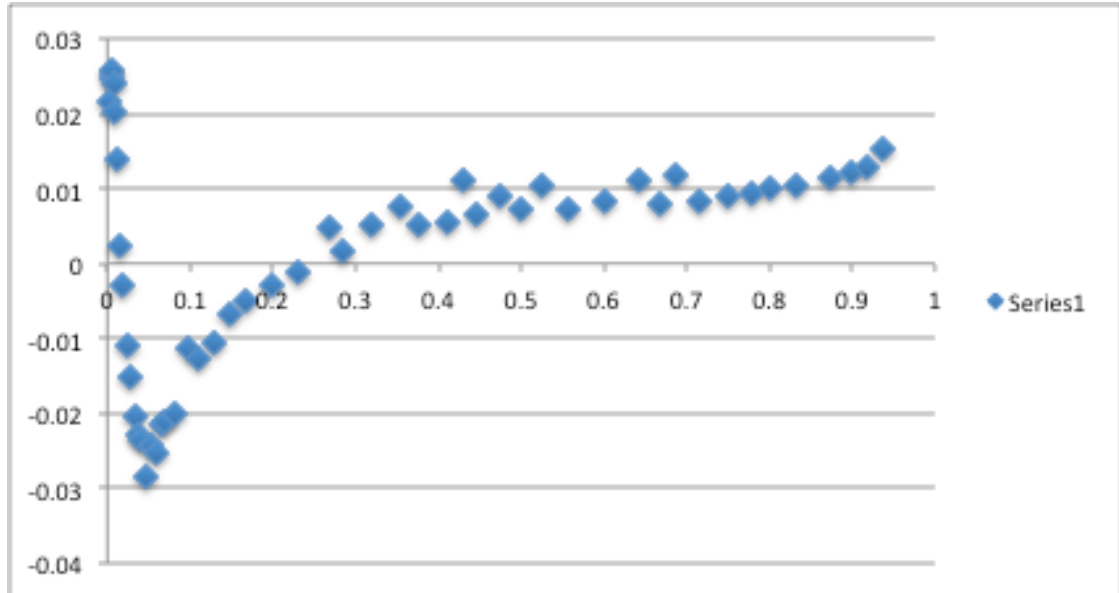
Graph F.2 – Non-linear least squares residuals for b_b/b = 0.01 residuals
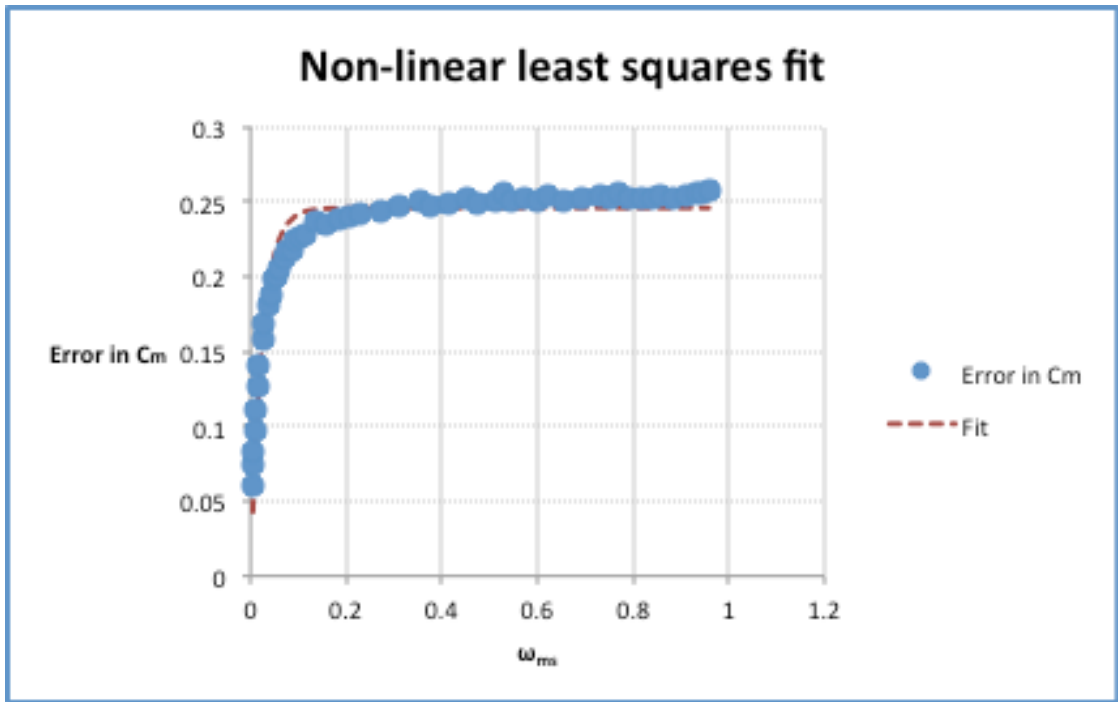
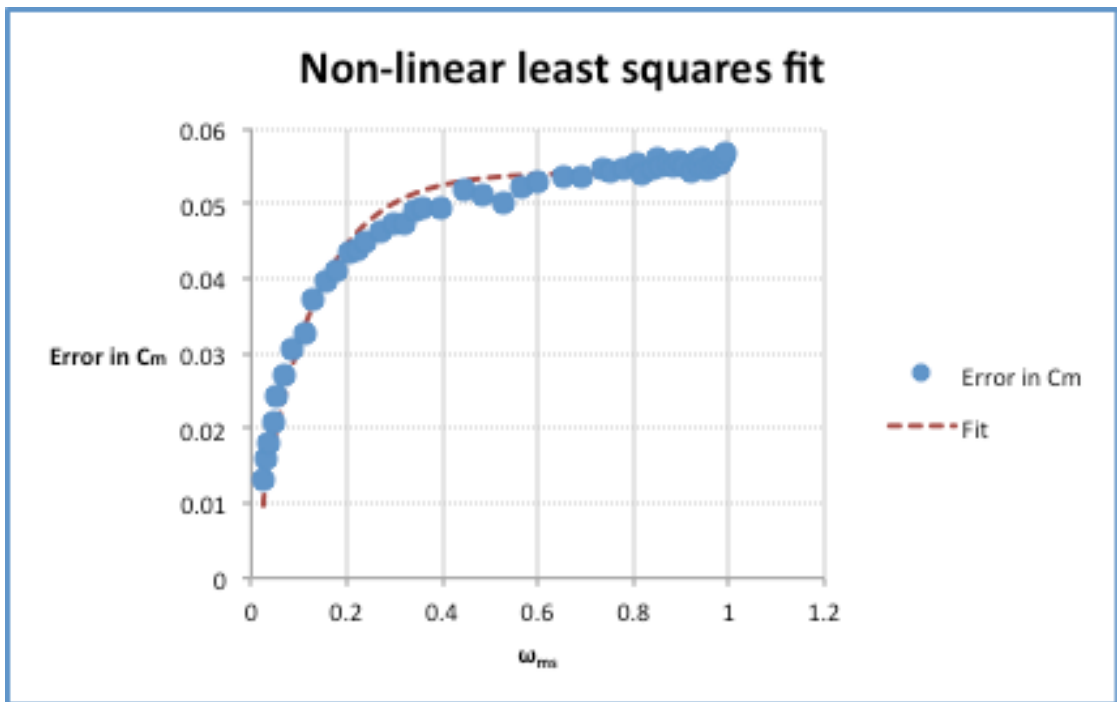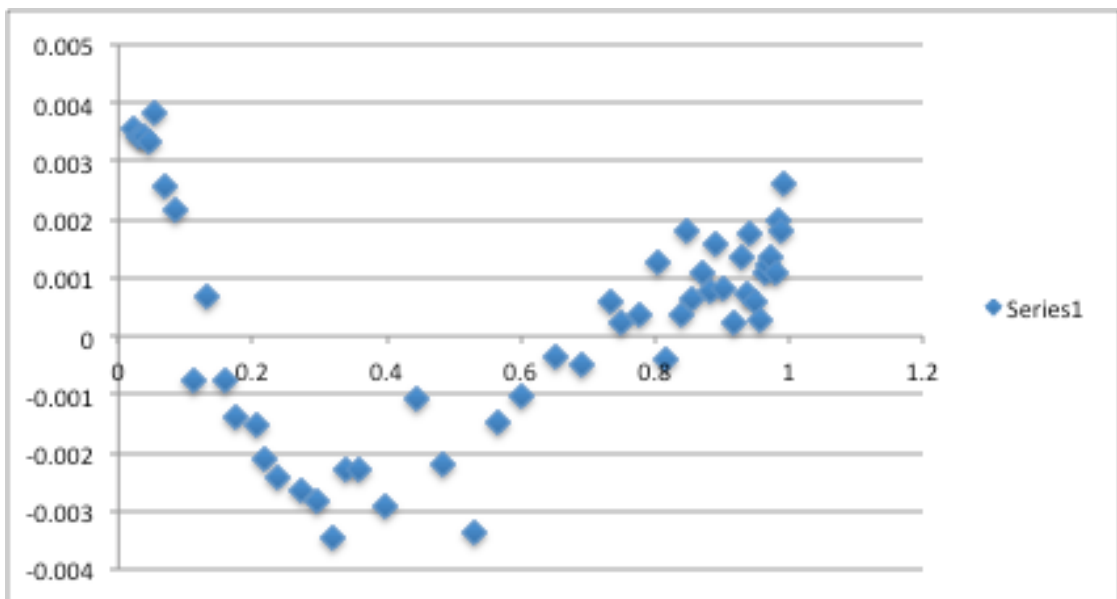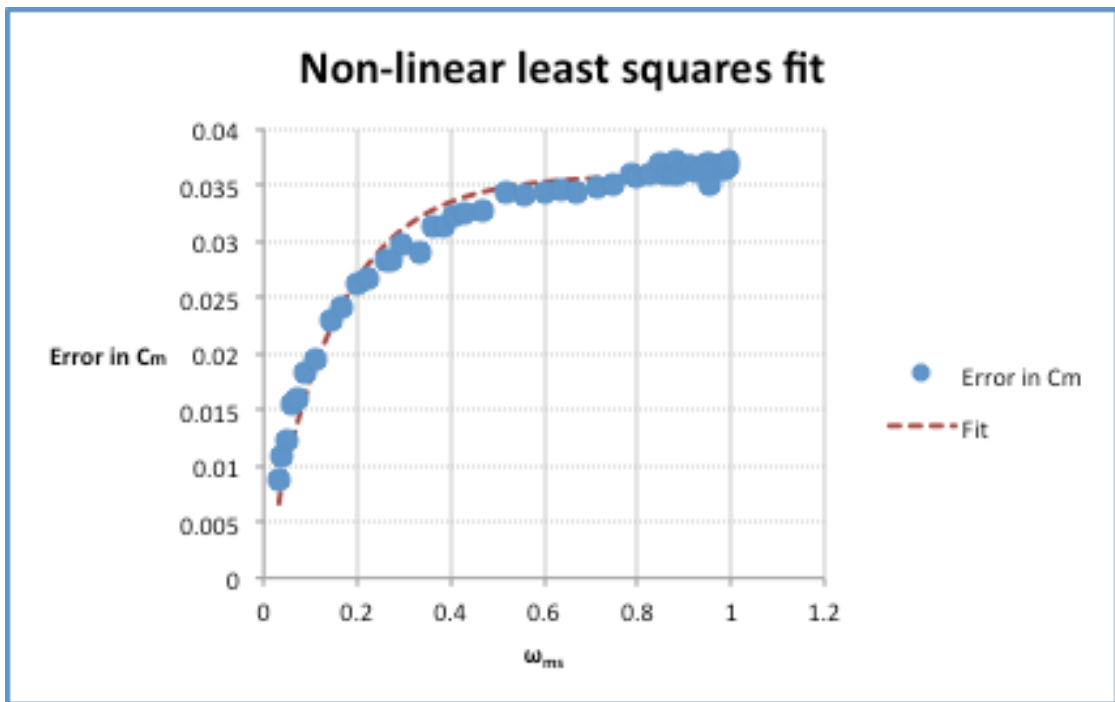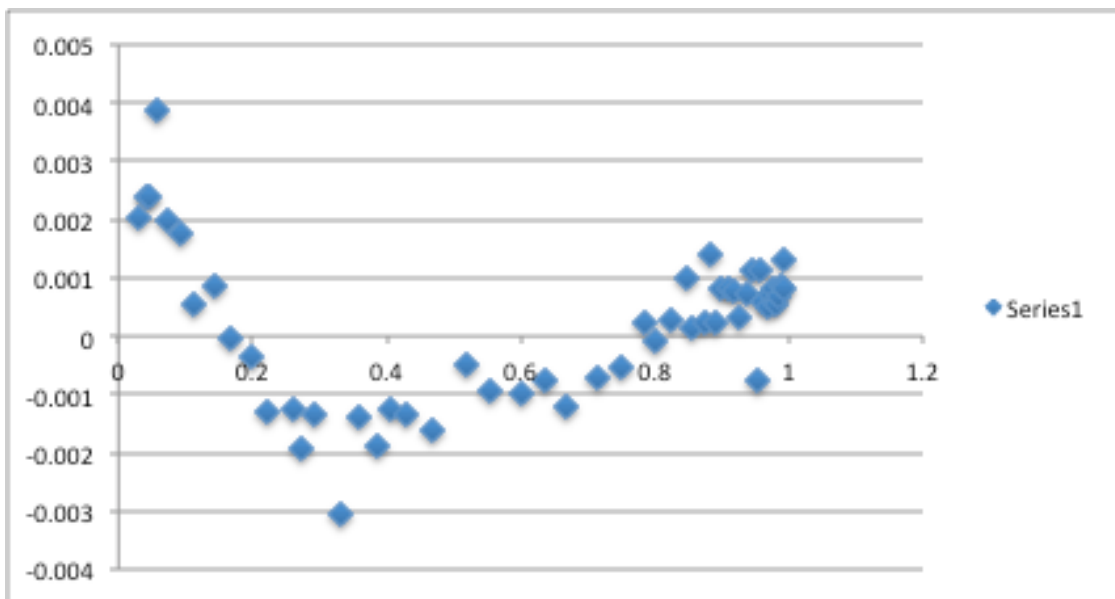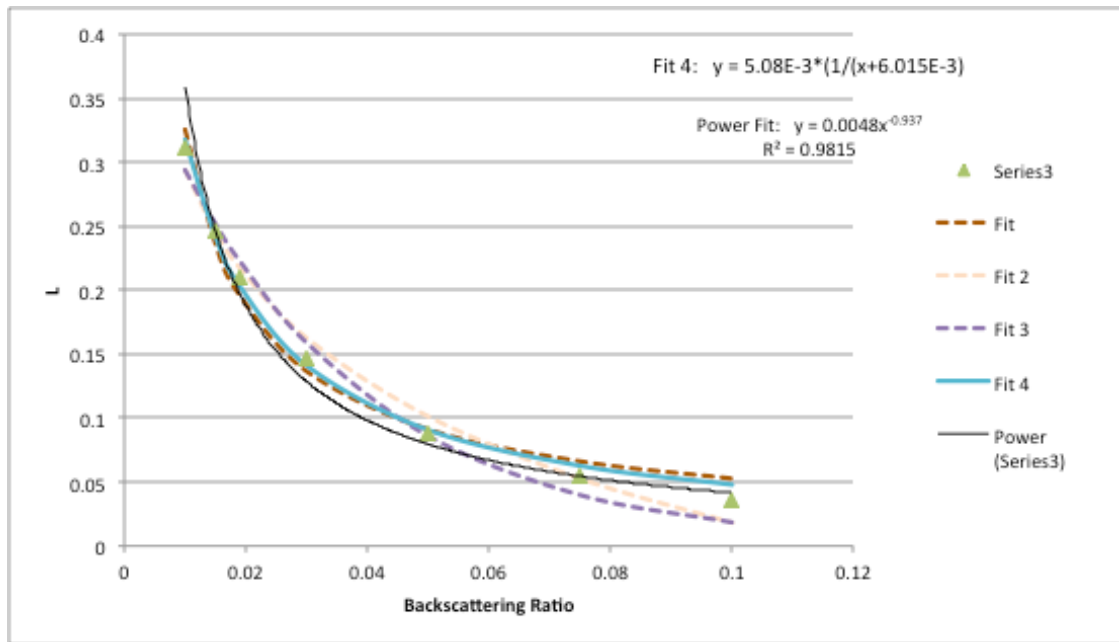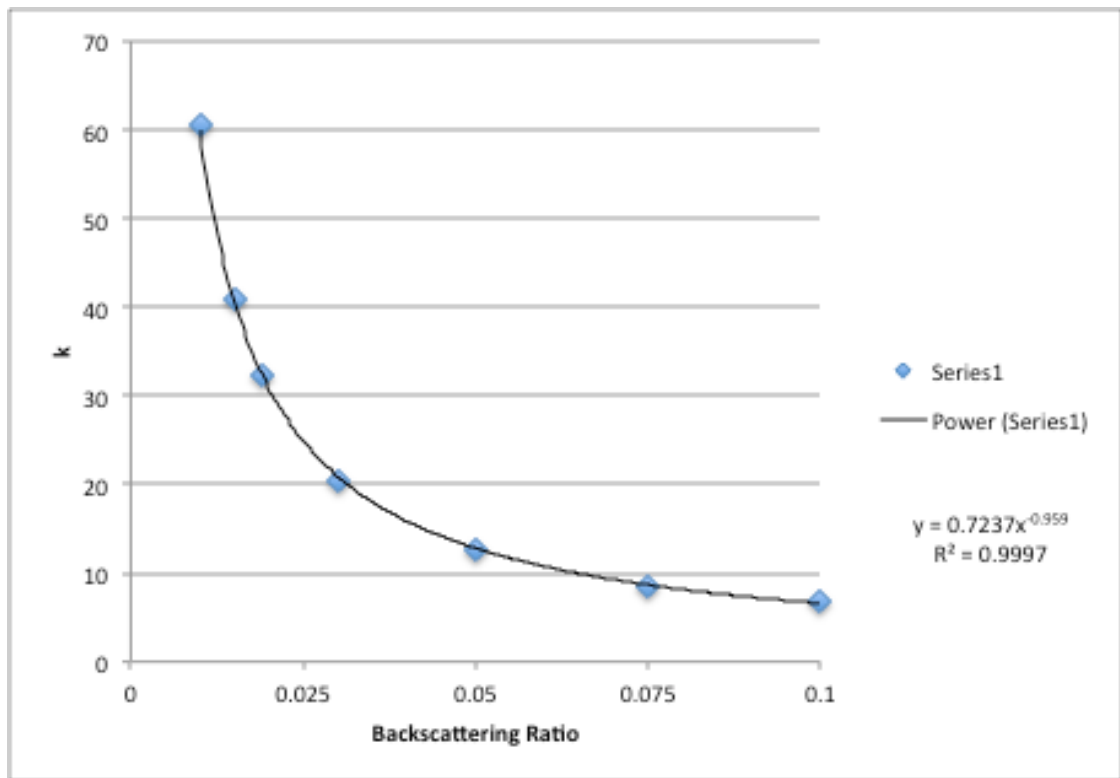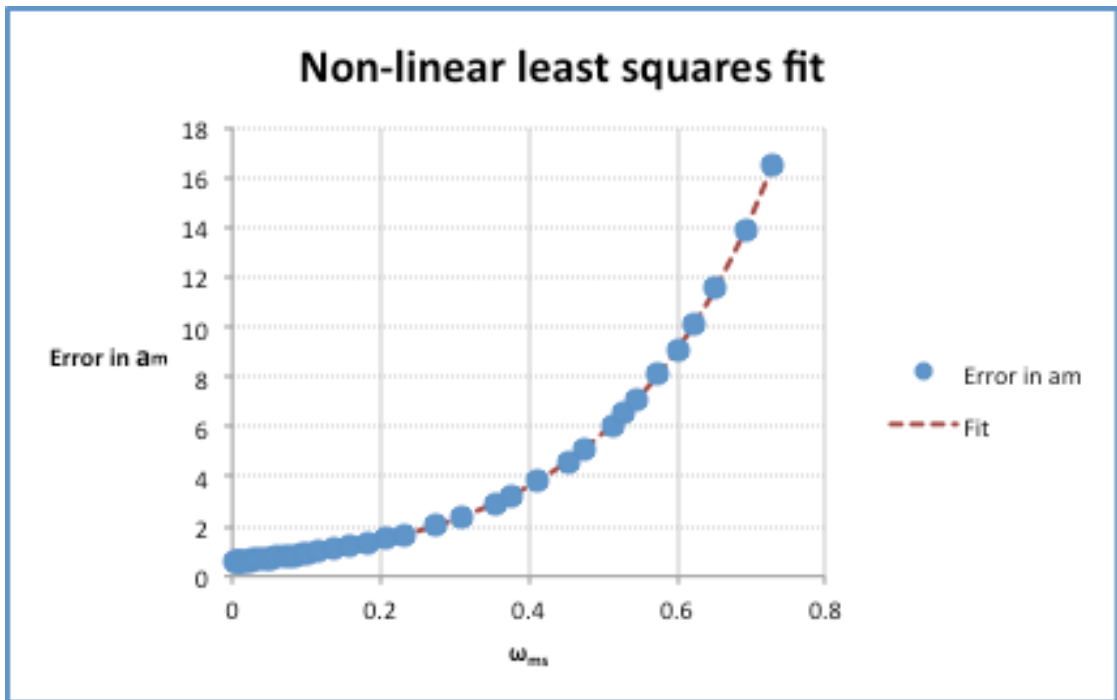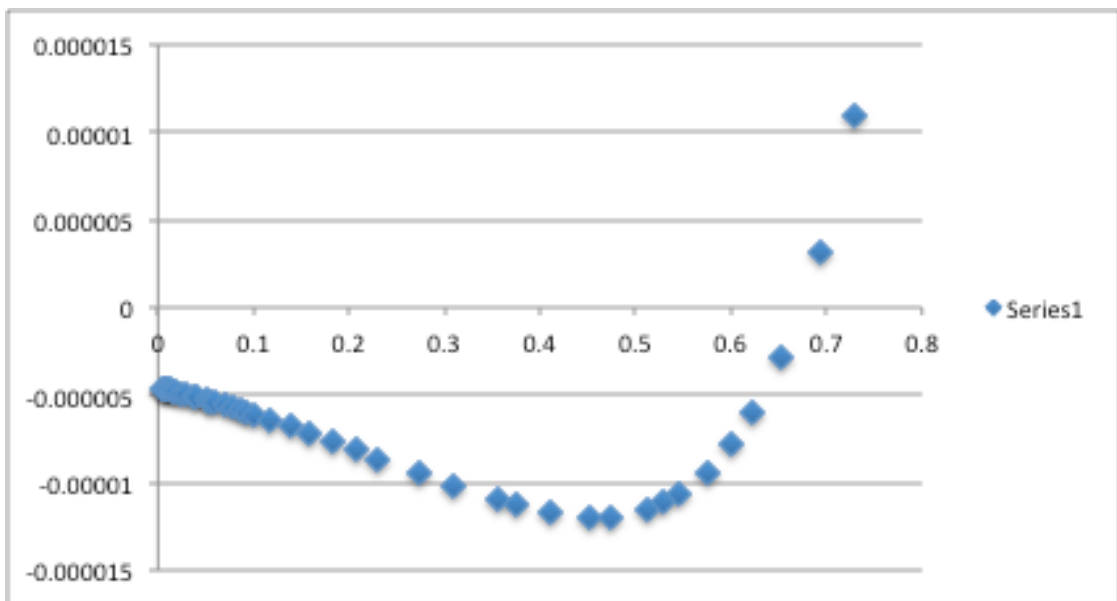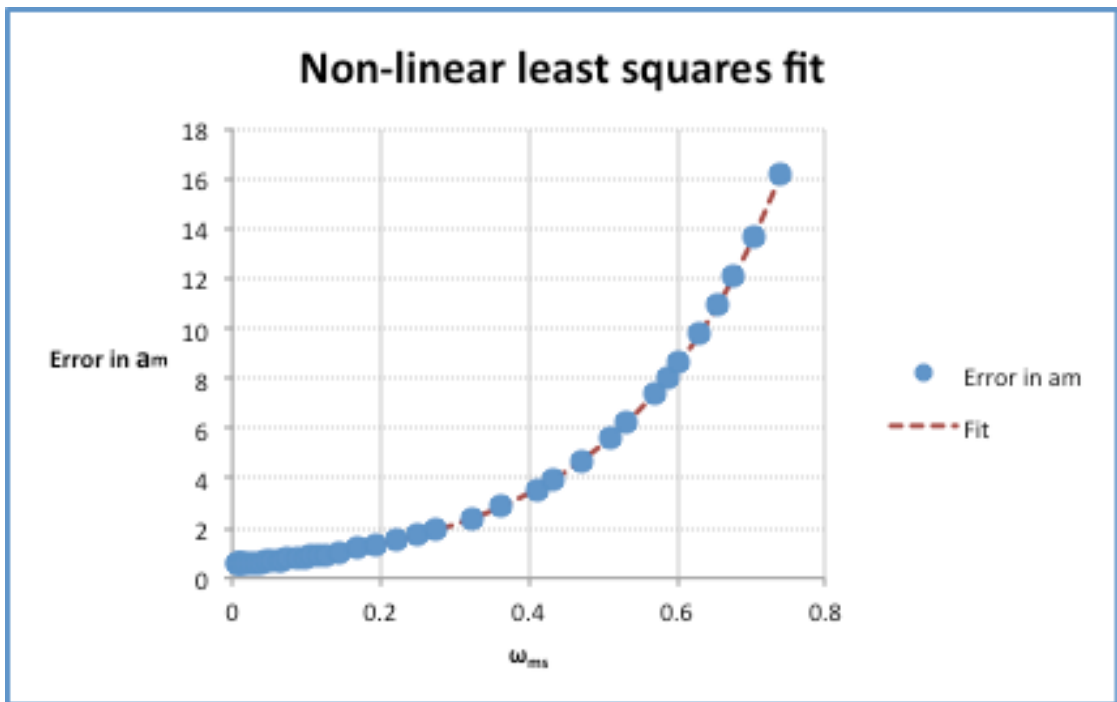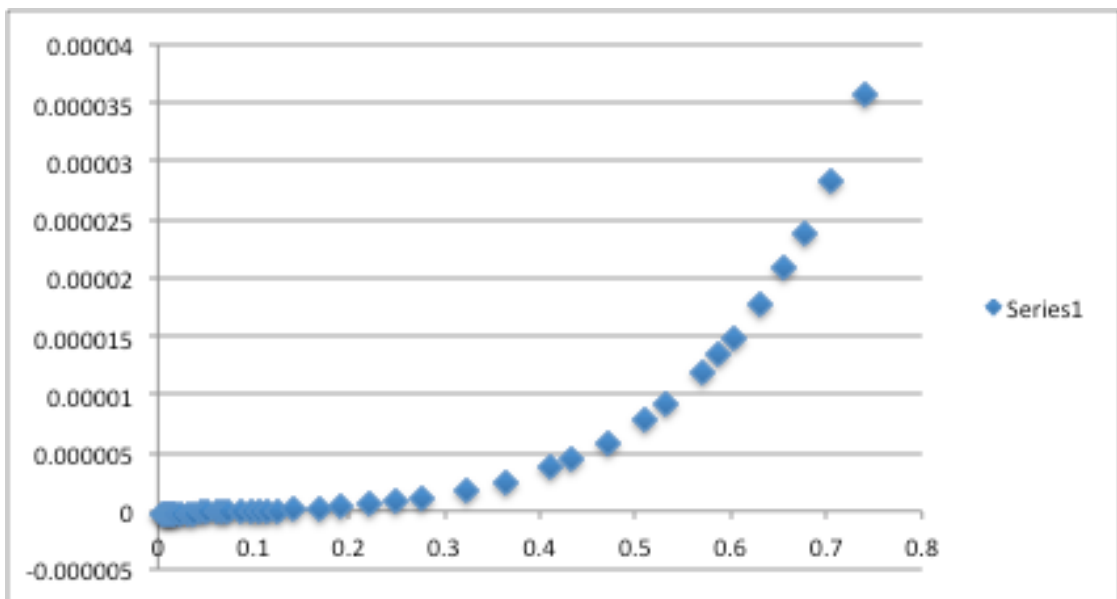**Graph F.3 – Non-linear least squares fit for b_b/b = 0.015**
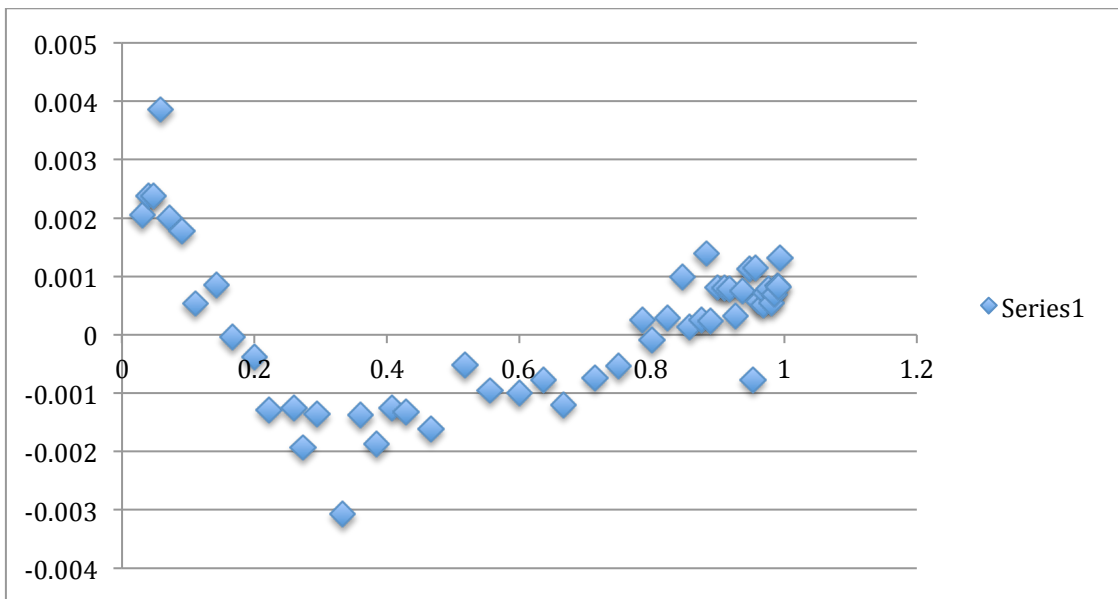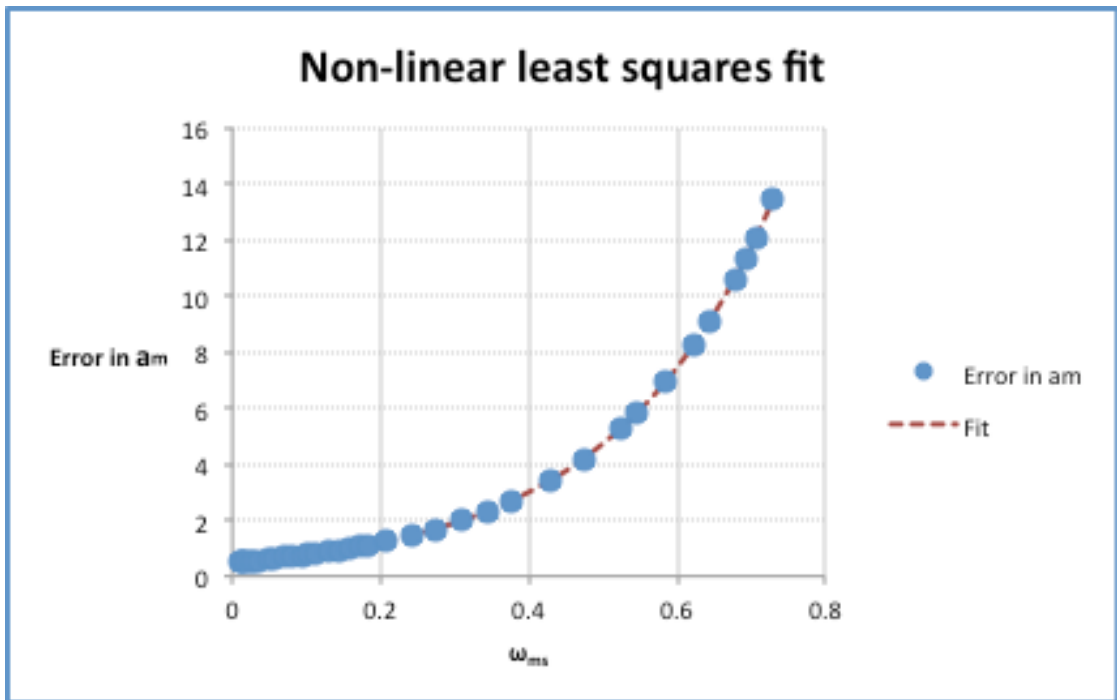

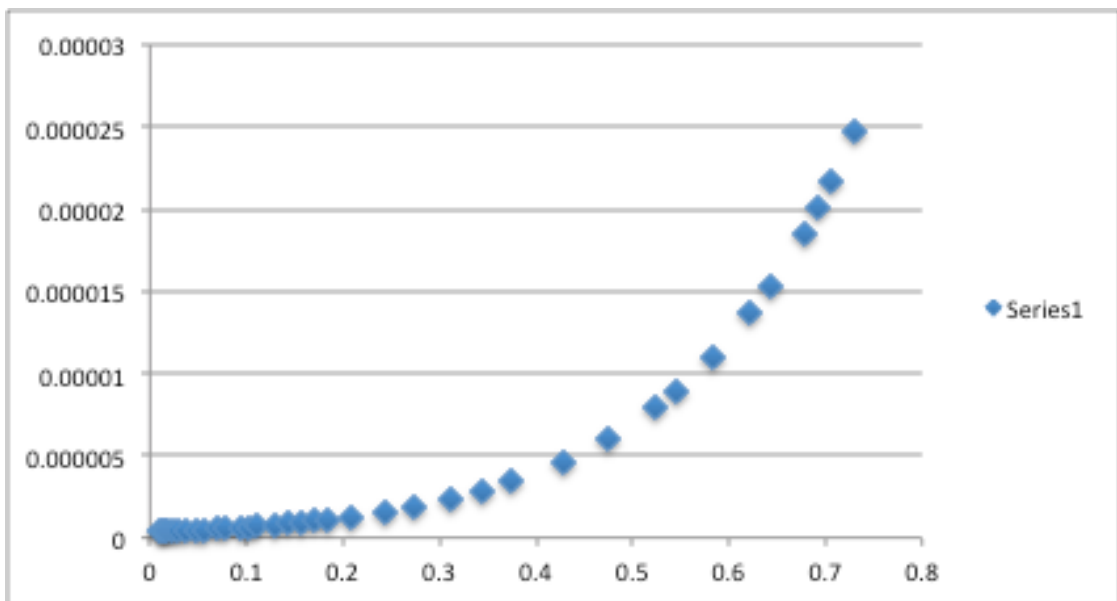**Graph F.4 – Non-linear least squares residuals for b_b/b = 0.015 residuals**
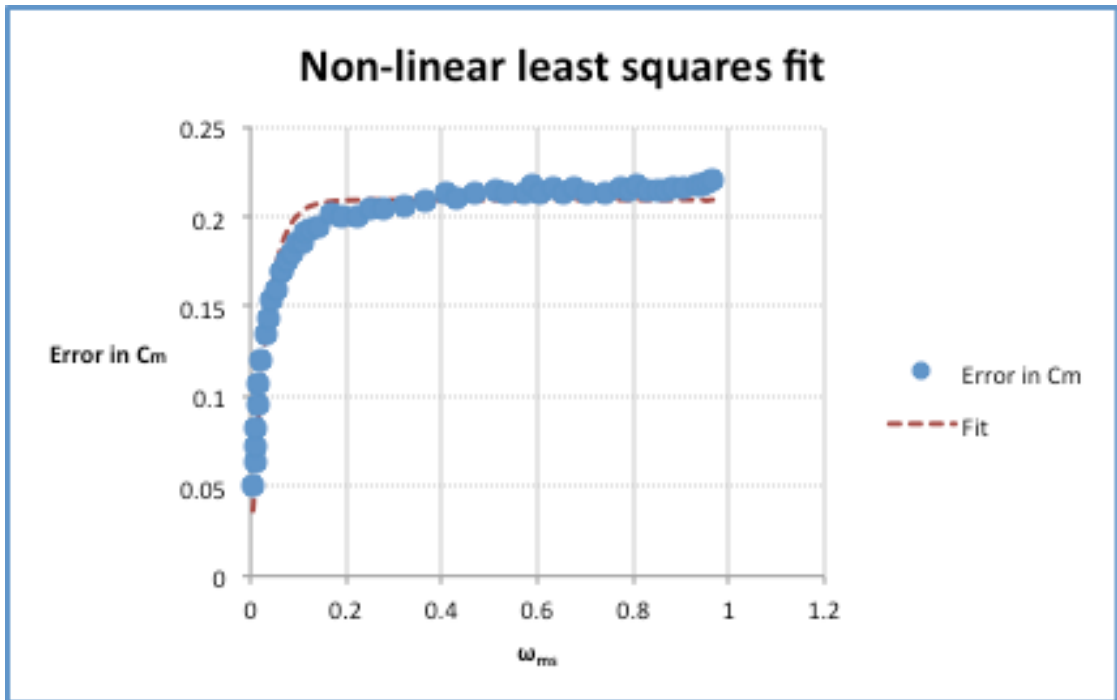
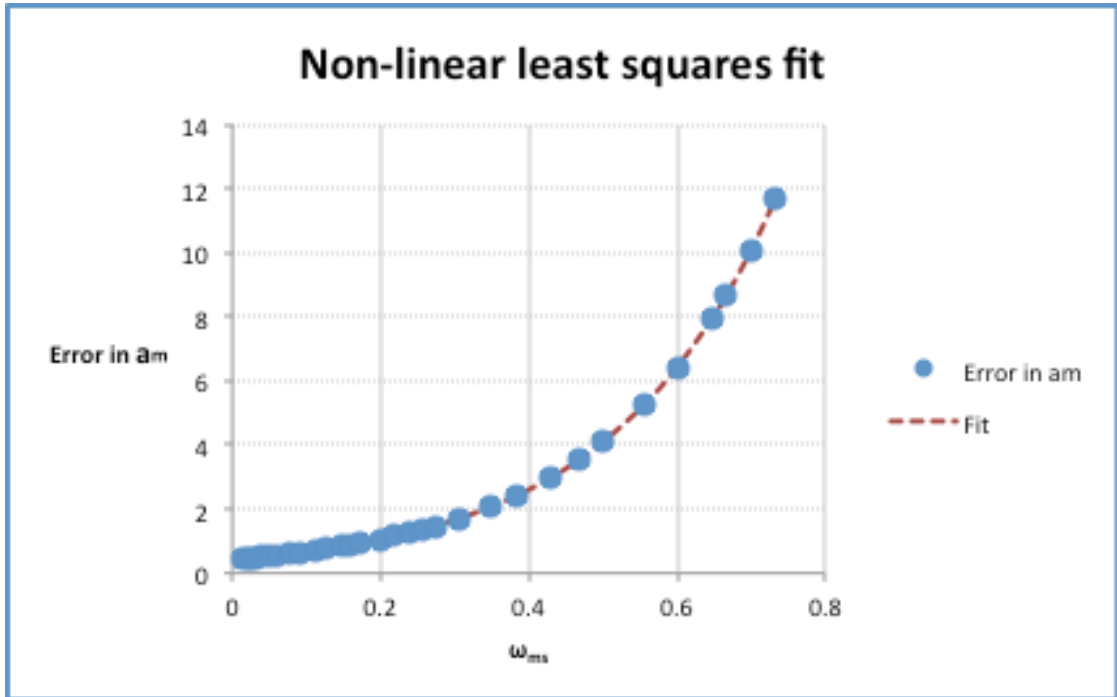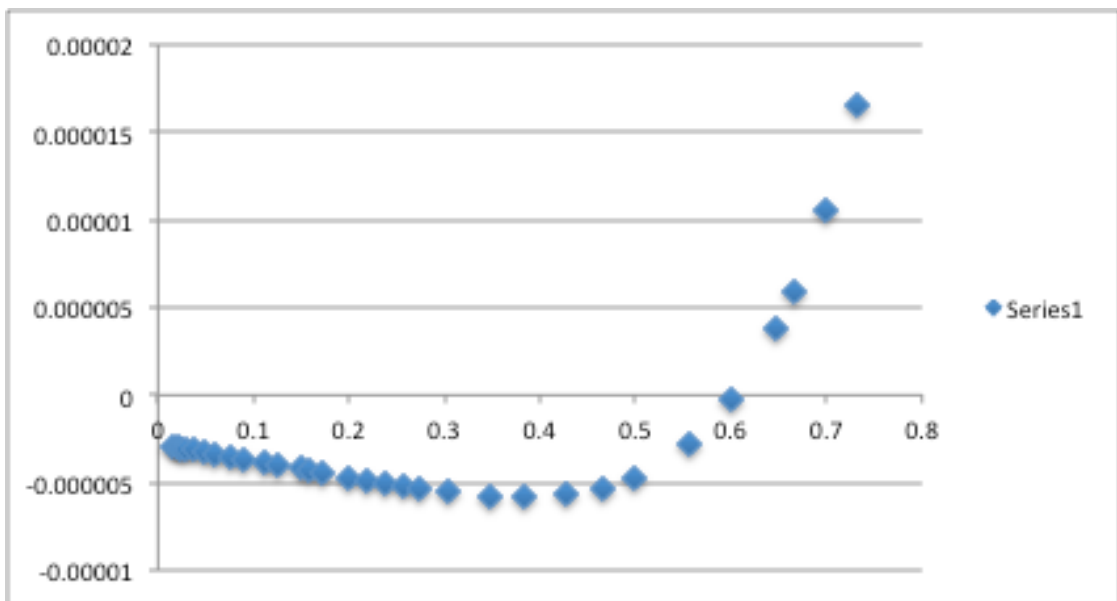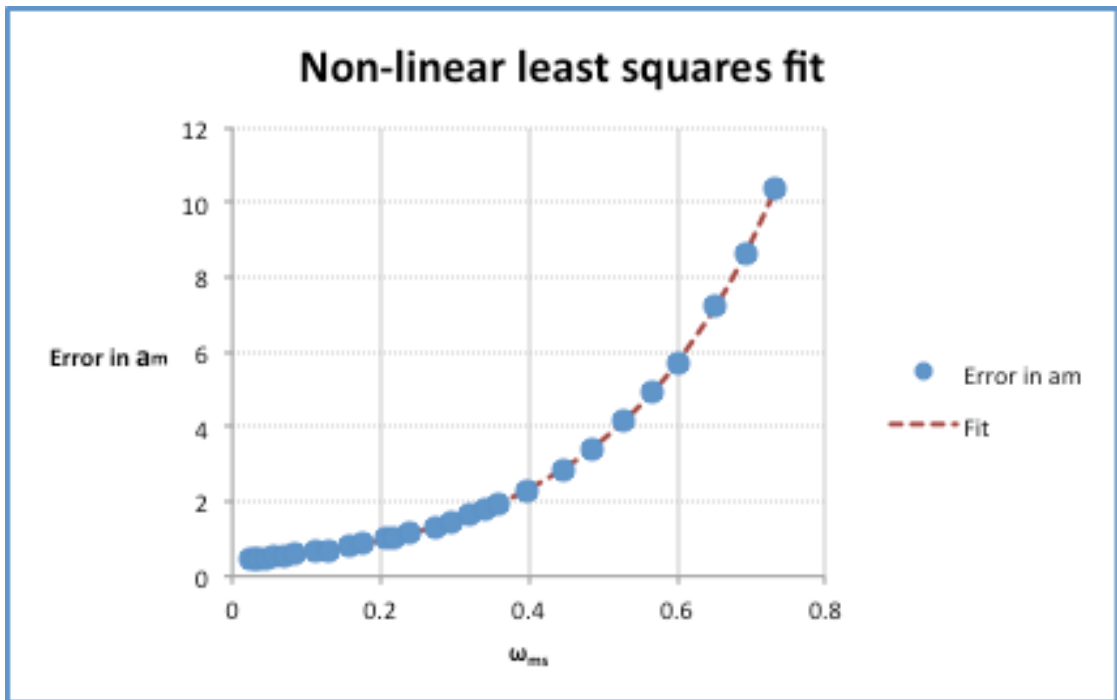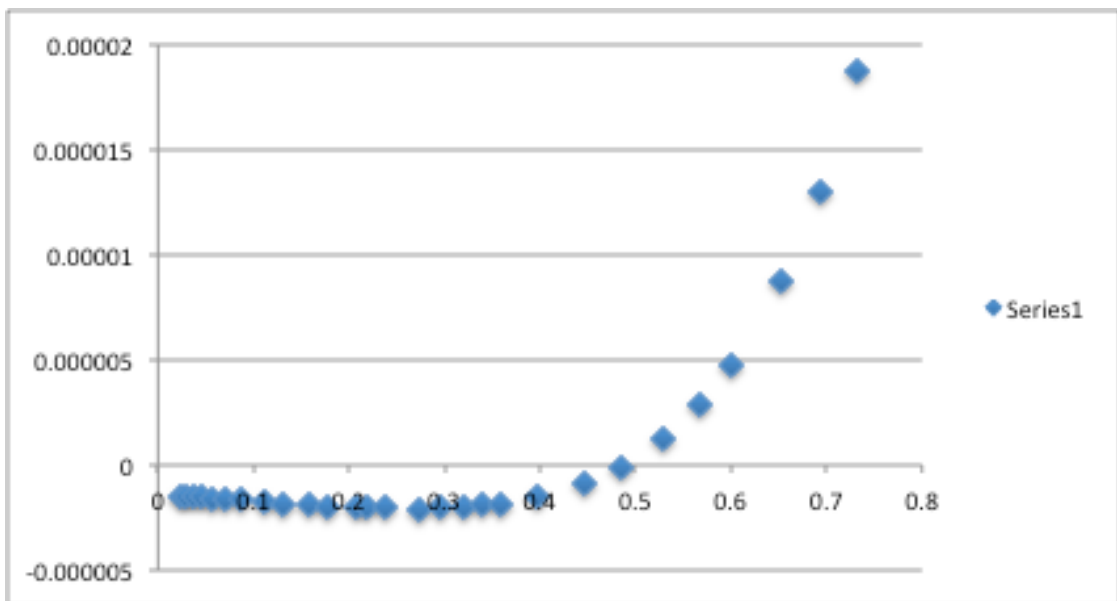**Graph F.5 – Non-linear least squares fit for $b_b/b = 0.019$**
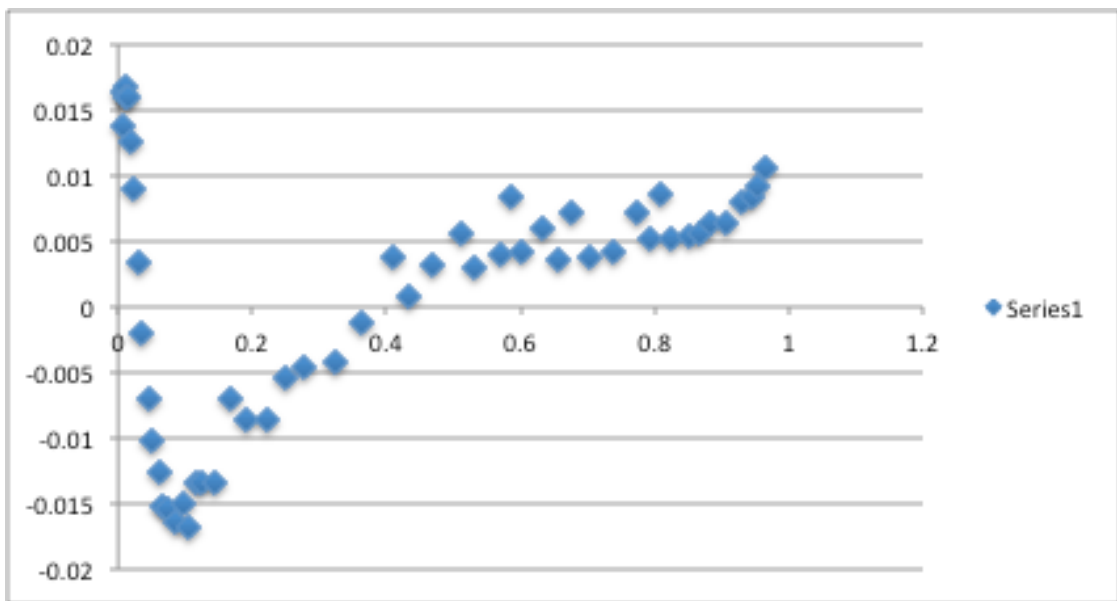
Graph F.6 – Non-linear least squares residuals for $b_b/b = 0.019$ residuals
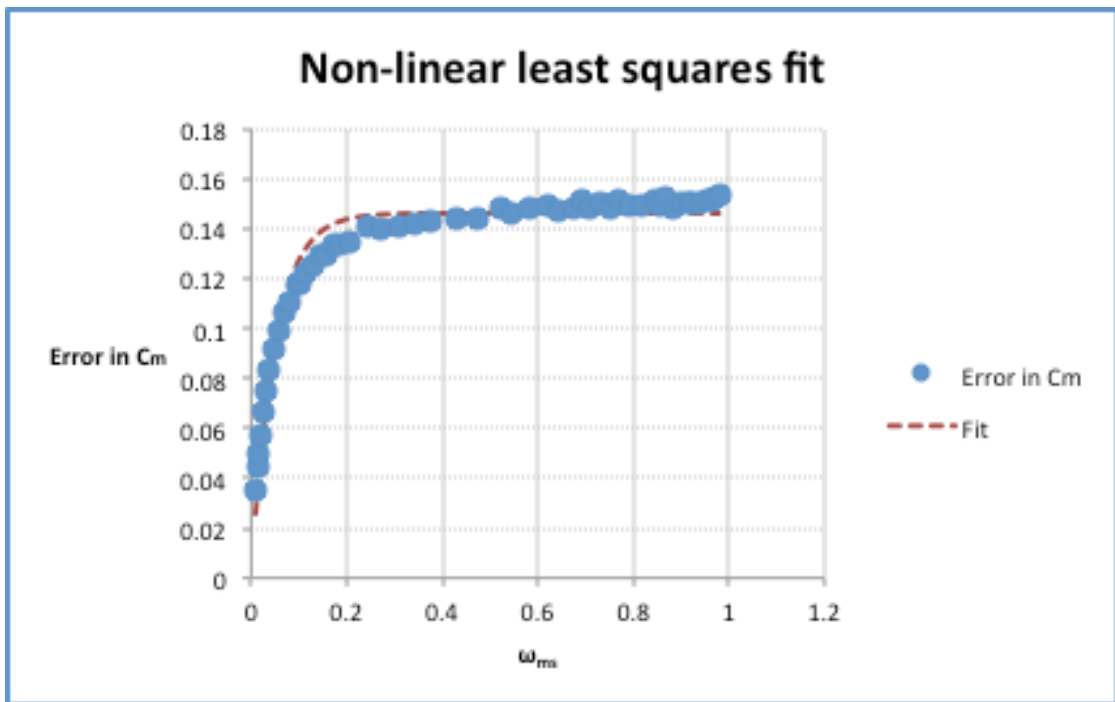
Graph F.7 – Non-linear least squares fit for $b_b/b = 0.03$
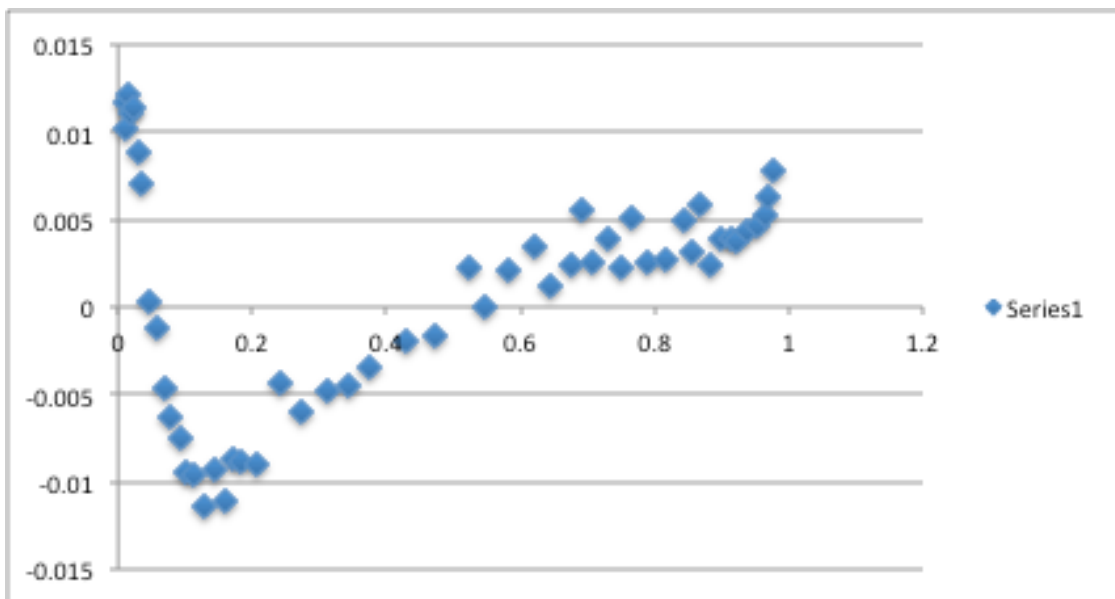
Graph F.8 – Non-linear least squares residuals for $b_b/b = 0.03$ residuals
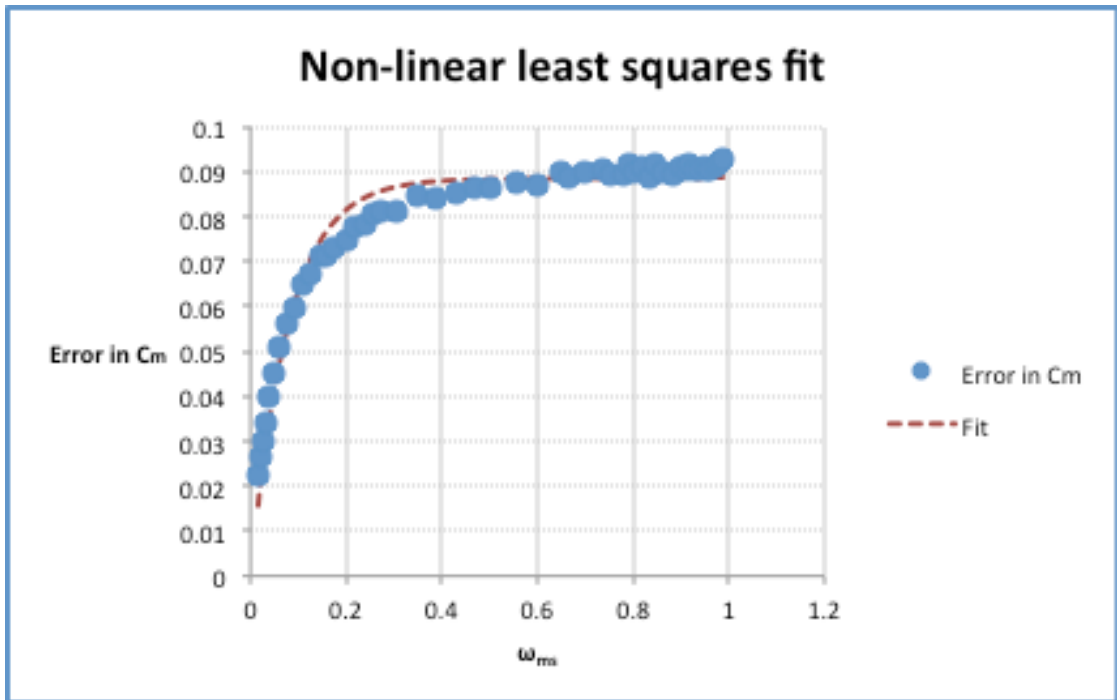
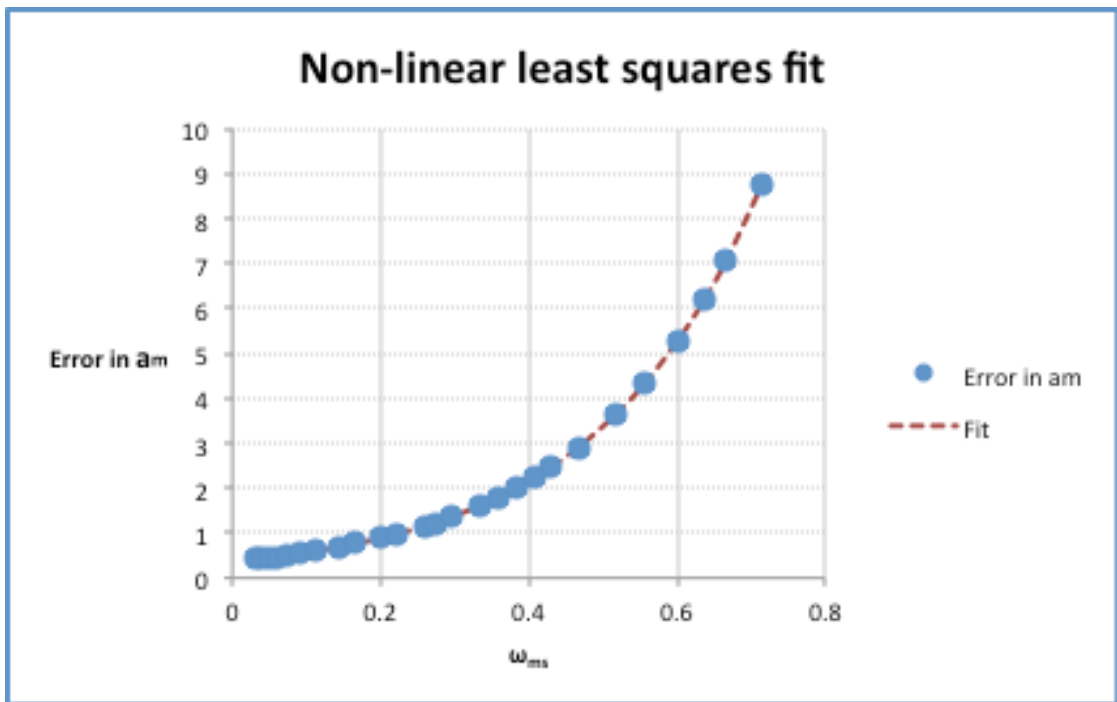**Graph F.9 – Non-linear least squares fit for b_b/b = 0.05**
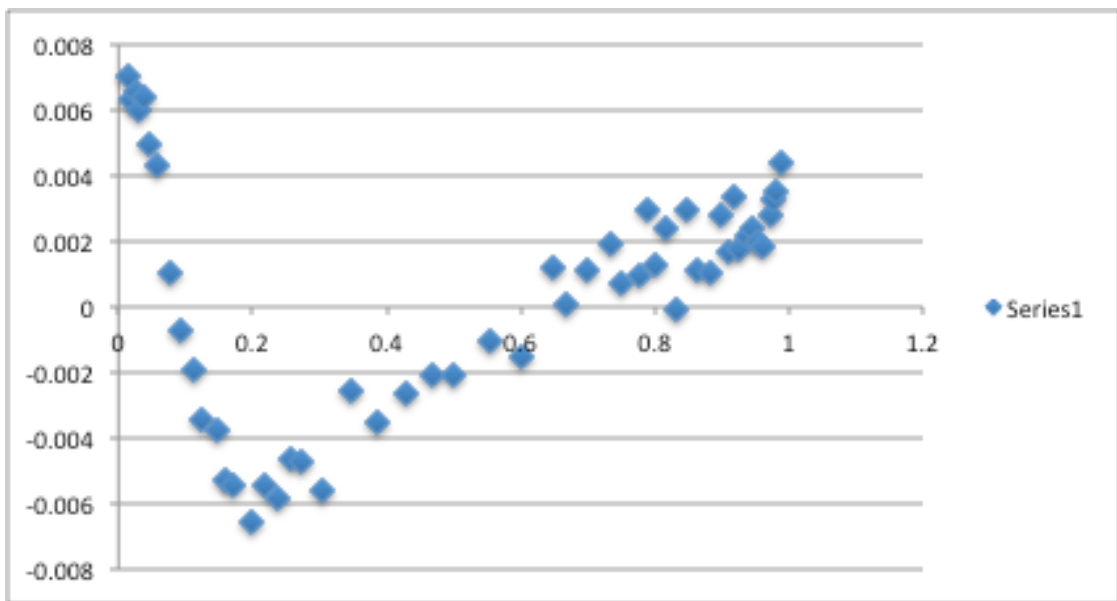
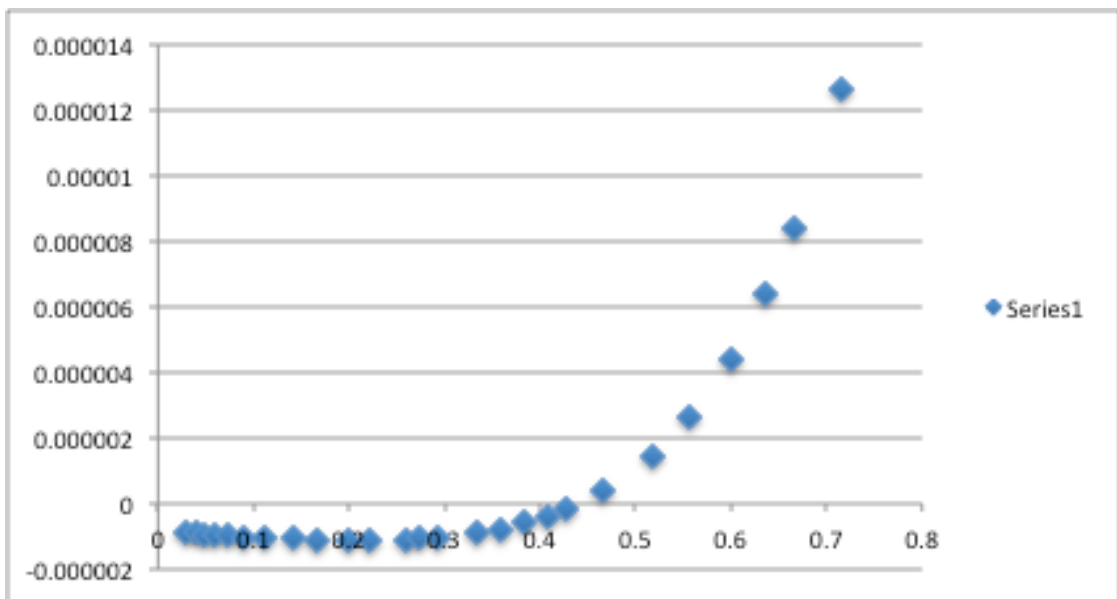**Graph F.10 – Non-linear least squares residuals for b_b/b = 0.05 residuals**

Graph F.11 – Non-linear least squares fit for b_b/b = 0.075

Graph F.12 – Non-linear least squares residuals for b_b/b = 0.075 residuals

**Graph F.13 – Non-linear least squares fit for $b_b/b = 0.1$**

Graph F.14 – Non-linear least squares residuals for $b_b/b = 0.1$

Table F.1 – Non-linear least squares fit coefficients

Coefficient Data					
bb/b = 0.01		bb/b = 0.015		bb/b = 0.019	
L	0.3121196	L	0.245749292	L	0.209322421
k	60.58402325	k	40.8813428	k	32.40465319
bb/b = 0.03		bb/b = 0.05		bb/b = 0.075	
L	0.146158323	L	0.088490652	L	0.05420596
k	20.50212725	k	12.68712342	k	8.604899751
bb/b = 0.1					
L	0.035894272				
k	6.743030075				

Graph F.15 – Fits for L as a function of b_b/b

Graph F.16 – Power fit for k values as a function of b_b/b

Appendix G – Absorption Fit Graphs
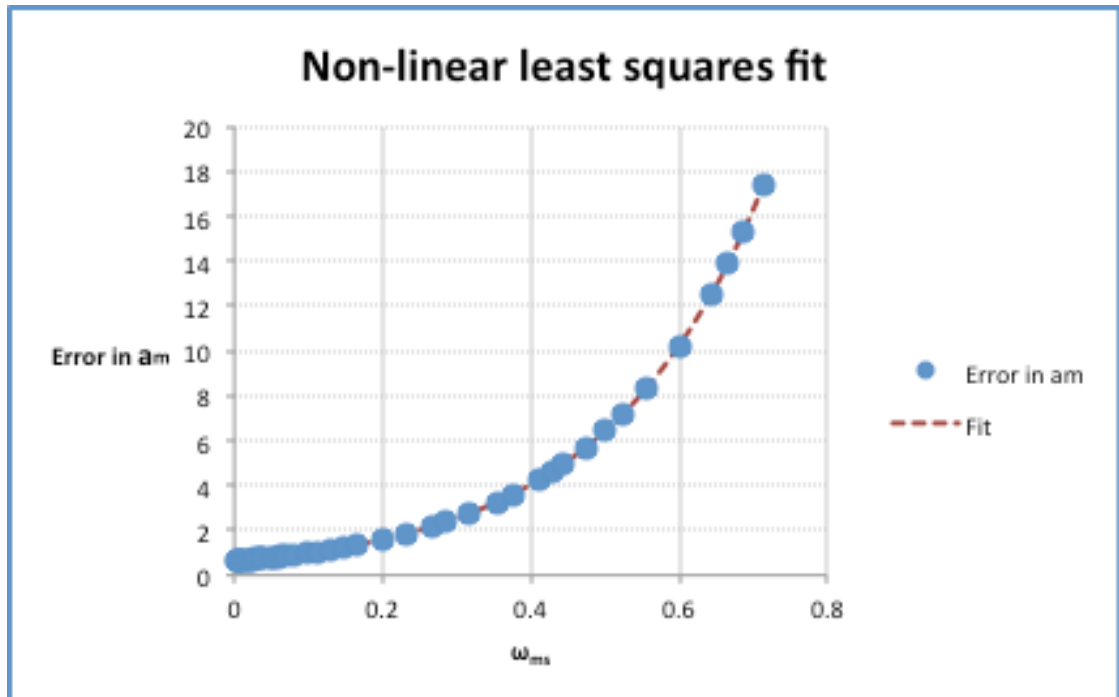
Graph G.1 – Non-linear least squares fit for b_b/b = 0.01
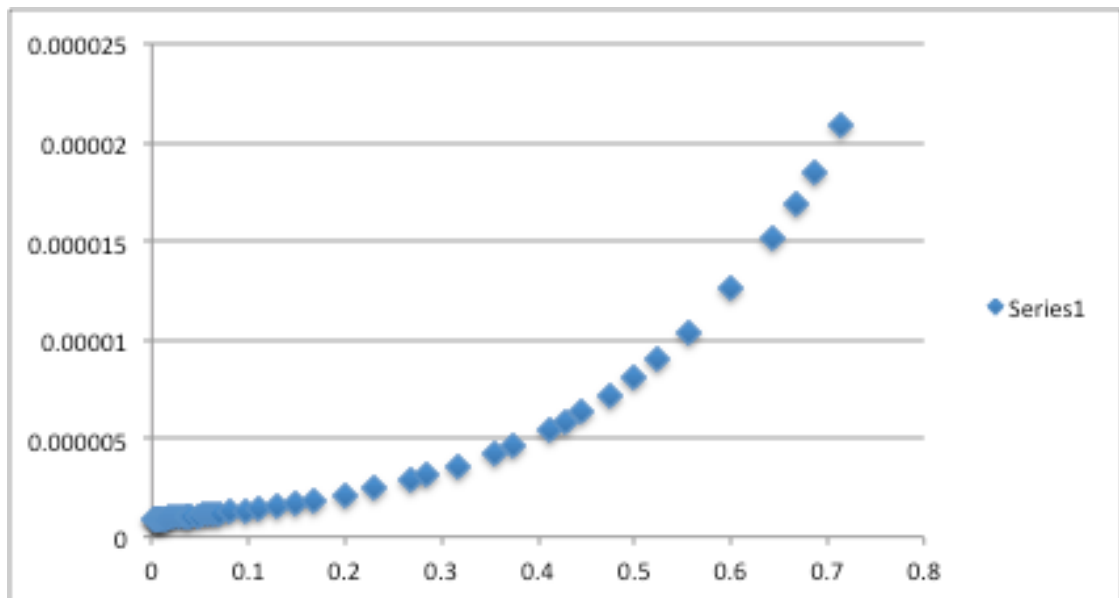
Graph G.2 – Non-linear least squares residuals for b_b/b = 0.01 residuals

Graph G.3 – Non-linear least squares fit for b_b/b = 0.015

Graph G.4 – Non-linear least squares residuals for b_b/b = 0.015 residuals

Graph G.5 – Non-linear least squares fit for $b_b/b = 0.019$

Graph G.6 – Non-linear least squares residuals for $b_b/b = 0.019$ residuals

Graph G.7 – Non-linear least squares fit for $b_b/b = 0.03$

Graph G.8 – Non-linear least squares residuals for $b_b/b = 0.03$ residuals

171

Graph G.9 – Non-linear least squares fit for b_b/b = 0.05

Graph G.10 – Non-linear least squares residuals for b_b/b = 0.05 residuals

Graph G.11 – Non-linear least squares fit for $b_b/b = 0.075$

Graph G.12 – Non-linear least squares residuals for $b_b/b = 0.075$ residuals

Graph G.13 – Non-linear least squares fit for $b_b/b = 0.1$

Graph G.14 – Non-linear least squares residuals for $b_b/b = 0.1$

Table G.1 – Non-linear least squares fit coefficients

Coefficient Data					
bb/b = 0.01		bb/b = 0.015		bb/b = 0.019	
L	0.633618939	L	0.572417095	L	0.527317048
k	4.617592258	k	4.6070430 4	k	4.632575233
bb/b = 0.03		bb/b = 0.05		bb/b = 0.075	
L	0.483439856	L	0.433248838	L	0.392882616
k	4.556665989	k	4.500466404	k	4.46277618
bb/b = 0.1					
L	0.360940761				
k	4.446778247				
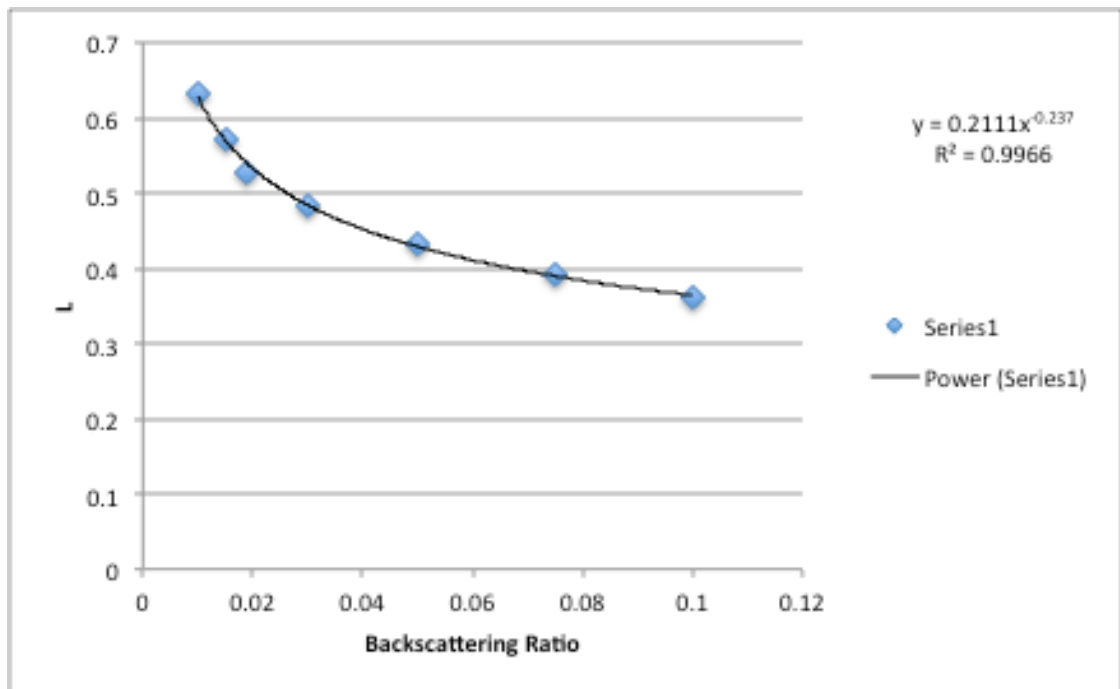
Graph G.15 – Fits for L as a function of b_b/b

175
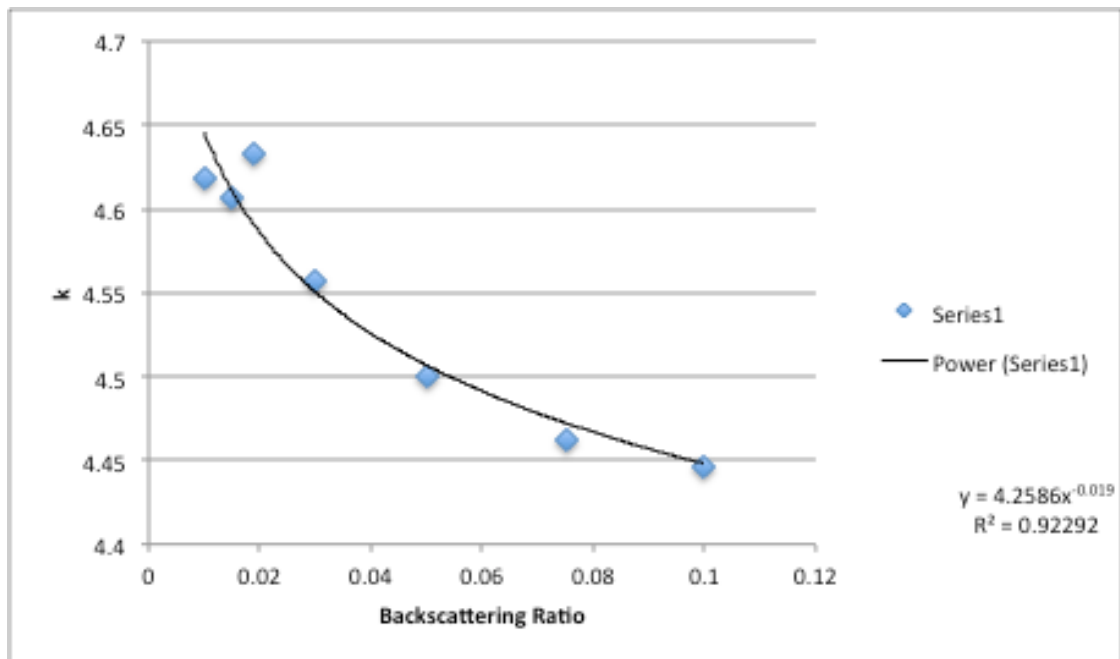
Graph G.16 – Power fit for k values as a function of b_b/b

Appendix H - ω_{ms} Limit Calculation

$$A_{TR} = A_{TR}(\lambda_o) e^{-s(\lambda - \lambda_o)}$$

$$\lambda_o = 550$$

$$\lambda - \lambda_o = 715 - 550$$

$$= 165$$

$$A_{TR} = 0.0038 e^{-0.0086 \times 165}$$

$$= 0.000919$$

$$\omega_m = \frac{b_b \, b}{b_b \, b + a}$$

$$b_b = 0.01 \quad b_b = 0.1$$

$$b = 0.25 \quad b = 15$$

$$a = 0.000919$$

$$\omega_m = \frac{0.01 \times 0.25}{0.01 \times 0.25 + 0.000919}$$

$$\boxed{= 0.7312}$$

$$\omega_m = \frac{0.01 \times 15}{0.01 \times 15 + 0.000919}$$

$$= 0.9939$$

$$\omega_m = \frac{0.1 \times 0.25}{0.1 \times 0.25 + 0.000919}$$

$$= 0.964543$$

$$\omega_m = \frac{0.1 \times 15}{0.1 \times 15 + 0.000919}$$

$$= 0.99938$$

Figure H.1 – Calculation of ω_{ms} limit for absorption graphs

Appendix I – Röttgers Sample Graphs
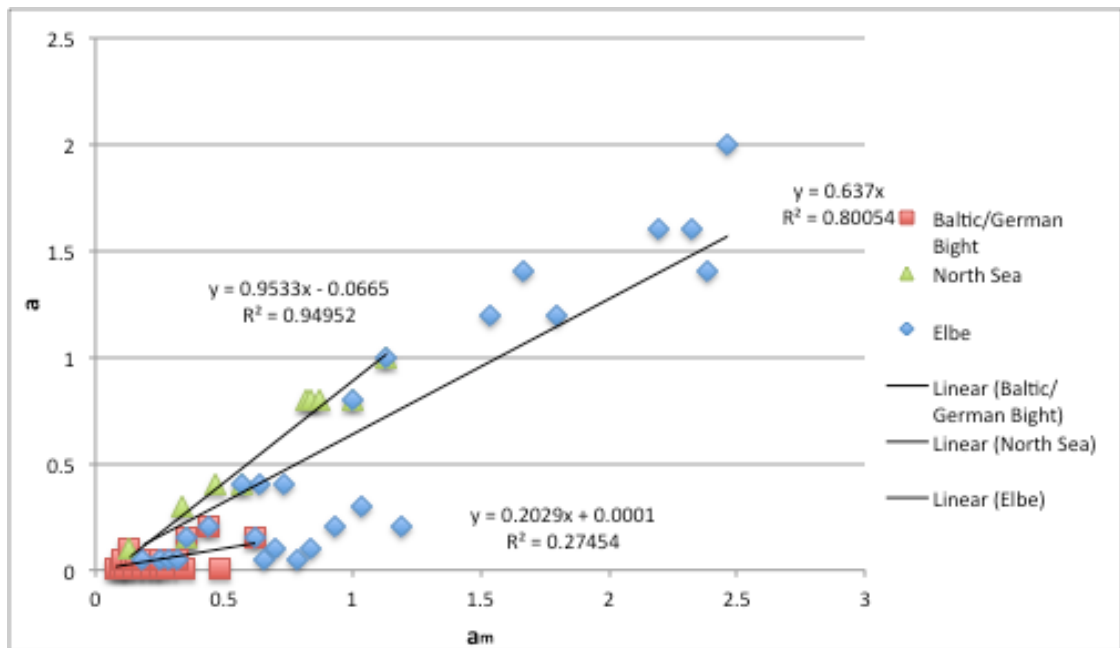
Graph I.1 – Röttger parameterised simulation results for bb/b = 0.01
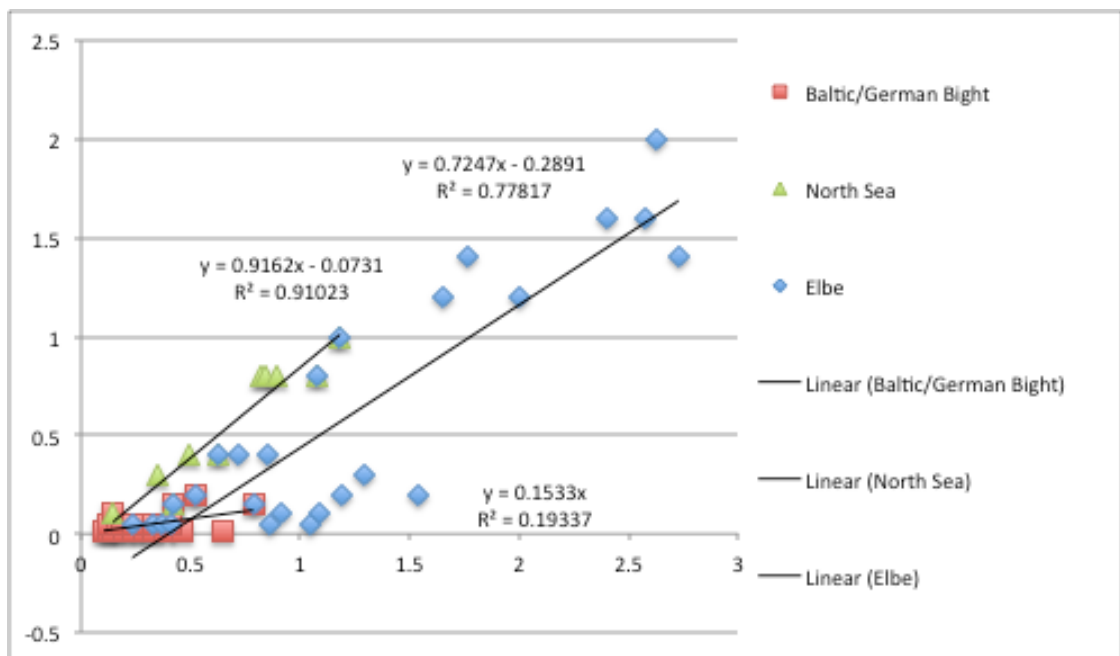
Graph I.2 – Röttger parameterised simulation results for bb/b = 0.01
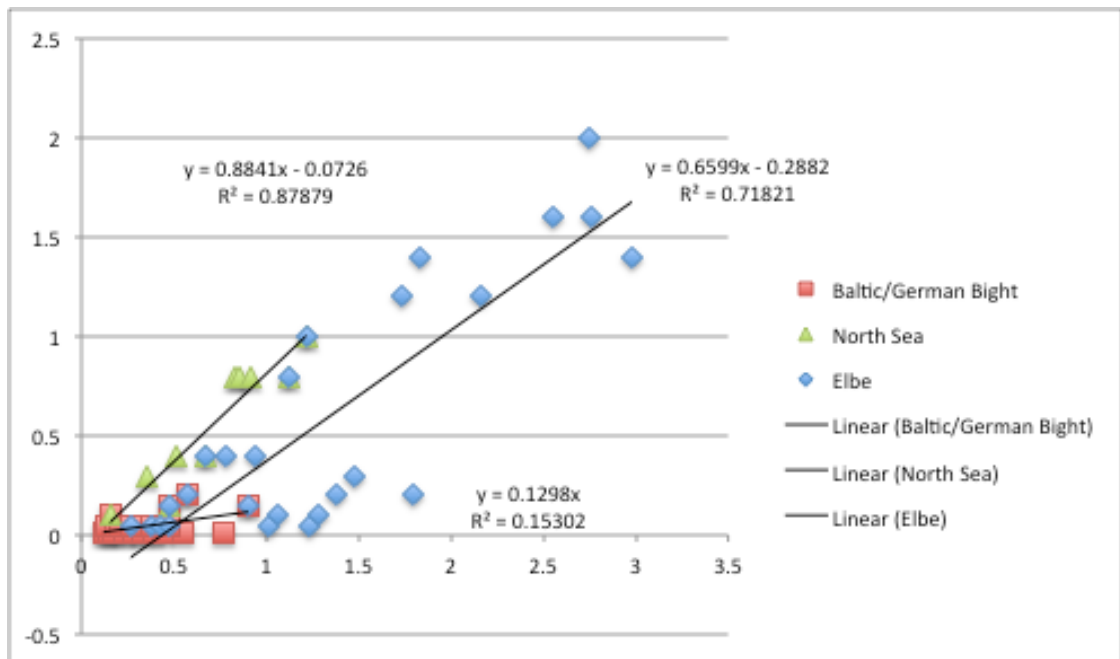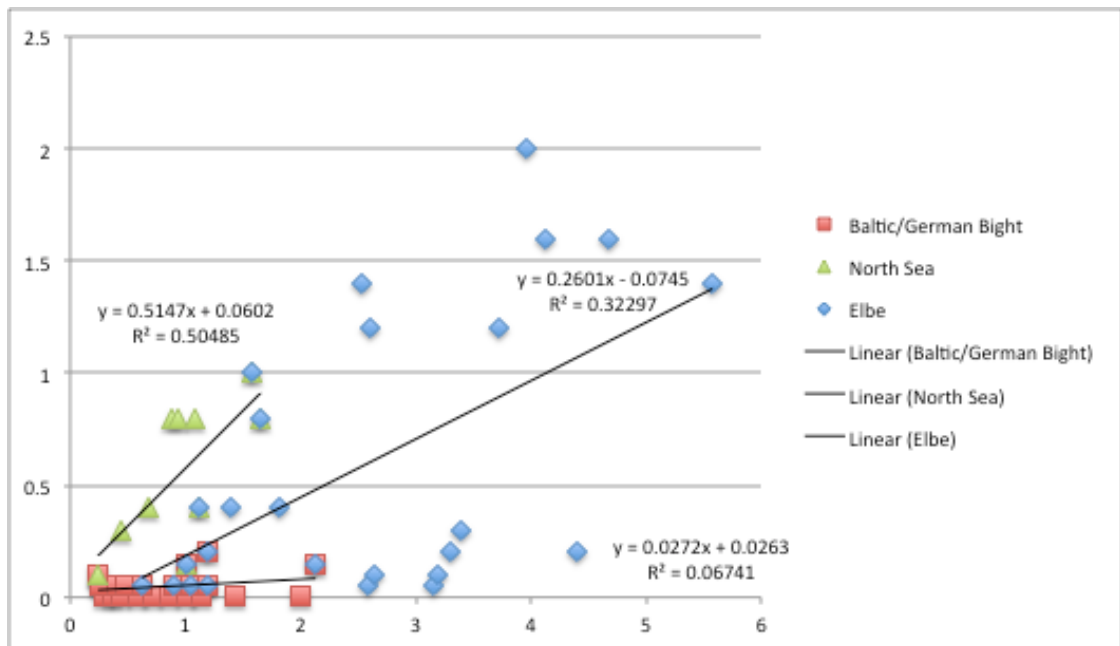
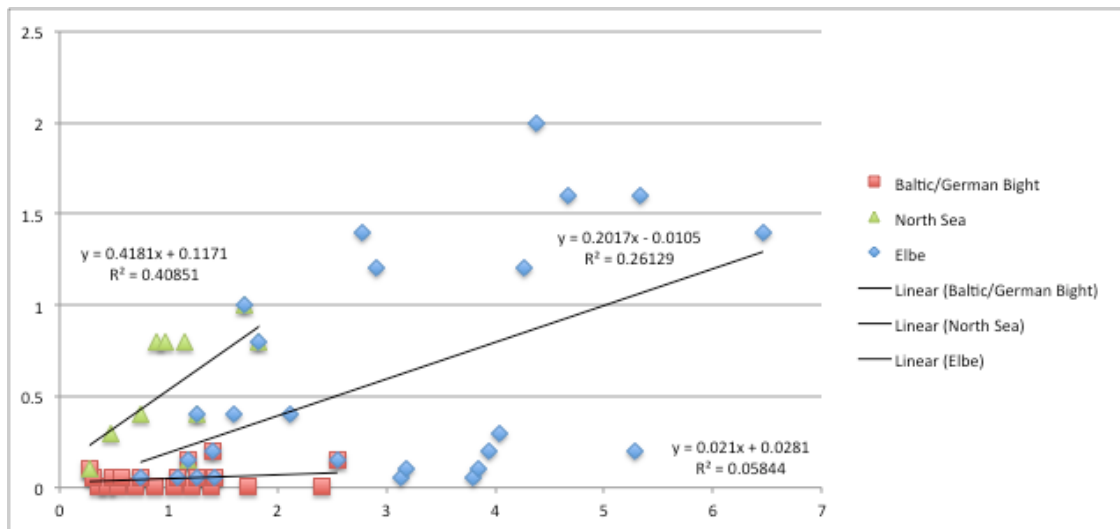**Graph I.3 – Röttger parameterised simulation results for bb/b = 0.01**
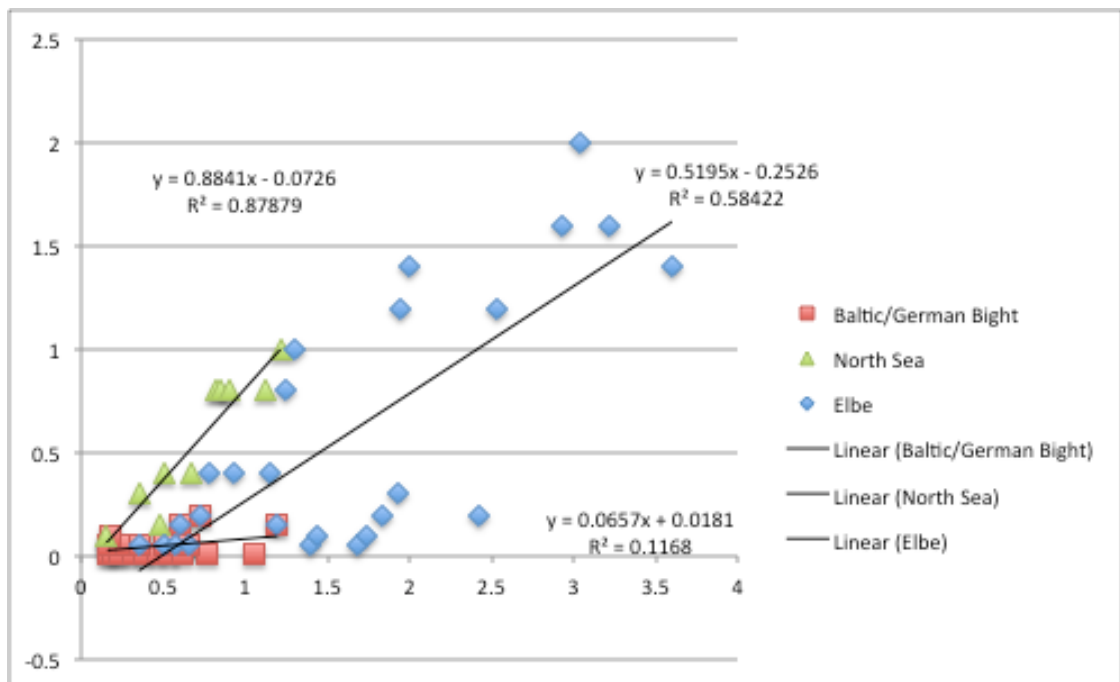
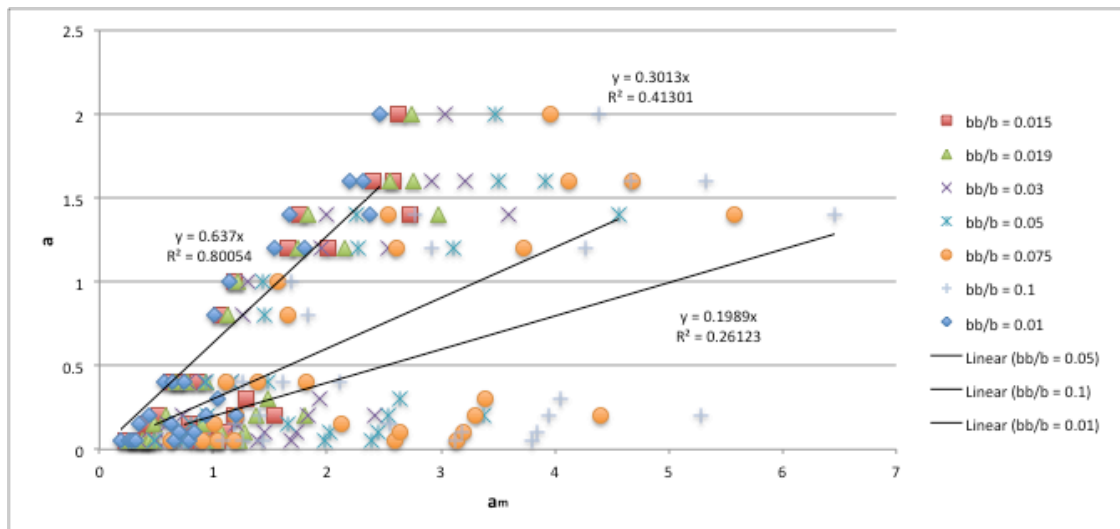**Graph I.4 – Röttger parameterised simulation results for bb/b = 0.01**
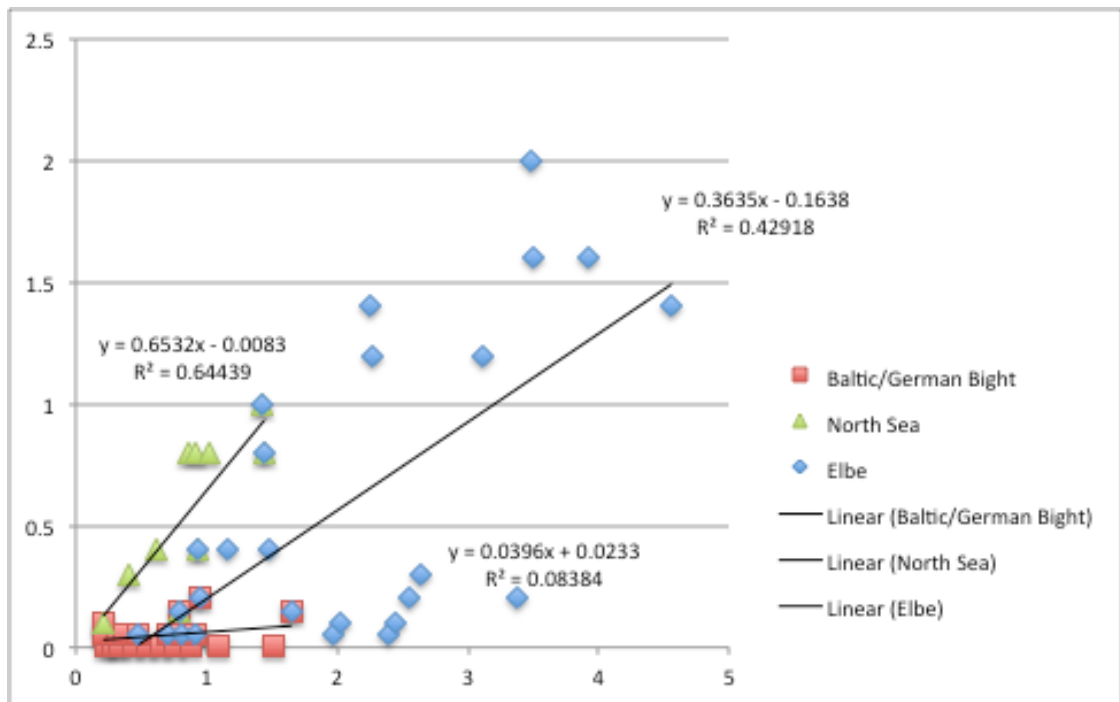
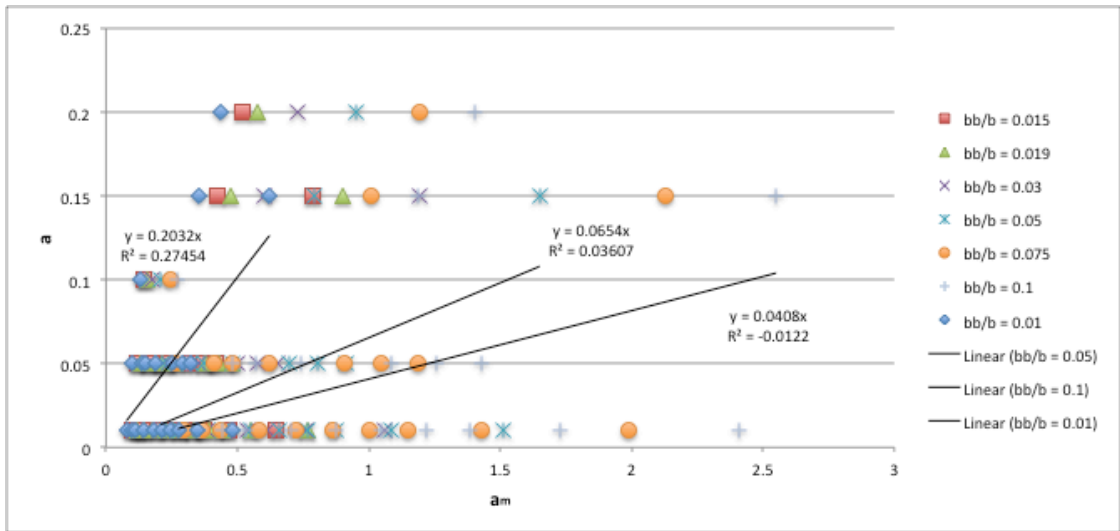**Graph I.5 – Röttger parameterised simulation results for bb/b = 0.01**

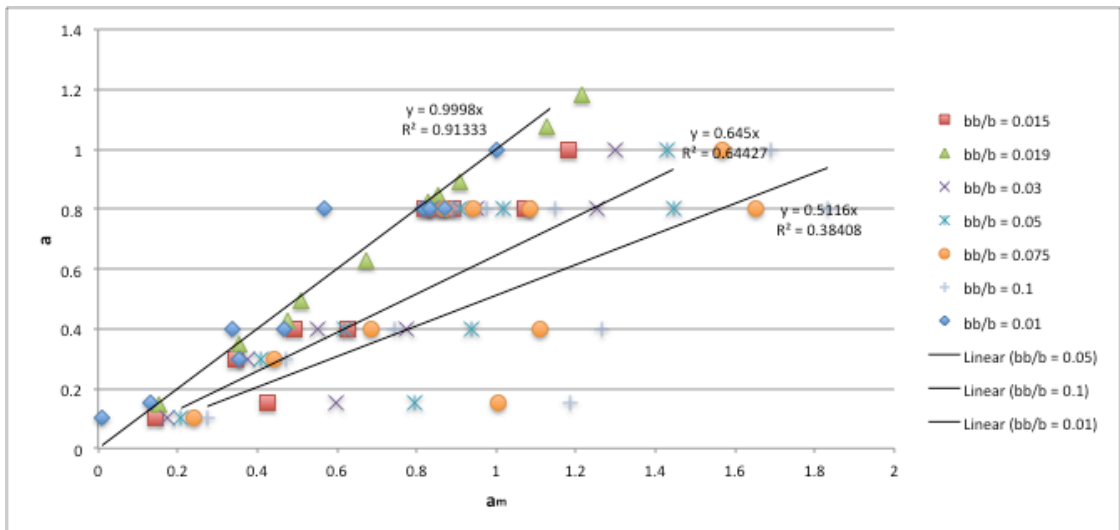**Graph I.6 – Röttger parameterised simulation results for bb/b = 0.01**

Graph I.7 – Röttger parameterised simulation results for bb/b = 0.01

Graph I.8 – Elbe parameterised samples for all tested backscatter ratios

Graph I.9 – Baltic/German Bight parameterised samples for all tested backscatter ratios

Graph I.10 - North Sea parameterised samples for all tested backscatter ratios